Electronic supporting information

Synthesis and Enantioseparation of Chiral Au_{13} Nanoclusters Protected by Bis-N-heterocyclic Carbene Ligands

Hong Yi,[a] Kimberly M. Osten,[a] Tetyana I. Levchenko,[b] Yoshitaka Aramaki*[a], Takashi Ooi*,[a,c]Masakazu Nambo,*[a] and Cathleen M. Crudden*[a,b]

[a] Institute of Transformative Bio-Molecules (WPI-ITbM) Nagoya University Furo, Chikusa, Nagoya 464-8602, Japan.

[b] Department of Chemistry, Queen's University, Chernoff Hall, Kingston, Ontario K7L 3N6, Canada.

[c] Department of Molecular and Macromolecular Chemistry, Graduate School of Engineering, Nagoya University, Nagoya 464-8601, Japan.

Table of Contents

1 Materials and instrumentation

1.1 Materials

All reactions and analyses were performed under ambient conditions unless otherwise specified. Benzimidazole, potassium carbonate, sodium borohydride, ammonium hexafluorophosphate, sodium trifluoroacetate, 1,2-bis(chloromethyl)benzene, 1,2-bis(bromomethyl)benzene, 1,3-bis(bromomethyl)benzene, 1,4-bis(bromomethyl)benzene, and 1-(bromomethyl)-2,3,4,5,6-pentafluorobenzene were purchased from TCI and Wako Chemical Corporation. Chloro(dimethylsulfide)gold(I),[1] 1-benzyl-*1H*-benzo[*d*]imidazole,[2] 1-benzyl-[2-^{13}C]-*1H*-benzo[*d*]imidazole,[3,2] 1-(4-fluorobenzyl)-*1H*-benzo[*d*]imidazole,[4] 1-(naphthalen-2-ylmethyl)-*1H*-benzo[*d*]imidazole,[5] 1-(pyridin-2-ylmethyl)-*1*H-benzo[*d*]imidazole,[6] and 1,2-bis((1H-benzo[d]imidazol-1-yl)methyl)benzene[7] were synthesized according to literature procedures. Hydrochloric acid (35.0–37.0 %), acetonitrile, ethyl acetate, methanol and dichloromethane (DCM) were purchased from Wako and Kanto Chemical Corporation. Absolute ethanol (99.5%) is purchased from Wako Chemical Corporation. All commercially obtained reagents and solvents were used as received.

1.2 NMR spectroscopy and elemental analysis

^{1}H, ^{13}C{^{1}H}, and COSY NMR spectra were recorded on a JEOL ECA-II 600 MHz spectrometer. ^{19}F NMR spectra were recorded on a JEOL ECA-II 400 MHz spectrometer. All ^{1}H NMR spectra were referenced to CD_2Cl_2 at 5.32 ppm or DMSO-d_6 at 2.50 ppm; all ^{13}C NMR spectra were referenced to CD_2Cl_2 at 53.84 ppm or DMSO- d_6 at 39.52 ppm. All spectra were recorded at room temperature. All NMR data was processed and displayed using MestReNova software. In cases of residual contaminants in the NMR spectra, these are noted on each spectrum. Elemental analyses were performed on a Yanaco MT-6 analyzer.

1.3 Mass spectrometry

Electrospray ionization mass spectra (ESI-MS) of clusters were recorded on a Bruker Compact QTOF mass spectrometer. Acetonitrile-dichloromethane (1:1 v/v) dispersions of samples (*ca.* 0.1 mg/mL) were infused at a flow rate of 180 μL/hr by a syringe pump. Parameters were as follows: end plate offset 500 V, capillary 3.6 kV, nebulizer 0.3 Bar, dry gas 3.0 L/min and dry temp 200 °C. The instrument was first calibrated with ESI Tuning Mix (Agilent Technologies) under the same parameters as an external reference.

1.4 UV-vis absorbance, fluorescence spectroscopy, and quantum yield measurements

UV-vis absorbance spectra were recorded on a Shimadzu UV-1800 spectrometer or on an Agilent Cary60 spectrophotometer using 1 cm pathlength quartz cuvettes as dilute dichloromethane, acetonitrile, or methanol solutions of cluster samples. The fluorescence excitation and emission spectra, and fluorescence excitation-emission matrix (EEM) data for cluster [**3a**]Cl_3 dissolved in dichloromethane were recorded on a Horiba Duetta Fluorescence and Absorbance Spectrometer with EzSpecTM software using a 1 cm pathlength quartz cuvettes. Relative fluorescence quantum yield (Φ_F) was determined by the

comparative method.[8] According to the method, the fluorescence quantum yield of a sample is related to that of a standard by the following expression:

$\Phi_F = (A_{std}/A)\ (F/F_{std})\ (n/n_{std})^2\ \Phi_{F(std)}$

where F and F_{std} are the areas under the fluorescence emission curves of the sample and the standard, respectively. A and A_{std} are the absorbances of the samples and standard at the excitation wavelengths, respectively. n and n_{std} are the refractive indices of solvents used for the sample and standard, respectively. Zinc phthalocyanine (ZnPc, Acros Organics) solution in freshly distilled pyridine was employed as the standard ($\Phi_{F(std)} = 0.30$).[9] The refractive indexes of the solvents were taken to be $n_{pyridine} = 1.5095$ and $n_{DCM} = 1.4242$ (both at 20 °C).[10] All solutions were filtered using 0.2 μm PTFE syringe filters (Basic™ Fisher), diluted to desired A, placed into 1 cm pathlength quartz fluorescence cuvettes with graded seal tube, sealed with rubber septa, and deoxygenated by purging with argon. In several independent measurements, sample and standard solutions were prepared to have equal absorbances (between 0.04 and 0.05) at their respective excitation wavelengths after purging. UV-vis absorbance spectra were recorded on an Agilent Cary60 spectrophotometer with the corresponding pure solvents for background correction. Fluorescence emission spectra were recorded for the same solutions on a Horiba Duetta Fluorescence and Absorbance Spectrometer with EzSpecTM software. Both the sample and standard were excited at the same relevant wavelength (indicated for each particular dataset). The spectra were corrected for wavelength-dependent instrument sensitivity. The areas under the fluorescence emission curves were calculated numerically using Origin Pro 2016 software. The absolute quantum yield of [**3a**]Cl_3 solutions in dichloromethane was measured on a C11347-11 Quantaurus-QY Absolute PL quantum yield spectrometer (Hamamatsu Photonics K.K.) equipped with 3.3 inch integrating sphere to measure all luminous flux and cooled, back-thinned CCD sensor for detection at 1024 photosensitive channels. The same procedure was implemented for the sample preparation as in the case of the relative quantum yield measurements.

1.5 Chiral high performance liquid chromatography

Chromatographic separation of cluster enantiomers was achieved on a Shimadzu LC-2010CHT HPLC system equipped with a Daicel CHIRALPAK IE-3 column (3μm, 250 mm×4.6 mm). A 10 mm path length UV-vis detector was used with the detection wavelength set to 350 nm. Analytes were eluted at a flow rate of 1.0 mL/min using MeOH/trifluoroacetic acid(TFA)/diethylamine(DEA) (100:0.1:0.1 volume ratio). For large-scale separations, a preparative scale Diacel CHIRALPAK IE-3 column (5μm, 250 mm×10.0 mm) was used with a flow rate of 2.0 mL/min and the same eluent system.

1.6 Circular dichroism spectroscopy

Circular dichroism (CD) spectra were recorded on a JASCO J-720WN CD-spectrometer using a 5 mm path length quartz cuvette. Samples were dissolved in dichloromethane, and a blank spectrum of solvent was subtracted from each sample spectrum. A scanning speed of 100 nm/min and data pitch of 0.1 nm was used to record four spectra, which were then averaged. All spectra were recorded at room temperature.

1.7 X-ray crystallography

Crystals of [**3a**]Cl_3 of appropriate quality for X-ray diffraction studies were covered with a thin layer of hydrocarbon oil (Paratone-N). A suitable crystal was then selected, attached to a glass fiber or a microsampler, and quickly placed in a low-temperature stream of nitrogen. Data were collected at Nagoya University using a Rigaku FR-X with Pilatus 200K with fine-focus sealed tube Mo K_α radiation (λ = 0.71073 Å), with the crystal cooled to −150 °C. The structure was solved using intrinsic phasing (SHELXT) and refined using SHELXL-2014.[11]

2 Experimental procedures

2.1 Synthesis of dibenzimidazolium salts 1a-g

General procedure for the synthesis of dibenzimidazolium salts 1a-e

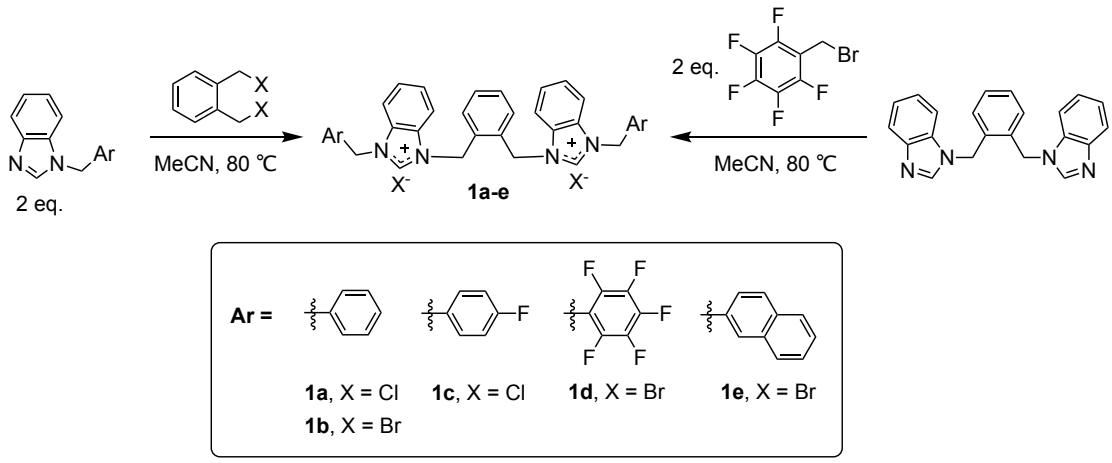

The following procedure for the preparation of dibenzimidazolium salts **1a-e** was adapted from the literature.[12] A 25 mL glass pressure tube was charged with: (1) for salts **1a-c** and **1e**, the appropriate mono-alkylated benzimidazole (2.0 mmol) and 1,2-bis(chloromethyl)- or 1,2-bis(bromomethyl)benzene (1.0 mmol); or (2) for salt **1d**, 1,2-bis((1H-benzo[d]imidazol-1-yl)methyl)benzene (1.0 mmol) and 1-(bromomethyl)-2,3,4,5,6-pentafluorobenzene (2.2 mmol). Acetonitrile (10 mL) was added, the tube was capped and the mixture was then heated in an 80 °C oil bath for 12 hours, and then cooled to room temperature. After cooling, the solvent was removed *in vacuo* to afford the crude solid. The crude solid was washed with EtOAc (3 x 10 mL) and dried *in vacuo* to afford the pure product as a white powder. Yields and characterization data for each compound are listed below.

Synthesis of 1,1'-(dibenzyl)-3,3'-(1,2-xylylene)dibenzimidazolium dichloride (1a)

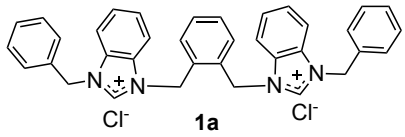

1-Benzyl-*1H*-benzo[*d*]imidazole (416.0 mg, 2.0 mmol) and 1,2-bis(chloromethyl)benzene (174.0 mg, 1.0 mmol) afforded the title compound **1a** in 81 % yield (480.1 mg). **^{1}H NMR (DMSO-d_6, 600 MHz):** δ 10.39 (s, 2H NC*H*N), 8.07 (d, ^3J = 7.8 Hz, 2H), 8.00 (d, ^3J = 7.8 Hz, 2H), 7.67 – 7.62 (m, 4H), 7.59 (d, ^3J = 7.8 Hz, 4H), 7.44 – 7.40 (m, 6H), 7.38 – 7.36 (m, 2H), 7.25 – 7.24 (m, 2H), 6.21 (s, 4H, NC*H*$_2$Ar), 5.86 (s, 4H, NC*H*$_2$Ar). **^{13}C{^{1}H} NMR (DMSO- d_6, 151 MHz):** δ 143.21 (N*C*HN), 134.06, 132.24, 131.44, 130.99, 129.36, 128.94, 128.76, 128.69, 128.34, 126.90, 126.78, 114.32, 114.05, 49.98 (N*C*H$_2$Ar), 47.69 (N*C*H$_2$Ar). **ESI-MS (*m/z*) for [$C_{36}H_{32}N_4Cl$]$^+$**: calculated 555.2310, found 555.2314.

Synthesis of 1,1'-(dibenzyl)-3,3'-(1,2-xylylene)di[2-^{13}C]benzimidazolium dichloride (^{13}C-1a)

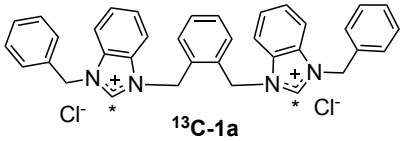

* = ^{13}C-labeled

1-Benzyl-[2-^{13}C]-*1H*-benzo[*d*]imidazole (209.0 mg, 1.0 mmol) and 1,2-bis(chloromethyl)benzene (87.0 mg, 0.5 mmol) afforded the title compound **^{13}C-1a** in 79 % yield (233.8 mg). **^{1}H NMR (DMSO- d_6, 600 MHz):** δ 10.24 (d, $^1J_{C\text{-}H}$ = 220.2 Hz, 2H, NC*H*N), 8.02 – 7.99 (m, 4H), 7.68 – 7.63 (m, 4H), 7.57 (d, ^3J = 7.6 Hz, 4H), 7.45 – 7.41 (m, 6H), 7.39 – 7.36 (m, 2H), 7.25 – 7.23 (m, 2H), 6.14 (d, $^3J_{C\text{-}H}$ = 4.2 Hz, 4H), 5.84 (d, $^3J_{C\text{-}H}$ = 4.2 Hz, 4H). **^{13}C{^{1}H} NMR (DMSO- d_6, 151 MHz):** δ 143.17 (N*C*HN), 134.01, 132.14, 131.44, 131.05, 129.40, 128.98, 128.76, 128.73, 128.33, 126.96, 126.82, 114.24, 114.07, 50.01 (N*C*H$_2$Ar), 47.63 (N*C*H$_2$Ar). **ESI-MS (*m/z*) for [$^{13}C_2C_{34}H_{32}N_4Cl$]$^+$**: calculated 557.2375, found 557.2378.

Synthesis of 1,1'-(dibenzyl)-3,3'-(1,2-xylylene)dibenzimidazolium dibromide (1b)

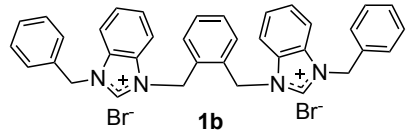

1-Benzyl-*1H*-benzo[*d*]imidazole (416.0 mg, 2.0 mmol) and 1,2-bis(bromomethyl)benzene (262.0 mg, 1.0 mmol) afforded the title compound **1b** in 96 % yield (651.2 mg). **^{1}H NMR (DMSO- d_6, 600 MHz):** δ 9.93 (s, 2H, NC*H*N), 8.01 (d, ^3J = 8.0 Hz, 2H), 7.93 (d, ^3J = 7.8 Hz, 2H), 7.70 – 7.66 (m, 4H), 7.54 (d, ^3J = 7.6 Hz, 4H), 7.46 – 7.42 (m, 6H), 7.40 – 7.39 (m, 2H), 7.26 – 7.24 (m, 2H), 6.03 (s, 4H, NC*H*$_2$Ar), 5.80 (s, 4H, NC*H*$_2$Ar). **^{13}C{^{1}H} NMR (DMSO- d_6, 151 MHz):** δ 142.98 (N*C*HN), 133.93, 132.02, 131.39, 131.06, 129.41, 128.97, 128.74, 128.33, 126.97, 126.84, 114.21, 114.10, 50.06 (N*C*H$_2$Ar), 47.72 (N*C*H$_2$Ar). Note that one carbon was not found, likely due to peak overlap. **ESI-MS (*m/z*) for [$C_{36}H_{32}N_4Br$]$^+$:** calculated 599.1805, found 599.1812.

Synthesis of 1,1'-(di-4-fluorobenzyl)-3,3'-(1,2-xylylene)dibenzimidazolium dichloride (1c)

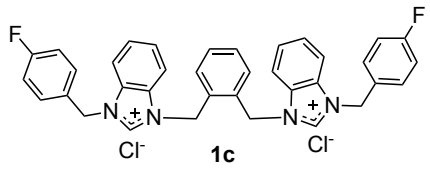

1c

1-(4-Fluorobenzyl)-*1H*-benzo[*d*]imidazole (452.0 mg, 2.0 mmol) and 1,2-bis(chloromethyl)benzene (174.0 mg, 1.0 mmol) afforded the title compound **1c** in 73 % yield (456.9 mg). **^{1}H NMR (DMSO- d_6, 600 MHz):** δ 10.35 (s, 2H NC*H*N), 8.05 (d, J = 7.9 Hz, 2H), 8.03 (d, J = 7.9 Hz, 2H), 7.70 – 7.64 (m, 8H), 7.44 – 7.42 (m, 2H), 7.27 – 7.24 (m, 6H), 6.18 (s, 4H, NCH_2Ar), 5.85 (s, 4H, NCH_2Ar). **^{13}C{1H} NMR (DMSO- d_6, 151 MHz):** δ 162.18 (d, $^{1}J_{F-C}$ = 245.2 Hz, C_6H_4F *C-4*), 143.19 (N*C*HN), 132.19, 131.45, 130.93, 130.87, 130.26, 129.37, 128.80, 126.91, 126.79, 115.80 (d, $^{2}J_{F-C}$ = 22.6 Hz, C_6H_4F *C-3*), 114.31, 114.04, 49.23 (N*C*H_2Ar), 47.69 (N*C*H_2Ar). **^{19}F NMR (DMSO- d_6, 376 MHz):** δ -113.04. **ESI-MS (*m/z*) for $[C_{36}H_{30}F_2N_4Cl]^+$:** calculated 591.2122, found 591.2121.

Synthesis of 1,1'-(di-pentafluorobenzyl)-3,3'-(1,2-xylylene)dibenzimidazolium dibromide (1d)

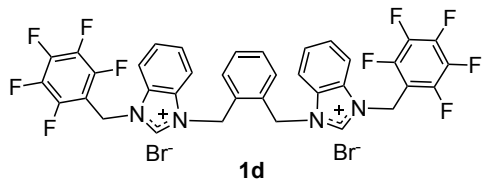

1d

Note that due to difficulty in isolating 1-(pentafluorobenzyl)-*1H*-benzo[*d*]imidazole, the procedure was modified from that used for other salts. This route is best suited to alkylation with benzyl bromides, and not chlorides, due to their lower reactivity with the starting material. 1,2-Bis((1H-benzo[d]imidazol-1-yl)methyl)benzene (338.0 mg, 1.0 mmol) and 1-(bromomethyl)-2,3,4,5,6-pentafluorobenzene (570.1 mg, 2.2 mmol) afforded the title compound **1d** in 92 % yield (781.0 mg). **^{1}H NMR (DMSO- d_6, 600 MHz):** δ10.15 (s, 2H NC*H*N), 8.08 (d, ^{3}J = 8.4 Hz, 2H), 7.96 (d, ^{3}J = 8.4 Hz, 2H), 7.79 (t, ^{3}J = 7.8 Hz, 2H), 7.70 (t, ^{3}J = 7.8 Hz, 2H), 7.37 (dd, J = 5.7, 3.3 Hz, 2H), 7.11 (dd, J = 5.4, 3.5 Hz, 2H), 6.15 (s, 4H, NCH_2Ar), 6.07 (s, 4H, NCH_2Ar). **^{13}C{^{1}H} NMR (DMSO- d_6, 151 MHz):** δ 145.34 (d, $^{1}J_{F-C}$ = 250.7 Hz, C_6F_5), 143.78 (N*C*HN), 141.37 (d, $^{1}J_{F-C}$ = 252.2 Hz, C_6F_5), 137.21 (d, $^{1}J_{F-C}$ = 253.7 Hz, C_6F_5), 131.84, 131.16, 131.00, 129.08, 127.82, 127.44, 127.02, 114.37, 113.47, 107.77 (t, $^{2}J_{F-C}$ = 16.6 Hz, C_6F_5), 47.77 (N*C*H_2Ar), 38.25 (N*C*H_2Ar). **^{19}F NMR (DMSO- d_6, 376 MHz):** δ -140.26 (d, ^{3}J = 22.6 Hz, 4F, *ortho*-C_6F_5), -152.64 (t, ^{3}J = 22.6 Hz. 2F, *para*-C_6F_5), -161.41 (t, ^{3}J = 22.6 Hz, 4F, *meta*-C_6F_5). **ESI-MS (*m/z*) for $[C_{36}H_{22}F_{10}N_4Br]^+$:** calculated 779.0863, found 779.0866.

Synthesis of 1,1'-(di(naphthalen-2-ylmethyl))-3,3'-(1,2-xylylene)dibenzimidazolium dibromide (1e)

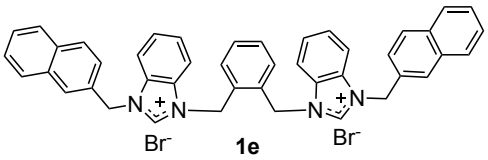

1e

1-(Naphthalen-2-ylmethyl)-*1H*-benzo[*d*]imidazole (516.0 mg, 2.0 mmol) and 1,2-bis(bromomethyl)benzene (262.0 mg, 1.0 mmol) afforded the title compound **1e** in 83 % yield (646.7 mg). **^{1}H NMR (DMSO- d_6, 600 MHz):** δ 10.11 (s, 2H NCHN), 8.17 (s, 2H), 8.05 (d, ^3J = 7.7 Hz, 2H), 7.98 (dd, J = 12.5, 8.3 Hz, 4H), 7.95 – 7.91 (m, 4H), 7.66 – 7.64 (m, 6H), 7.57 – 7.55 (m, 4H), 7.46 (dd, J = 5.5, 3.3 Hz, 2H), 7.28 (dd, J = 5.2, 3.6 Hz, 2H), 6.14 (s, 4H, NCH_2Ar), 6.00 (s, 4H, NCH_2Ar). **^{13}C{^{1}H} NMR (DMSO- d_6, 151 MHz):** δ 143.16 (N*C*HN), 132.72, 132.69, 132.06, 131.43, 131.35, 131.19, 129.39, 128.77, 128.68, 127.87, 127.70, 127.63, 127.00, 126.84, 126.78, 126.76, 125.71, 114.22, 114.14, 50.32 (N*C*H_2Ar), 47.77 (N*C*H_2Ar). **ESI-MS (*m/z*) for [$C_{44}H_{36}N_4Br$]$^+$:** calculated 699.2118, found 699.2114.

Synthesis of 1,1'-(dibenzyl)-3,3'-(1,3-xylylene)dibenzimidazolium dibromide (1f)

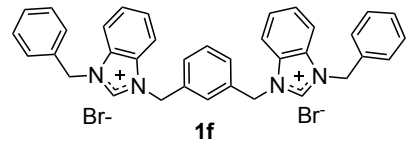

1f

The general procedure for the synthesis of **1a-e** was used, with the exception of the use of 1,3-bis(bromomethyl)benzene as starting material. 1-Benzyl-*1H*-benzo[*d*]imidazole (416.0 mg, 2.0 mmol) and 1,3-bis(bromomethyl)benzene (262.0 mg, 1.0 mmol) afforded the title compound **1f** in 87 % yield (589.8 mg). **^{1}H NMR (DMSO- d_6, 600 MHz):** δ 10.31 (s, 2H NC*H*N), 7.98 (d, ^3J = 8.4 Hz, 2H), 7.91 (d, ^3J = 8.1 Hz, 3H), 7.62 (t, ^3J = 7.8 Hz, 2H), 7.59 – 7.52 (m, 8H), 7.50 – 7.46 (m, 1H), 7.43 – 7.41 (m, 4H), 7.39 – 7.37 (m, 2H), 5.85 (s, 4H, NCH_2Ar), 5.84 (s, 4H, NCH_2Ar). **^{13}C{^{1}H} NMR (DMSO- d_6, 151 MHz):** δ 142.82 (N*C*HN), 134.75, 133.95, 131.02, 130.95, 129.75, 129.00, 128.75, 128.69, 128.63, 128.36, 126.79, 126.70, 114.05, 114.01, 50.03 (N*C*H_2Ar), 49.77 (N*C*H_2Ar). **ESI-MS (*m/z*) for [$C_{36}H_{32}N_4Br$]$^+$:** calculated 599.1805, found 599.1804.

Synthesis of 1,1'-(di(naphthalen-2-ylmethyl))-3,3'-(1,4-xylylene)dibenzimidazolium dibromide (1g)

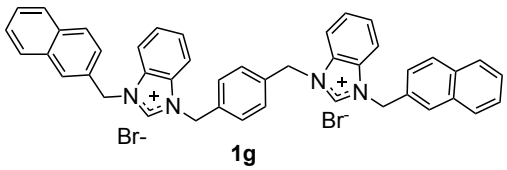

1g

The general procedure for the synthesis of **1a-e** was used, with the exception of the use of 1,4-bis(bromomethyl)benzene as starting material. 1-(Naphthalen-2-ylmethyl)-*1H*-benzo[*d*]imidazole (516.0 mg, 2.0 mmol) and 1,4-bis(bromomethyl)benzene (262.0 mg, 1.0 mmol) afforded the title compound **1g** in 83 % yield (645.74 mg). **^{1}H NMR (DMSO- d_6, 600 MHz):** δ 10.22 (s, 2H NC*H*N), 8.14 (s, 2H), 8.05 – 8.02 (m, 2H), 8.00 – 7.90 (m, 8H), 7.67 – 7.59 (m, 10H), 7.57 – 7.56 (m, 4H), 5.98 (s, 4H, NCH_2Ar), 5.83 (s, 4H, NCH_2Ar). **^{13}C{^{1}H} NMR (DMSO- d_6, 151 MHz):** δ 142.90 (N*C*HN), 134.53, 132.74, 132.69, 131.30, 131.17, 131.02, 128.91, 128.81, 127.88, 127.73, 127.70, 126.84, 126.79, 126.78, 125.73, 114.10, 113.99, 50.26 (N*C*H_2Ar), 49.57 (N*C*H_2Ar). Note that one carbon was not found, likely due to peak overlap. **ESI-MS (*m/z*) for [$C_{44}H_{36}N_4Br$]$^+$:** calculated 699.2118, found 699.2117.

2.2 Synthesis of bis-NHC dinuclear gold(I) halide complexes 2a-g

General procedure for the synthesis of complexes 2a-g

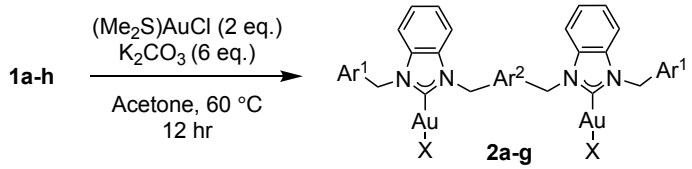

A 25 mL glass pressure tube was charged with the appropriate benzimidazolium salt **1a-g** (0.30 mmol), $(Me_2S)AuCl$ (0.60 mmol), K_2CO_3 (1.8 mmol) and acetone (10 mL). The mixture was heated in a 60 °C oil bath for 12 hours, and then cooled to room temperature. After cooling, the solvent was removed *in vacuo* to afford the crude residue. Purification of the residue by flash column chromatography on silica gel (Fuji Silysia Chromatorex PSQ60AB silica; 20:1 DCM/MeOH eluent; ~3x10 cm column size, R_f (DCM) = 0.4) afforded the pure complex as a white powder. Yields and characterization data for each compound are listed below.

Synthesis of 1,1'-(dibenzyl)-3,3'-(1,2-xylylene)dibenzo[*d*]imidazol-2-ylidene digold(I) dichloride (2a)

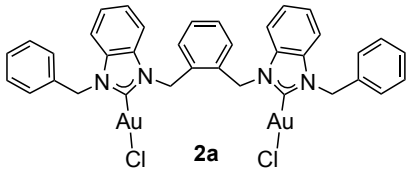

1a (177.0 mg, 0.30 mmol) afforded complex **2a** in 61 % yield (179.7 mg). **^{1}H NMR (DMSO- d_6, 600 MHz):** δ 7.82 (d, ^3J = 7.4 Hz, 2H), 7.70 (d, ^3J = 7.2 Hz, 2H), 7.51 (d, ^3J = 7.6 Hz, 4H), 7.48 – 7.45 (m, 4H), 7.41 (t, ^3J = 7.5 Hz, 4H), 7.35 – 7.34 (m, 2H), 7.21 -7.19 (m, 2H), 6.65 – 6.58 (m, 2H), 6.17 (s, 4H, NCH_2Ar), 5.87 (s, 4H, NCH_2Ar). **^{13}C{^{1}H} NMR (DMSO- d_6, 151 MHz):** δ 178.80 (N*C*N), 135.75, 133.31, 133.09, 132.79, 128.90, 128.19, 128.15, 127.31, 125.42, 125.00, 124.90, 112.74, 112.68, 51.64 (N*C*H_2Ar), 48.63 (N*C*H_2Ar). **ESI-MS (*m/z*) for $[C_{36}H_{30}Au_2N_4Cl]^+$:** calculated 947.1485, found 947.1487.

Synthesis of 1,1'-(dibenzyl)-3,3'-(1,2-xylylene)di[2-^{13}C]benzo[*d*]imidazol-2-ylidene digold(I) dichloride (^{13}C-2a)

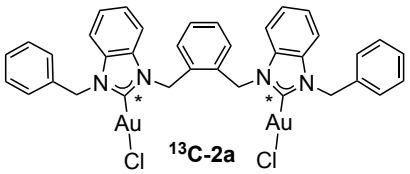

^{13}C-1a (177.6 mg, 0.30 mmol) afforded complex **^{13}C-2a** in 58 % yield (171.4 mg). **^{1}H NMR (DMSO- d_6, 600 MHz):** δ 7.84 – 7.79 (m, 2H), 7.70 (d, ^3J = 7.1 Hz, 2H), 7.50 (d, ^3J = 7.6 Hz, 4H), 7.47 – 7.45 (m, 4H), 7.40 (t, ^3J = 7.5 Hz, 4H), 7.35 – 7.34 (m, 2H), 7.20 (dd, J = 5.7, 3.3 Hz, 2H), 6.61 (dd, J = 5.1, 3.7 Hz, 2H), 6.17 (d, $^3J_{C\text{-}H}$ = 5.1 Hz, 4H, NCH_2Ar), 5.87 (d, $^3J_{C\text{-}H}$ = 5.3 Hz, 4H, NCH_2Ar). **^{13}C{^{1}H} NMR (DMSO- d_6, 151 MHz):** δ 178.82 (N*C*N), 135.76, 133.32, 133.10, 132.79, 128.91, 128.21, 128.17, 127.33, 125.42, 125.02, 124.91, 112.75, 112.68, 51.74 (N*C*H_2Ar), 48.77 (N*C*H_2Ar). **ESI-MS (*m/z*) for $[^{13}C_2C_{34}H_{30}Au_2N_4Cl]^+$:** calculated 949.1555, found 949.1550.

Synthesis of 1,1'-(dibenzyl)-3,3'-(1,2-xylylene)dibenzo[*d*]imidazol-2-ylidene digold(I) dibromide (2b)

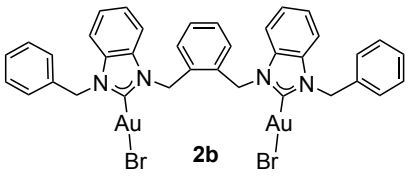

1b (203.4 mg, 0.30 mmol) afforded complex **2b** in 65 % yield (208.6 mg). **^{1}H NMR (DMSO- d_6, 600 MHz):** δ 7.83 – 7.81 (m, 2H), 7.71 – 7.68 (m, 2H), 7.51 (d, ^3J = 7.4 Hz, 4H), 7.49 – 7.45 (m, 4H), 7.40 (t, ^3J = 7.6 Hz, 4H), 7.35 – 7.34 (m, 2H), 7.20 (dd, J = 5.7, 3.3 Hz, 2H), 6.64 (dd, J = 5.5, 3.5 Hz, 2H), 6.17 (s, 4H, NCH_2Ar), 5.87 (s, 4H, NCH_2Ar). **^{13}C{^{1}H} NMR (DMSO- d_6, 151 MHz):** δ 181.63 (N*C*N), 135.72, 133.31, 133.02, 132.73, 128.90, 128.21, 127.34, 125.54, 125.05, 124.94, 112.78, 112.71, 51.59 (N*C*H$_2$Ar), 48.58 (N*C*H$_2$Ar). Note that one carbon was not found, likely due to peak overlap. **ESI-MS (*m/z*) for [$C_{36}H_{30}Au_2N_4Br$]$^+$:** calculated 991.0979, found 991.0981.

Synthesis of 1,1'-(di-4-fluorobenzyl)-3,3'-(1,2-xylylene)dibenzo[*d*]imidazol-2-ylidene digold(I) dichloride (2c)

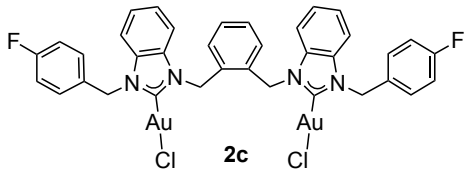

1c (187.8 mg, 0.30 mmol) afforded complex **2c** in 53 % yield (161.8 mg). **^{1}H NMR (DMSO- d_6, 600 MHz):** δ 7.84 (d, ^3J = 7.9 Hz, 2H), 7.69 (d, ^3J = 7.9 Hz, 2H), 7.57 (dd, J = 8.5, 5.5 Hz, 4H), 7.47 – 7.45 (m, 4H), 7.24 (t, ^3J = 8.8 Hz, 4H), 7.20 (dd, J = 5.7, 3.3 Hz, 2H), 6.61 (dd, J = 5.3, 3.6 Hz, 2H), 6.16 (s, 4H, NCH_2Ar), 5.85 (s, 4H, NCH_2Ar). **^{13}C{^{1}H} NMR (DMSO- d_6, 151 MHz):** δ 178.76 (N*C*N), 161.84 (d, $^1J_{F\text{-}C}$ = 244.6 Hz, C_6H_4F *C-4*), 133.27, 133.10, 132.71, 132.00, 129.61, 129.55, 128.17, 125.46, 125.04, 124.94, 115.78 (d, $^2J_{F\text{-}C}$ = 22.65 Hz, C_6H_4F *C-3*), 112.69, 50.88 (N*C*H$_2$Ar), 48.67 (N*C*H$_2$Ar). **^{19}F NMR (DMSO- d_6, 376 MHz**): δ -113.82. **ESI-MS (*m/z*) for [$C_{36}H_{28}Au_2F_2N_4Cl$]$^+$:** calculated 983.1296, found 983.1293.

Synthesis of 1,1'-(dipentafluorobenzyl)-3,3'-(1,2-xylylene)dibenzo[*d*]imidazol-2-ylidene digold(I) dibromide (2d)

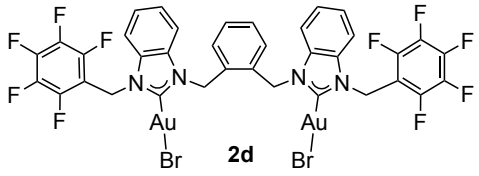

1d (257.4 mg, 0.30 mmol) afforded complex **2d** in 65 % yield (208.6 mg). **^{1}H NMR (DMSO- d_6, 600 MHz):** δ 7.94 (d, ^3J = 8.3 Hz, 2H), 7.66 (d, ^3J = 8.2 Hz, 2H), 7.57 (t, ^3J = 7.8 Hz, 2H), 7.49 (t, ^3J = 7.8 Hz, 2H), 7.19 – 7.13 (m, 2H), 6.62 – 6.54 (m, 2H), 6.09 (s, 4H, NCH_2Ar), 5.92 (s, 4H, NCH_2Ar). **^{13}C{^{1}H} NMR (DMSO- d_6, 151 MHz):** δ 182.18 (N*C*N), 145.20 (d, $^1J_{F\text{-}C}$ = 256.7 Hz, C_6F_5), 140.60 (d, $^1J_{F\text{-}C}$ = 119.3 Hz, C_6F_5), 136.97 (d, $^1J_{F\text{-}C}$ = 125.3 Hz, C_6F_5), 133.29, 133.15, 132.28, 128.09, 125.46, 125.17, 112.73, 112.23, 110.19 (t, $^2J_{F\text{-}C}$ = 28.7 Hz, C_6F_5), 49.05 (N*C*H$_2$Ar), 40.06 (N*C*H$_2$Ar). **^{19}F NMR (DMSO- d_6, 376 MHz**): -140.22 (d, ^3J = 22.6 Hz, 4F, *ortho*-C_6F_5), -153.87 (t, ^3J = 22.7 Hz, 2F, *para*-C_6F_5), -161.61 (t, ^3J = 22.6 Hz, 4F, *meta*-C_6F_5). **ESI-MS (*m/z*) for [$C_{36}H_{20}Au_2F_{10}N_4Br$]$^+$:** calculated 1171.0037, found 1171.0048.

Synthesis of 1,1'-(di(naphthalen-2-ylmethyl))-3,3'-(1,2-xylylene)dibenzo[*d*]imidazol-2-ylidene digold(I) dibromide (2e)

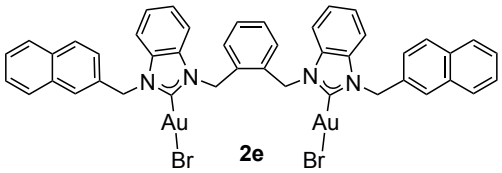

1e (233.7 mg, 0.30 mmol) afforded complex **2e** in 55 % yield (178.5 mg, R_f (DCM) = 0.3). **^{1}H NMR (DMSO- d_6, 600 MHz):** δ 8.03 (s, 2H), 7.95 (d, J = 8.5 Hz, 2H), 7.92 – 7.85 (m, 6H), 7.76 – 7.69 (m, 2H), 7.64 (d, ^3J = 8.4 Hz, 2H), 7.58 – 7.50 (m, 4H), 7.49 – 7.42 (m, 4H), 7.22 (dd, J = 5.5, 3.4 Hz, 2H), 6.71 – 6.65 (m, 2H), 6.21 (s, 4H, NCH_2Ar), 6.04 (s, 4H, NCH_2Ar). **^{13}C{^{1}H} NMR (DMSO- d_6, 151 MHz):** δ 181.81 (N*C*N), 133.37, 133.28, 133.06, 132.85, 132.68, 132.54, 128.71, 128.21, 127.83, 127.67, 126.67, 126.44, 125.59, 125.05, 124.97, 112.79, 112.74, 51.84 (N*C*H$_2$Ar), 48.64 (N*C*H$_2$Ar). Note that two carbons were not found, likely due to peak overlap. **ESI-MS (*m/z*) for [$C_{44}H_{34}Au_2N_4Br$]$^+$:** calculated 1091.1298, found 1091.1307.

Synthesis of 1,1'-(dibenzyl)-3,3'-(1,3-xylylene)dibenzo[*d*]imidazol-2-ylidene digold(I) dibromide (2f)

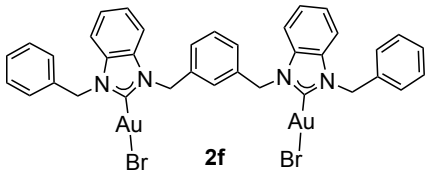

1f (203.4 mg, 0.30 mmol) afforded complex **2f** in 45 % yield (144.6 mg, 45 % yield). **^{1}H NMR (DMSO- d_6, 600 MHz):** δ 7.73 (d, ^3J = 8.2 Hz, 2H), 7.65 – 7.58 (m, 3H), 7.48 – 7.46 (m, 6H), 7.43 – 7.35 (m, 7H), 7.32 – 7.30 (m, 4H), 5.81 (s, 4H, NCH_2Ar), 5.74 (s, 4H, NCH_2Ar). **^{13}C{^{1}H} NMR (DMSO- d_6, 151 MHz):** δ 180.52 (N*C*N), 136.24, 135.68, 132.62, 132.50, 129.36, 128.81, 128.14, 127.34, 126.21, 124.69, 124.65, 112.63, 112.46, 51.63 (N*C*H$_2$Ar), 51.12 (N*C*H$_2$Ar). Note that one carbon was not found, likely due to peak overlap. **ESI-MS (*m/z*) for [$C_{36}H_{30}Au_2N_4Br$]$^+$:** calculated 991.0979, found 991.0976.

Synthesis of 1,1'-(di(naphthalen-2-ylmethyl))-3,3'-(1,4-xylylene)dibenzo[*d*]imidazol-2-ylidene digold(I) dibromide (2g)

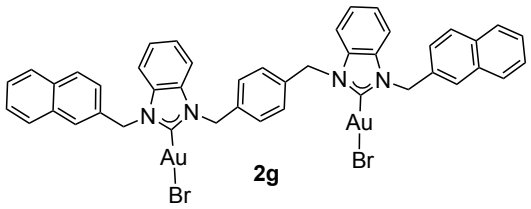

1g (233.4 mg, 0.30 mmol) afforded complex **2g** in 33 % yield (115.8 mg). **^{1}H NMR (DMSO- d_6, 600 MHz):** δ 7.96 (s, 2H), 7.92 – 7.87 (m, 4H), 7.87 – 7.84 (m, 2H), 7.78 – 7.76 (m, 2H), 7.75 – 7.70 (m, 2H), 7.56 (d, ^3J = 8.3 Hz, 2H), 7.54 – 7.50 (m, 4H), 7.47 (s, 4H), 7.38 (dd, J = 6.0, 3.1 Hz, 4H), 5.94 (s, 4H, NCH_2Ar), 5.79 (s, 4H, NCH_2Ar). **^{13}C NMR (DMSO- d_6, 151 MHz):** δ 180.76 (N*C*N), 135.73, 133.22, 132.81, 132.66, 132.64, 132.51, 128.64, 127.77, 127.64, 126.65, 126.44, 126.38, 124.96, 124.80, 112.66, 51.70 (N*C*H$_2$Ar), 51.07 (N*C*H$_2$Ar). Note that three carbons were not found, likely due to peak overlap. **ESI-MS (*m/z*) for [$C_{44}H_{34}Au_2N_4Br$]$^+$:** calculated 1091.1292, found 1091.1296.

2.3 Synthesis of $[Au_{13}(bisNHC)_5X_2]X_3$ clusters

General procedure for synthesis of gold nanoclusters $[3a\text{-}e]X_3$

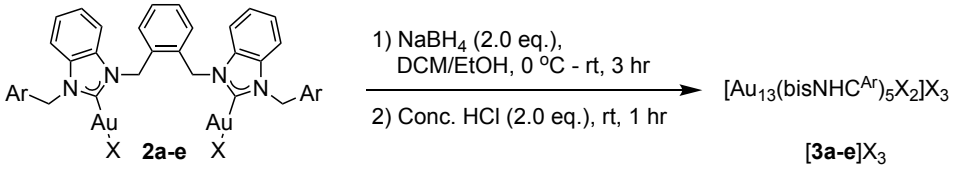

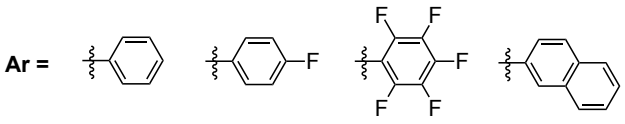

3a, X = Cl **3c**, X = Cl **3d**, X = Br **3e**, X = Br
3b, X = Br

The synthesis of gold nanoclusters $[\mathbf{3a\text{-}e}]X_3$ was adapted from previously published procedures.[13] In a 50 mL round bottom flask, the appropriate gold complex **2a-e** (ca. 40 mg, 0.04 mmol) was suspended in DCM/EtOH (2:1 v/v, 30 mL). The mixture was sonicated to form a homogenous suspension, then cooled to 0 °C in an ice bath. To the stirring solution was added a sonicated solution of sodium borohydride (3.0 mg, 0.08 mmol) in ethanol (99.5%, 10 mL). The mixture was stirred for 1 hour, then removed from the ice bath and stirred 2 hours at room temperature. Concentrated HCl (6.5 µL, 0.08 mmol) was added (see Figure S1 showing the positive effect of HCl treatment on cluster distribution), and the mixture was stirred for 1 hour at room temperature, then pumped to dryness *in vacuo*. The crude residue was extracted with EtOH (4 x 2 mL), and the supernatant solutions were filtered through celite, removing a beige to brown precipitate. The eluent from this filtration was dried *in vacuo* yielding the crude cluster mixture as a red-orange to dark red residue. The crude cluster mixtures were purified by silica gel column chromatography (Fuji Silysia Chromatorex PSQ60AB silica; 9:1 to 3:1 DCM/MeOH eluent; ~3x10 cm column size). The final red band on column yields the purified clusters $[\mathbf{3a\text{-}e}]X_3$ (cluster R_f (9:1 DCM/MeOH) = 0.3-0.4). See below for yields (based on Au) and characterization data.

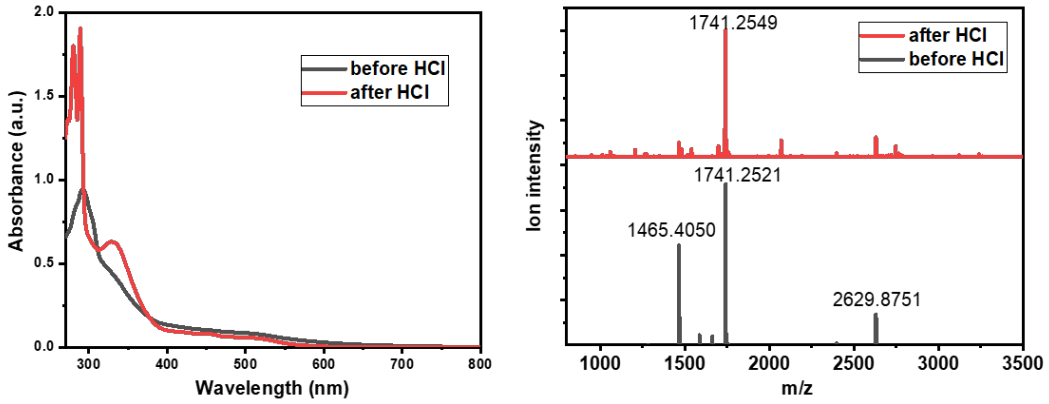

Figure S1. UV-vis spectrum (left) and ESI-MS (right) of crude **3a** cluster mixture before (red) and after (black) HCl treatment.

Synthesis of $[Au_{13}(bisNHC^{Ph})_5Cl_2]Cl_3$ ($[\mathbf{3a}]Cl_3$)

2a (78.5 mg, 0.08 mmol) afforded the desired nanocluster [**3a**]Cl_3 as a red solid in 43 % yield after column purification (28.1 mg). Red needle crystals of [**3a**]Cl_3 suitable for X-ray crystallography were grown from a solution of column purified cluster (13.4 mg) in DCM (~2 mL, 6 mg/mL) layered with hexanes (~2 mL) left capped at room temperature for one day. The crystals were washed with DCM-Hex (1:4 v/v; 3 x 1 mL), removing an orange powdery precipitate and pale orange supernatant solution, which were dried *in vacuo* (3.9 mg and 3.6 mg, respectively). Several crystals were reserved under DCM-Hex (1:4 v/v) for X-ray analysis. The remaining were dried *in vacuo* yielding dark red needles (3.4 mg, 25 % recovery). **^{1}H NMR (CD_2Cl_2, 600 MHz):** δ 7.88 (d, ^3J = 8.4 Hz, 5H), 7.55 (t, ^3J = 8.1 Hz, 5H), 7.47 (d, ^2J = 16.2 Hz, 5H, d-NCH_2Ar), 7.38 (d, ^3J = 7.8 Hz, 5H), 7.25 (t, ^3J = 8.1 Hz, 5H), 7.19 (d, ^2J = 16.2 Hz, 5H, b-NCH_2Ar), 7.17 (t, ^3J = 7.5 Hz, 5H), 7.07 (t, ^3J = 8.1 Hz, 5H), 7.01 (d, ^3J = 8.4 Hz, 5H), 7.00 (t, ^3J = 7.5 Hz, 5H), 6.95 (t, ^3J = 7.5 Hz, 5H), 6.88 (t, ^3J = 7.5 Hz, 5H), 6.87 (d, ^2J = 15.0 Hz, 5H, c-NCH_2Ar), 6.82 (d, ^3J = 7.2 Hz, 10H), 6.78 (d, ^2J = 13.8 Hz, 5H, a-NCH_2Ar), 6.71 (d, ^3J = 7.2 Hz, 10H), 6.52 (t, ^3J = 7.8 Hz, 10H), 6.50 – 6.46 (m, 15H), 6.42 (d, ^3J = 6.6 Hz, 5H), 6.15 (t, ^3J = 7.5 Hz, 5H), 6.13 (d, ^3J = 7.8 Hz, 5H), 5.40 (d, ^2J = 16.2 Hz, 5H, d-NCH_2Ar), 4.79 (d, ^2J = 15.0 Hz, 5H, c-NCH_2Ar), 4.53 (d, ^2J = 16.2 Hz, 5H, b-NCH_2Ar), 3.48 (d, ^2J = 13.8 Hz, 5H, a-NCH_2Ar). **UV-vis (DCM):** characteristic absorbances at 287, 325, 454, and 526 nm. **ESI-MS (*m/z*):** major peak $[Au_{13}(C_{36}H_{30}N_4)_5Cl_2]^{3+}$: calculated 1741.2477, found 1741.2606; minor peak $[Au_{13}(C_{36}H_{30}N_4)_5Cl_2]Cl^{2+}$: calculated 2629.8532, found 2629.8871. **Elemental analysis**: calculated (%) for $C_{180}H_{150}Au_{13}Cl_5N_{20}$: C, 40.55; H, 2.86; N, 5.25; found: C, 40.60; H, 3.30; N, 4.87.

Synthesis of $[Au_{13}(bisNHC^{Ph})_5Cl_2][PF_6]_3$ and $[Au_{13}(bisNHC^{Ph})_5Cl_2][CO_2CF_3]_3$ ($[\mathbf{3a}][PF_6]_3$ and $[\mathbf{3a}][CO_2CF_3]_3$)

Anion exchange of cluster [**3a**]Cl_3 was performed to isolate PF_6 as well as trifluoroacetate (CO_2CF_3) salts of the cluster for comparison by NMR spectroscopy. The general procedure for anion exchange is as follows. To a methanol (3 mL) solution of the cluster (5 mg, 9 x 10^{-4} mmol) was added an excess of the desired anion salt, either NH_4PF_6 or $Na(CO_2CF_3)$ (10 eq., 0.009 mmol). The solution was stirred for 1 hour, then dried *in vacuo*. The residue was dissolved in DCM and syringe filtered (<0.45 μm PTFE filter) to remove excess salts. The filtrate was dried *in vacuo* yielding the anion exchanged clusters [**3a**]$[PF_6]_3$ and [**3a**]$[CO_2CF_3]_3$ in 88 and 57 % yields, respectively. Some notable shift differences were observed in the ^{1}H NMR spectra of the clusters depending on the anion, especially for two of the NCH_2Ar proton peaks (see below and Figures S58-61).

$[\mathbf{3a}][PF_6]_3$: ^{1}H NMR (CD_2Cl_2, 600 MHz): δ 7.52 (d, ^2J = 16.1 Hz, 5H, d-NCH_2Ar), 7.21 (d, ^2J = 17.1 Hz, 5H, b-NCH_2Ar), 6.90 (d, ^2J = 14.6 Hz, 5H, c-NCH_2Ar), 6.78 (d, ^2J = 13.7 Hz, 5H, a-NCH_2Ar), 4.91 (d, ^2J = 16.2 Hz, 5H, d-NCH_2Ar), 4.49 (d, ^2J = 16.6 Hz, 5H, b-NCH_2Ar), 4.16 (d, ^2J = 14.7 Hz, 5H, c-NCH_2Ar), 3.48 (d, ^2J = 13.7 Hz, 5H, a-NCH_2Ar).

$[\mathbf{3a}][CO_2CF_3]_3$: ^{1}H NMR ($CD_2Cl_2$, 600 MHz): δ 7.52 (d, ^2J = 16.3 Hz, 5H, d-NCH_2Ar), 7.21 (d, ^2J = 15.9 Hz, 5H, b-NCH_2Ar), 6.86 (d, ^2J = 14.6 Hz, 5H, c-NCH_2Ar), 6.77 (d, ^2J = 13.7 Hz, 5H, a-NCH_2Ar), 5.18 (d, ^2J = 16.2 Hz, 5H, d-NCH_2Ar), 4.53 (d, ^2J = 16.1 Hz, 5H, b-NCH_2Ar), 4.50 (d, ^2J = 14.3 Hz, 5H, c-NCH_2Ar), 3.48 (d, ^2J = 13.7 Hz, 5H, a-NCH_2Ar).

Synthesis of [2-^{13}C]-labeled [Au_{13}(bisNHC^{Ph})$_5$$Cl_2$]$Cl_3$ (^{13}C-[3a]Cl_3)

^{13}**C-2a** (46.7 mg, 0.047 mmol) afforded the desired nanocluster ^{13}**C**-[**3a**]Cl_3 as a red solid in 49 % yield after column chromatography (19.1 mg). After purification, the cluster was washed with DCM-Hex (1:4 v/v; 3 x 1 mL) and pentane (3 x 1 mL) and dried *in vacuo* yielding a red powder (15.3 mg, 39 %). Note that the cluster still contained some gold complex impurities by NMR spectroscopy; therefore, a portion of the purified cluster (5.16 mg, 9.7 x 10^{-4} mmol) was anion exchanged to the PF_6 salt as described above, yielding ^{13}**C**-[**3a**][PF_6]$_3$ as a red solid (5.1 mg, 93 % yield). The PF_6 salt was crystallized by dissolving the residue in DCM (~1 mL) and adding hexanes until a precipitate formed (~1 mL). The precipitate was redissolved by adding DCM dropwise, then the vial was capped and left at room temperature for 3 days, after which red needles had formed. The crystals were washed with DCM/Hexanes (1:4 v/v; 2 x 1 mL), then pentane (2 x 1 mL) before being dried *in vacuo* for several hours (1.8 mg, 35 % crystal yield). **^{13}C-[3a]Cl_3: ^{1}H NMR (CD_2Cl_2, 600 MHz):** δ 7.87 (m, 5H), 7.56 (t, ^3J = 7.7 Hz, 5H), 7.49 – 7.37 (m, 10H), 7.27 – 7.17 (m, 15H), 7.09 – 6.93 (m, 20H), 6.89 – 6.76 (m, 25H), 6.71 (d, ^3J = 7.4 Hz, 10H), 6.53 – 6.46 (m, 25H), 6.40 (d, ^3J = 7.4 Hz, 5H), 6.16 – 6.11 (m, 10H), 5.37 (dd, $^2J_{H\text{-}H}$ = 16.1 Hz, $^3J_{C\text{-}H}$ = 6.4 Hz, 5H, d-NCH_2Ar), 4.74 (dd, $^2J_{H\text{-}H}$ = 14.9 Hz, $^3J_{C\text{-}H}$ = 2.9 Hz, 5H, c-NCH_2Ar), 4.52 (dd, $^2J_{H\text{-}H}$ = 16.4 Hz, $^3J_{C\text{-}H}$ = 3.3 Hz, 5H, b-NCH_2Ar), 3.48 (dd, $^2J_{H\text{-}H}$ = 13.9 Hz, $^3J_{C\text{-}H}$ = 4.3 Hz, 5H, a-NCH_2Ar).

^{13}C{^{1}H} NMR (CD_2Cl_2, 151 MHz): δ 207.51 (d, J = 9.7 Hz, carbene), 207.05 (d, J = 7.6 Hz, unknown), 206.61 (d, J = 9.8 Hz, carbene), 206.06 (d, J = 9.9 Hz, unknown). **ESI-MS (*m/z*):** major peak [Au_{13}($^{13}C_2C_{34}H_{30}N_4$)$_5Cl_2$]$^{3+}$: calculated 1744.5923, found 1744.5972. **^{13}C-[3a][PF_6]$_3$: ^{1}H NMR (CD_2Cl_2, 600 MHz):** δ 7.70 (d, ^3J = 8.4 Hz, 5H), 7.58 (t, ^3J = 7.3 Hz, 5H), 7.52 (dd, $^2J_{H\text{-}H}$ = 16.0 Hz, $^3J_{C\text{-}H}$ = 4.6 Hz, 5H, d-NCH_2Ar), 7.38 (d, ^3J = 8.2 Hz, 5H), 7.30 (t, ^3J = 7.3 Hz, 5H), 7.23 (t, ^3J = 7.6 Hz, 5H), 7.20 (dd, $^2J_{H\text{-}H}$ = 15.4 Hz, $^3J_{C\text{-}H}$ = 4.6 Hz, 5H, b-NCH_2Ar), 7.11 (t, ^3J = 7.3 Hz, 5H), 7.03 – 6.97 (m, 10H), 6.95 – 6.92 (m, 10H), 6.89 (dd, $^2J_{H\text{-}H}$ = 14.7 Hz, $^3J_{C\text{-}H}$ = 4.7 Hz, 5H, c-NCH_2Ar), 6.77 (d, $^2J_{H\text{-}H}$ = 13.7 Hz, $^3J_{C\text{-}H}$ = 4.8 Hz, 5H, a-NCH_2Ar), 6.74 – 6.64 (m, 20H), 6.54 – 6.47 (m 25H), 6.20 (t, ^3J = 7.4 Hz, 5H), 6.14 (d, ^3J = 8.7 Hz, 10H), 4.90 (d, $^2J_{H\text{-}H}$ = 16.1 Hz, $^3J_{C\text{-}H}$ = 6.5 Hz, 5H, d-NCH_2Ar), 4.49 (d, $^2J_{H\text{-}H}$ = 16.6 Hz, $^3J_{C\text{-}H}$ = 3.5 Hz, 5H, b-NCH_2Ar), 4.16 (d, $^2J_{H\text{-}H}$ = 14.8 Hz, $^3J_{C\text{-}H}$ = 2.8 Hz, 5H, c-NCH_2Ar), 3.48 (d, $^2J_{H\text{-}H}$ = 13.6 Hz, $^3J_{C\text{-}H}$ = 4.4 Hz, 5H, a-NCH_2Ar). **^{13}C{^{1}H} NMR (CD_2Cl_2, 151 MHz):** δ 207.51 (d, J = 9.6 Hz, carbene), 207.03 (d, J = 8.8 Hz, unknown), 206.55 (d, J = 9.9 Hz, carbene), 205.98 (d, J = 10.0 Hz, unknown).

Synthesis of $[Au_{13}(bisNHC^{Ph})_5Br_2]Br_3$ ($[\mathbf{3b}]Br_3$)

2b (41.7 mg, 0.04 mmol) afforded nanocluster [**3b**]Br_3 as a red solid in 27 % yield after column chromatography (9.1 mg). The cluster was crystallized by dissolving the residue in DCM (~1 mL) and adding hexanes until a precipitate formed (~2 mL). The precipitate was redissolved by adding DCM dropwise, then the vial was capped and left at room temperature for 3 days, after which small red needles had formed. The crystals were washed with hexanes (2 x 0.5 mL) before being dried *in vacuo* for several hours (4.1 mg, 12 % crystal yield). **^{1}H NMR (CD_2Cl_2, 600 MHz):** δ 7.91 (d, ^3J = 8.4 Hz, 5H), 7.55 (t, ^3J = 7.8 Hz, 5H), 7.44 (d, ^2J = 16.1 Hz, 5H, d-NCH_2Ar), 7.40 (d, ^3J = 8.0 Hz, 5H), 7.24 (t, ^3J = 8.0 Hz, 5H), 7.20 (d, ^2J = 16.6 Hz, 5H, b-NCH_2Ar), 7.18 (t, ^3J = 7.8 Hz, 5H), 7.08 (t, ^3J = 7.6 Hz, 5H), 7.02 (t, ^3J = 7.5 Hz, 5H), 7.01 (d, ^3J = 8.3 Hz, 5H), 6.96 (t, ^3J = 8.1 Hz, 5H), 6.89 (d, ^2J = 15.0 Hz, 5H, c-NCH_2Ar), 6.86 – 6.84 (m, 15H), 6.78 (d, ^2J = 13.8 Hz, 5H, a-NCH_2Ar), 6.63 (d, ^3J = 7.4 Hz, 10H), 6.53 (t, ^3J = 7.7 Hz, 20H), 6.43 (d, ^3J = 7.5 Hz, 5H), 6.40 (d, ^3J = 8.4 Hz, 5H), 6.16 – 6.12 (m, 10H), 5.40 (d, ^2J = 16.2 Hz, 5H, d-NCH_2Ar), 4.77 (d, ^2J = 14.7 Hz, 5H, c-NCH_2Ar), 4.57 (d, ^2J = 16.6 Hz, 5H, b-NCH_2Ar), 3.47 (d, ^2J = 13.8 Hz, 5H, a-NCH_2Ar).. **UV-vis (DCM):** characteristic absorbances at 318, 338, 407, 455, and 516 nm. **ESI-MS (*m/z*):** major peak $[Au_{13}(C_{36}H_{30}N_4)_5Br_2]^{3+}$: calculated 1771.2134, found 1771.2202; minor peak $[Au_{13}(C_{36}H_{30}N_4)_5Br_2]Br^{2+}$: calculated 2696.7768, found 2696.7931.

Synthesis of $[Au_{13}(bisNHC^{Ar})_5Cl_2]Cl_3$ (Ar = 4-fluorophenyl, $[\mathbf{3c}]Cl_3$)

2c (40.7 mg, 0.04 mmol) afforded nanocluster [**3c**]Cl_3 as a red powder in 22 % yield after column chromatography (7.6 mg). **^{1}H NMR (CD_2Cl_2, 600 MHz):** δ 7.93 (d, ^3J = 8.2 Hz, 5H), 7.56 (t, ^3J = 7.7 Hz, 5H), 7.45 (d, ^2J = 16.3 Hz, 5H, d-NCH_2Ar), 7.36 (d, ^3J = 7.8 Hz, 5H), 7.28 (t, ^3J = 7.8 Hz, 5H), 7.19 – 7.09 (m, 20H, ArH + b-NCH_2Ar), 7.01 – 6.97 (m, 5H), 6.90 – 6.81 (m, 20H, ArH + c-NCH_2Ar), 6.78 – 6.75 (m, 10H), 6.67 (d, ^2J = 13.8 Hz, 5H, a-NCH_2Ar), 6.50 (d, ^3J = 7.2 Hz, 5H), 6.46 (d, ^3J = 8.3 Hz, 5H), 6.30 – 6.23 (m, 20H), 6.14 (d, ^3J = 8.2 Hz, 5H), 5.62 (d, ^2J = 16.3 Hz, 5H, d-NCH_2Ar), 5.05 (d, ^2J = 14.7 Hz, 5H, c-NCH_2Ar), 4.53 (d, ^2J = 16.4 Hz, 5H, b-NCH_2Ar), 3.43 (d, ^2J = 14.0 Hz, 5H, a-NCH_2Ar).

^{19}F NMR (**DMSO-d6, 376 MHz**): δ -111.47 (s, 5F), -112.65 (s, 5F). **UV-vis (DCM):** characteristic absorbances at 292, 326, 409, 455, and 516 nm. **ESI-MS (*m/z*):** major peak $[Au_{13}(C_{36}H_{28}N_4F_2)_5Cl_2]^{3+}$: calculated 1801.2163, found 1801.2099; minor peak $[Au_{13}(C_{36}H_{28}N_4F_2)_5Cl_2]Cl^{2+}$: calculated 2719.8061, found 2719.8191. **Elemental analysis**: calculated (%) for $C_{180}H_{140}Au_{13}Cl_5F_{10}N_{20}$: C, 39.23; H, 2.56; N, 5.08; found: C, 38.93; H, 2.90; N, 4.68.

Synthesis of $[Au_{13}(bisNHC^{Ar})_5Br_2]Br_3$ (Ar = pentafluorophenyl, [3d]Br_3)

2d (45.0 mg, 0.04 mmol) afforded nanocluster [**3d**]Br_3 **as a red solid** in 25 % yield after column chromatography (10.0 mg). **^{1}H NMR (CD_2Cl_2, 600 MHz):** δ 7.78 (d, ^3J = 8.4 Hz, 5H), 7.62 (t, ^3J = 7.5 Hz, 5H), 7.58 (d, ^2J = 16.5 Hz, c-NCH_2Ar), 7.39 (t, ^3J = 7.5 Hz, 5H), 7.25 (d, ^3J = 7.9 Hz, 5H), 7.21 (t, ^3J = 7.9 Hz, 5H), 7.19 – 7.17 (m, 10H), 6.91 (t, ^3J = 7.4 Hz, 5H), 6.79 (d, ^2J = 14.7 Hz, 5H, b-NCH_2Ar), 6.65 (d, ^3J = 6.6 Hz, 5H), 6.59 (d, ^2J = 14.7 Hz, 5H, a-NCH_2Ar), 6.39 (d, ^2J = 15.7 Hz, 5H, d-NCH_2Ar), 6.32 (d, ^3J = 8.4 Hz, 5H), 6.19 (d, ^3J = 7.4 Hz, 5H), 5.74 (d, ^2J = 15.8 Hz, 5H, d-NCH_2Ar), 5.46 (d, ^2J = 16.5 Hz, 5H, c-NCH_2Ar), 5.22 (d, ^2J = 14.8 Hz, 5H, b-NCH_2Ar), 3.94 (d, ^2J = 14.7 Hz, 5H, a-NCH_2Ar). **^{19}F NMR (DMSO- d_6 376 MHz)**: -141.07 (br m, 15F, *ortho*-C_6F_5), -143.20 (br m, 5F, *ortho*-C_6F_5), -151.16 (t, ^3J = 22.3 Hz, 5F, *para*-C_6F_5), -152.23 (t, ^3J = 20.5 Hz, 5F, *para*-C_6F_5), -160.05 (br m, 10F, *meta*-C_6F_5), -162.39 (br m, 10F, *meta*-C_6F_5). **UV-vis (DCM):** characteristic absorbances at 281, 292, 325, 446, and 517 nm. **ESI-MS (*m/z*):** major peak $[Au_{13}(C_{36}H_{20}N_4F_{10})_5Br_2]^{3+}$: calculated 2071.0564, found 2071.0750; minor peak $[Au_{13}(C_{36}H_{20}N_4F_{10})_5Br_2]Br^{2+}$: calculated 3146.5413, found 3146.5816.

Synthesis of $[Au_{13}(bisNHC^{Ar})_5Br_2]Br_3$ (Ar = 2-naphthyl, [3e]Br_3)

2e (46.6 mg, 0.04 mmol) afforded nanocluster [**3e**]Br_3 as a red solid in 30 % yield after column chromatography (11.2 mg). **^{1}H NMR (CD_2Cl_2, 600 MHz):** δ 7.97 (d, ^3J = 8.3 Hz, 5H), 7.71 (d, ^2J = 16.0 Hz, 5H, d-NCH_2Ar), 7.61 (d, ^3J = 7.8 Hz, 5H), 7.57 (t, ^3J = 7.7 Hz, 5H), 7.46 (d, ^2J = 16.9 Hz, 5H, c-NCH_2Ar), 7.42 (d, ^3J = 8.1 Hz, 5H), 7.32 – 7.16 (m, 45H), 7.07 (d, ^3J = 8.1 Hz, 5H), 6.97 (d, ^2J = 13.5 Hz, 5H, a-NCH_2Ar), 6.93 – 6.90 (m, 10H, ArH + b-NCH_2Ar), 6.82 – 6.71 (m, 30H), 6.58 (d, ^3J = 8.5 Hz, 5H), 6.50 (d, ^3J = 7.3 Hz, 5H), 6.42 (t, ^3J = 7.9 Hz, 5H), 5.69 (d, ^3J = 8.3 Hz, 5H), 5.63 (d, ^3J = 8.4 Hz, 5H), 5.57 (d, ^2J = 16.0 Hz, d-NCH_2Ar), 5.02 (d, ^2J = 16.7 Hz, c-NCH_2Ar), 4.86 (d, ^2J = 14.4 Hz, b-NCH_2Ar), 3.71 (d, ^2J = 13.6 Hz, a-NCH_2Ar). **UV-vis (DCM):** characteristic absorbances at 287, 320, 343, 410, 457, 517 nm. **ESI-MS (*m/z*):** major peak $[Au_{13}(C_{44}H_{34}N_4)_5Br_2]^{3+}$: calculated 1937.5978, found 1937.9344; minor peak $[Au_{13}(C_{44}H_{34}N_4)_5Br_2]Br^{2+}$: calculated 2947.3567, found 2946.8617.

Reduction of complexes 2f and 2g

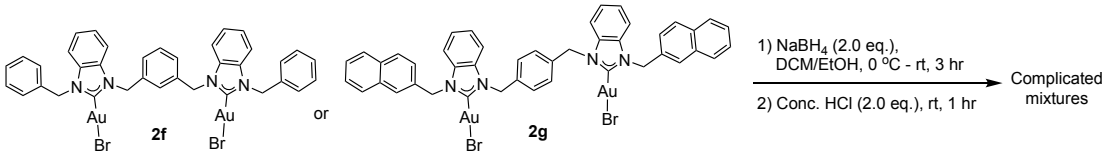

Complexes **2f** and **2g** were reduced with sodium borohydride using the general method described above. The crude cluster mixtures were characterized by ESI-MS and showed only complicated mixtures of smaller gold complexes and some trace unidentifiable clusters, with no Au_{13} clusters present (see Figure S2). Attempts to purify the crude clusters by column chromatography yielded only mixtures, therefore further attempts at cluster synthesis using complexes **2f** and **2g** were not pursued.

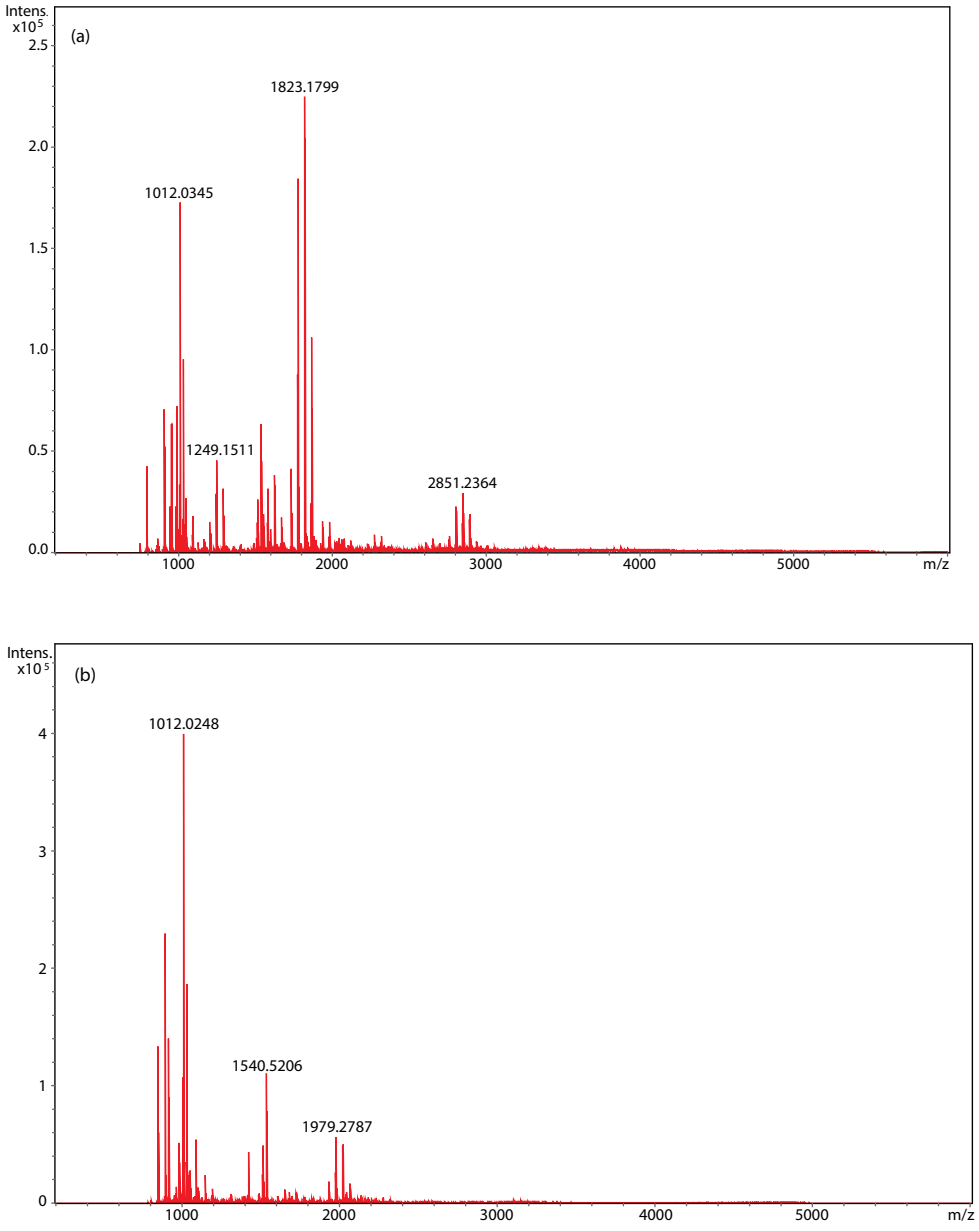

Figure S2. ESI-MS of the crude mixtures from the reduction of (a) **2g** and (b) **2h** under standard conditions.

2.4 Chiral separation and cluster stability tests

Experimental procedure for large scale separation of racemic 3a by chiral HPLC

Cluster [**3a**]Cl_3 (5.0 mg) was dissolved in 1.0 mL MeOH. Chromatographic separation of the cluster enantiomers was then carried out on a Shimadzu LC-2010CHT HPLC system equipped with a Diacel CHIRALPAK IE-3 column (5µm, 250 mm×10.0 mm) by direct injection of this solution. MeOH/TFA/DEA (1:0.1:0.1 volume ratio) was used as eluent with a flow rate of 2.0 mL/min. Once the first cluster peak started to elute, the column eluent was collected into a 50 mL vial. Due to partial peak overlap of the two enantiomers, the intermediate fractions at the tail end of the first enantiomer peak and the beginning of the second enantiomer peak were not collected in order to avoid significant mixing of the two enantiomers. The remainder of second enantiomer was then collected into a 50 mL vial. After separation, the solvents were removed *in vacuo*. To remove excess acid and amine impurities, the residues were dissolved in DCM and washed with water until the extracted aqueous phase was a neutral pH. The organic phase was then dried *in vacuo* to yield the cluster enantiomers as red residues (enantiomer 1: 2.0 mg; enantiomer 2: 1.5 mg). Each fraction was then re-evaluated by chiral HPLC to check the enantiomeric excess of the isolated fractions, as well as characterized by UV-vis spectroscopy (Figure S3). ESI-MS and NMR spectroscopic data indicated partial anion exchange to the trifluoroacetate species [**3a**][CO_2CF_3]$_3$ had most likely taken place, therefore each enantiomer was anion exchanged to the PF_6 salt via the method described previously, which resulted in identical ^{1}H NMR spectroscopic peaks for each cluster enantiomer, which were consistent with independently prepared and isolated [**3a**][PF_6]$_3$ (see Figures S4-5). We have checked the separation of **3c-3e** by chiral HPLC under the same conditions as **3a**. Au_{13} nanoclusters **3c** and **3d** can be separated, while 3e can't be separated (Figure S6).

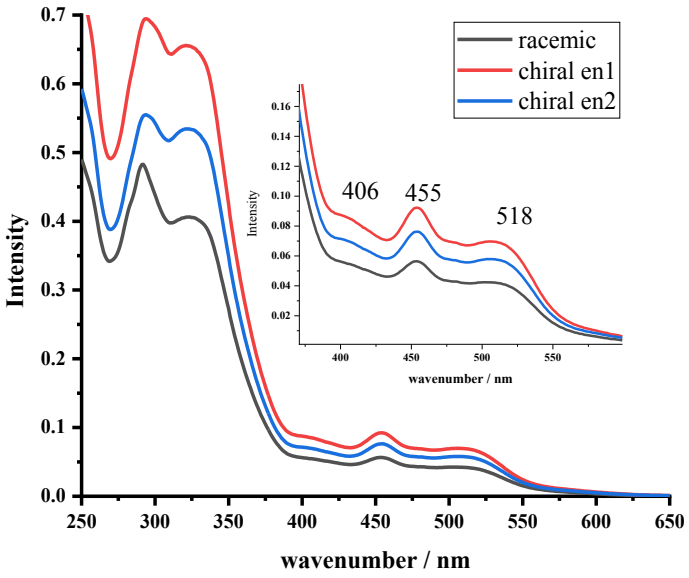

Figure S3. UV-vis spectra (DCM) of the two cluster fractions isolated by chiral HPLC separation of racemic [**3a**]Cl_3.

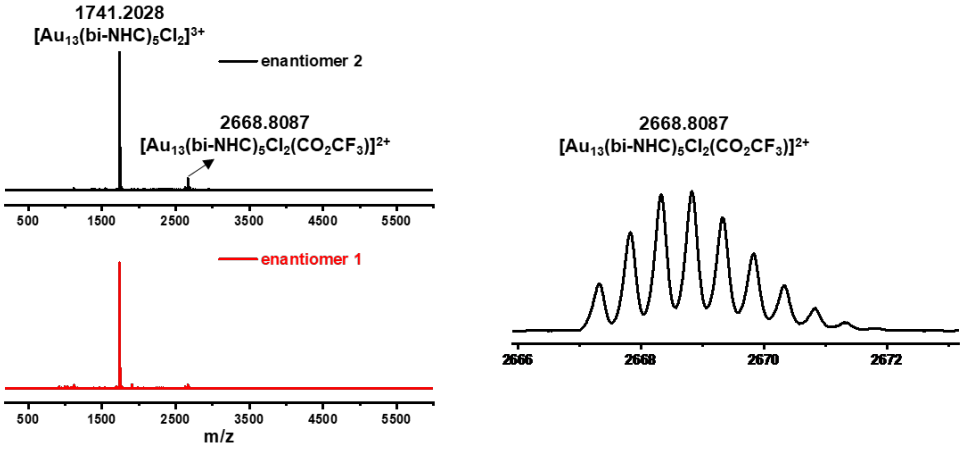

Figure S4. ESI-MS spectra of the two cluster fractions isolated by chiral HPLC separation of racemic [**3a**]Cl_3.

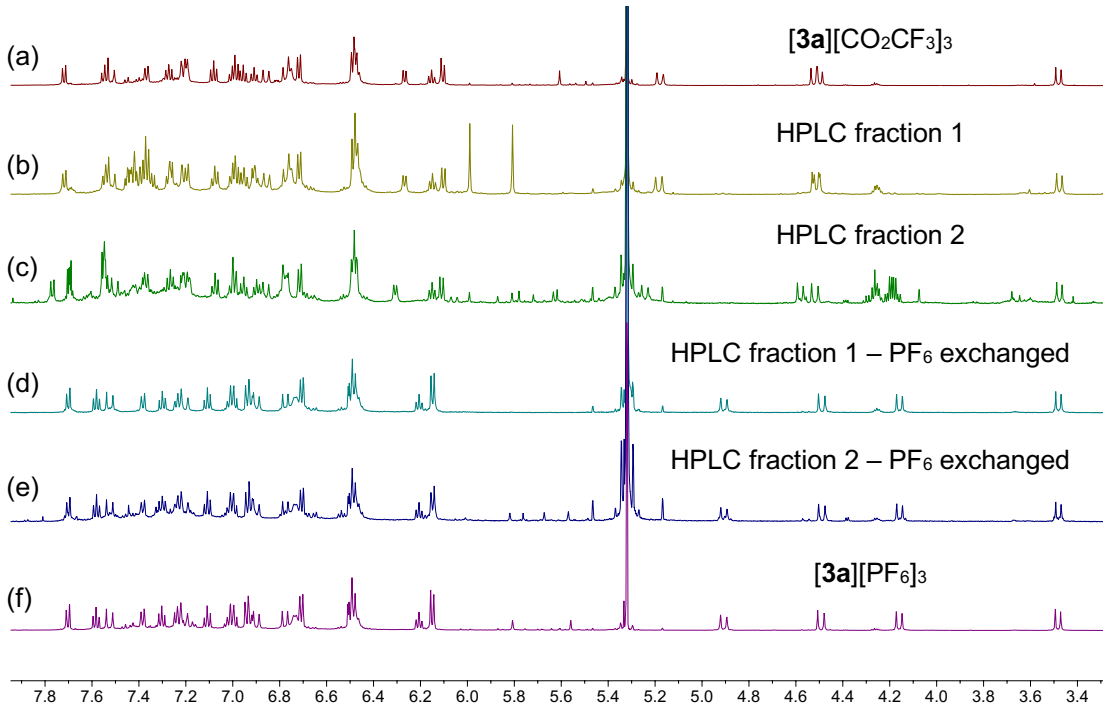

Figure S5. ^{1}H NMR (CD_2Cl_2, 600 MHz) spectra of (a) independently isolated [**3a**][CO_2CF_3]$_3$, (b) first cluster enantiomer fraction isolated by chiral HPLC separation of racemic [**3a**]Cl_3, (c) second cluster enantiomer fraction isolated by chiral HPLC separation of racemic [**3a**]Cl_3, (d) first cluster enantiomer fraction exchanged to [**3a**][PF_6]$_3$, (c) second cluster enantiomer fraction enantiomer fraction exchanged to [**3a**][PF_6]$_3$, and (d) independently isolated [**3a**][PF_6]$_3$.

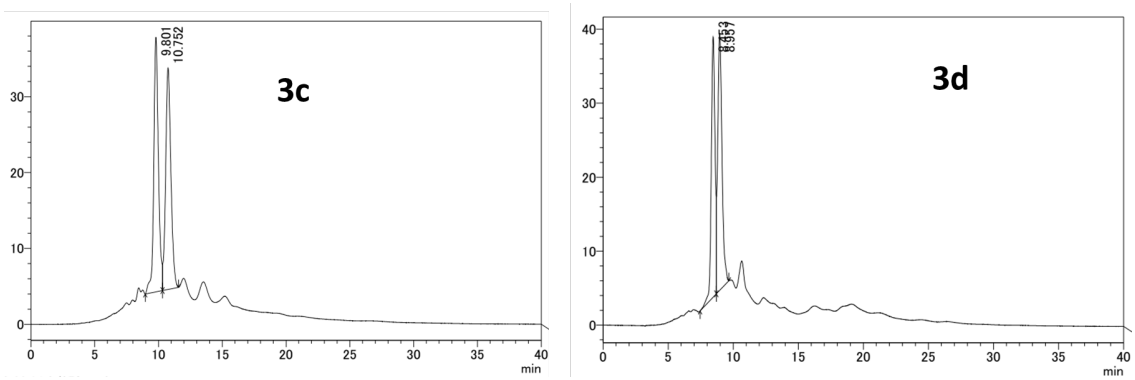

Figure S6. Enantioseparation of **3c** and **3d** could be affected under the same conditions employed for **3a**, however cluster **3e** could not be resolved under these conditions.

Thermal stability of cluster 3a

Cluster [**3a**]Cl_3 (0.3 mg) was dissolved in acetonitrile (3.0 mL). The sample was then transferred into a 1 cm^2 quartz cuvette fitted with a sealable screw cap top. The sample was heated at 60 ^oC in an oil bath, and changes to the UV-vis spectrum were monitored over time. The UV-vis spectrum showed no discernible changes over 3 days of heating (see Figure 6A in manuscript). The emission spectra of Cluster [**3a**]Cl_3 for 3 days at 60 ^oC in MeCN solution are checked. No obvious change of emission spectra was observed after 3 days (Figure S7).

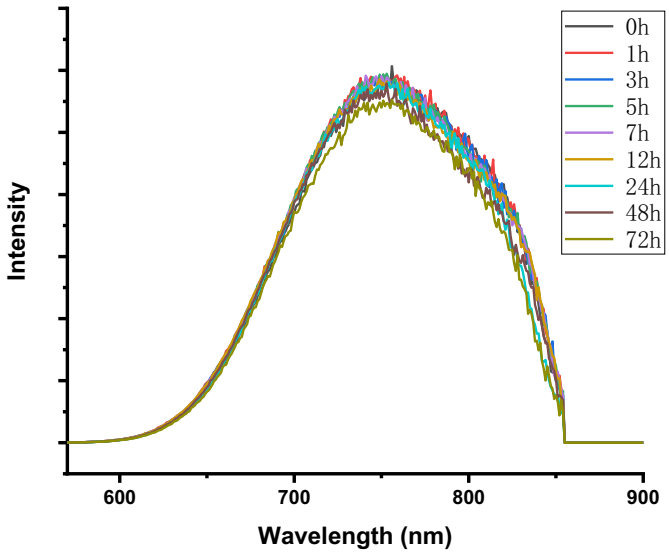

Figure S7. Emission spectra of Cluster [**3a**]Cl_3 for 3 days at 60 ^oC in MeCN

Chiral stability of cluster 3a under thermal treatment

The isolated enantiomer 1 (1.2 mg, 88 % ee) from chiral HPLC separation of racemic [**3a**]Cl_3 was dissolved in MeOH (3.0 mL). The sample was transferred to three separate glass reaction tubes (1.0 mL each) and the tubes were sealed with Teflon lined caps. The three solutions were then heated for 1 hour at 60 ^oC, 80 ^oC and 100 ^oC, after which they were cooled and the cluster

enantiomeric excess was measured again by chiral HPLC (see Figure S8). Note that the samples heated at 80 ºC and 100 ºC were run with a fresh eluent batch, and therefore had slightly higher retention times. The CD spectrum of **3a-en1** after 100 ºC was also measured (Figure S9). We re-confirmed the assignment of the enantiomer retention times by independently running a sample of racemic [**3a**]Cl_3 using the new eluent.

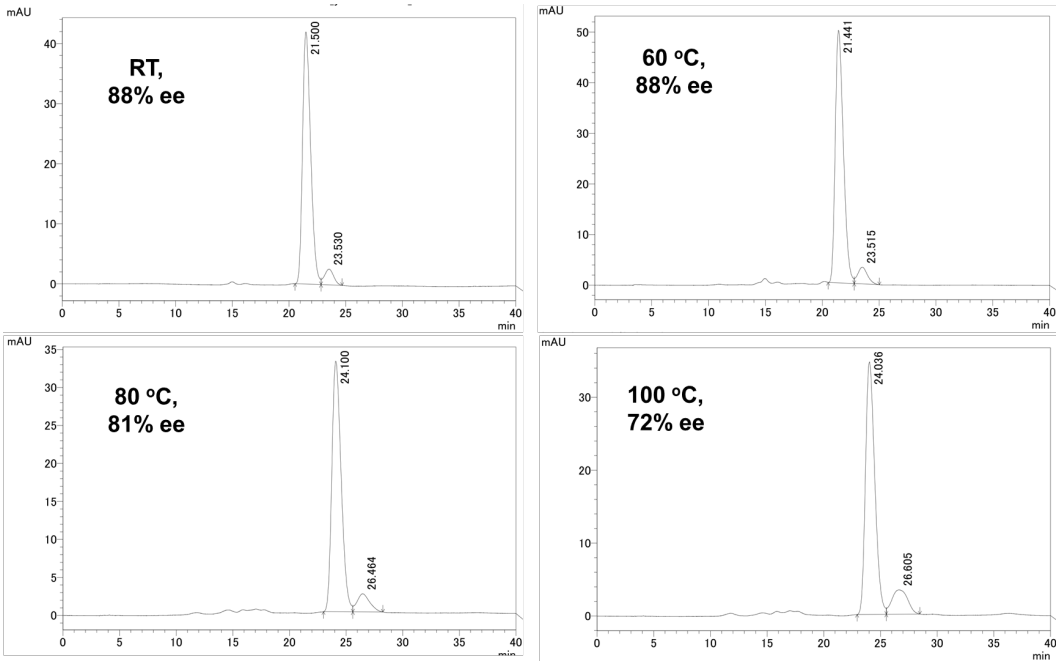

Figure S8. HPLC chromatograms for enantiomer 1 isolated from chiral HPLC of racemic [**3a**]Cl_3 (a) prior to heating (88% ee) and after 1 hour of heating at (b) 60 ºC (88 % ee), (c) 80 ºC (81% ee), and (d) 100 ºC (72% ee).

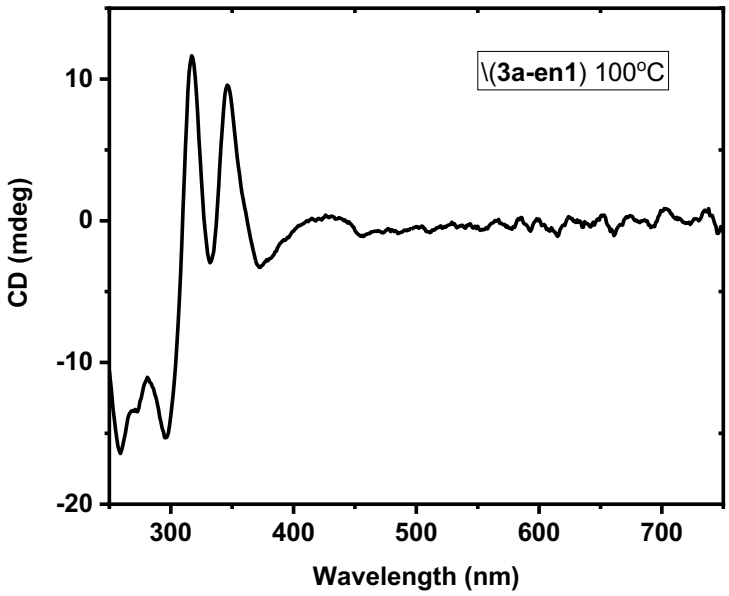

Figure S9. CD spectrum of **3a-en1** after heating at 100 ºC for 1h.

3 Characterization data

3.1 UV-vis, fluorescence and ESI mass spectra of clusters

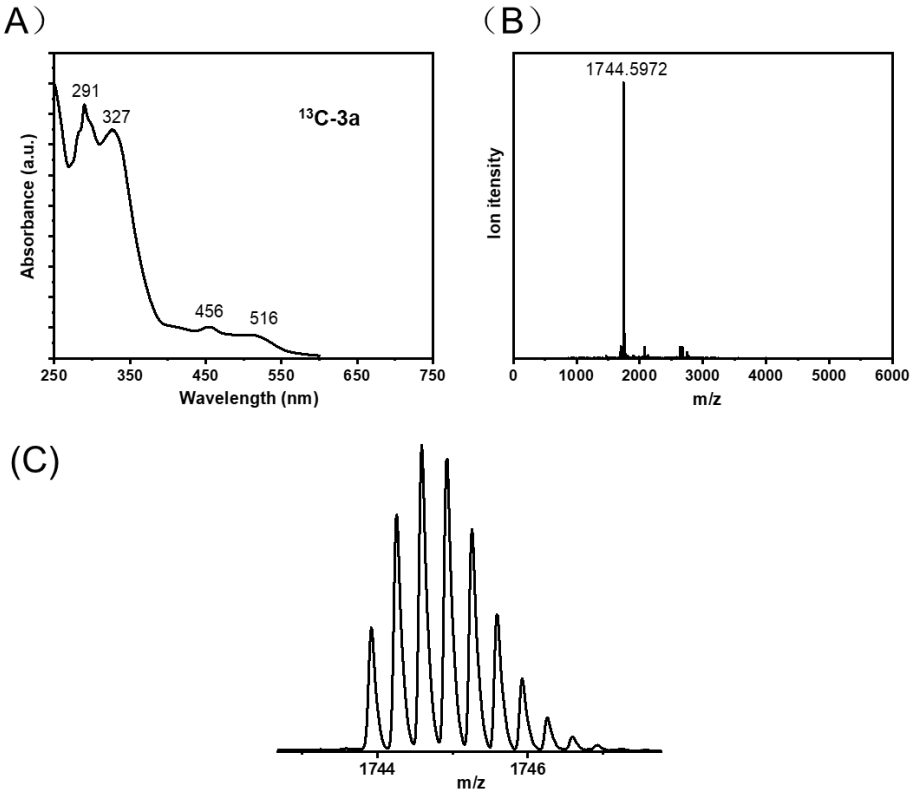

Figure S10. (A) UV-vis spectrum of cluster ^{13}**C**-[**3a**]Cl_3 in DCM, (B) ESI-MS of ^{13}**C**-[**3a**][Cl_3 and (C) expansions of the cluster peak in the ESI-MS showing the major $[Au_{13}(^{13}C_2C_{34}H_{30}N_4)_5Cl_2]^{3+}$ peak. A signal due to $[Au_{13}(^{13}C_2C_{34}H_{30}N_4)_5Cl_2]Cl^{2+}$ was not observed.

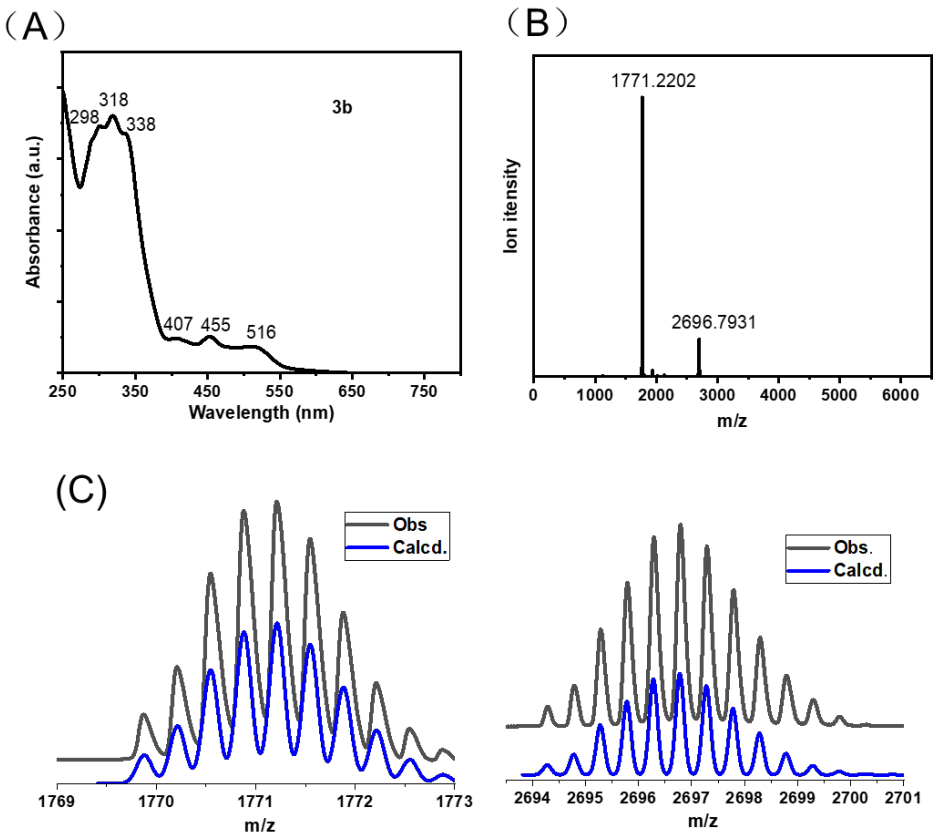

Figure S11. (A) UV-vis spectrum of cluster [**3b**]Br_3 in DCM, (B) ESI-MS of [**3b**]Br_3 and (C) expansions of the cluster peaks in the ESI-MS showing the major $[Au_{13}(C_{36}H_{30}N_4)_5Br_2]^{3+}$ (left) and minor $[Au_{13}(C_{36}H_{30}N_4)_5Br_2]Br^{2+}$ (right) peaks (black) overlayed with their simulated isotope patterns (blue).

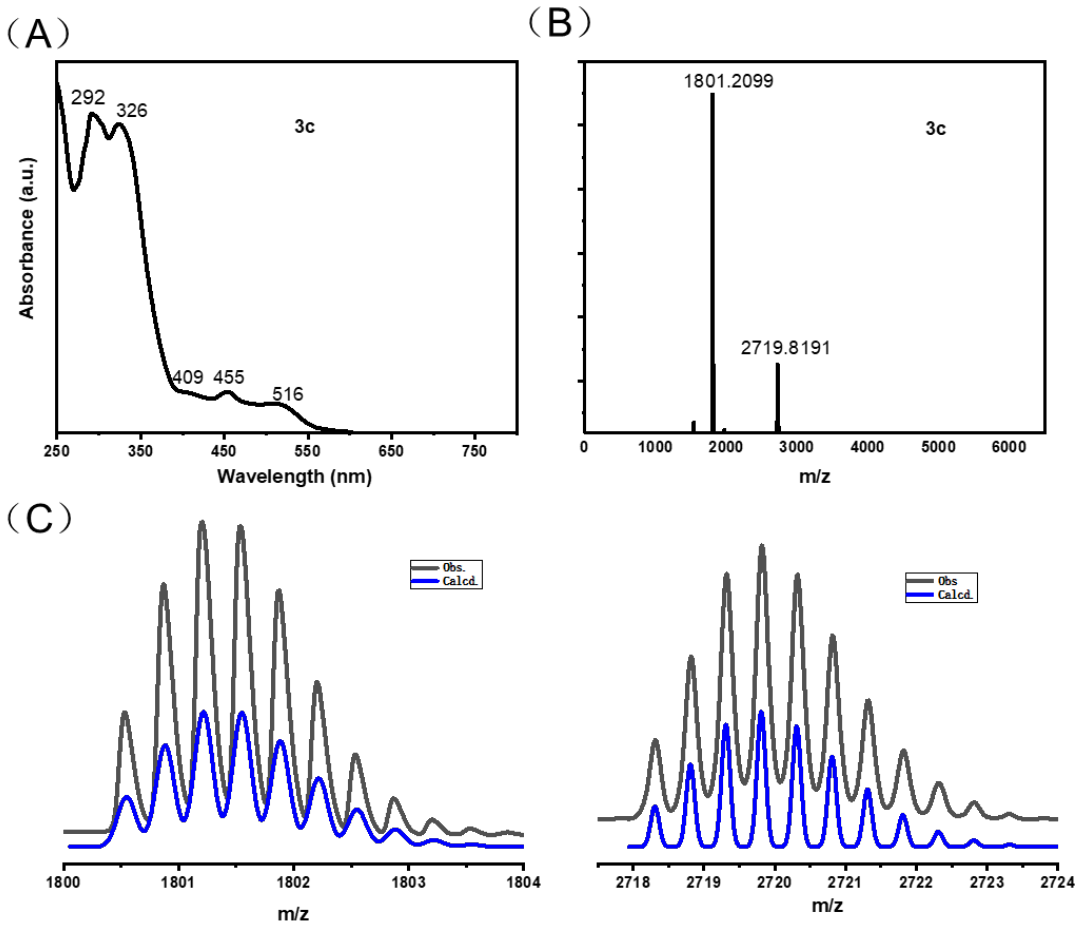

Figure S12. (A) UV-vis spectrum of cluster [**3c**]Cl_3 in DCM, (B) ESI-MS of [**3c**]Cl_3 and (C) expansions of the cluster peaks in the ESI-MS showing the major $[Au_{13}(C_{36}H_{28}N_4F_2)_5Cl_2]^{3+}$ (left) and minor $[Au_{13}(C_{36}H_{28}N_4F_2)_5Cl_2]Cl^{2+}$ (right) peaks (black) overlayed with their simulated isotope patterns (blue).

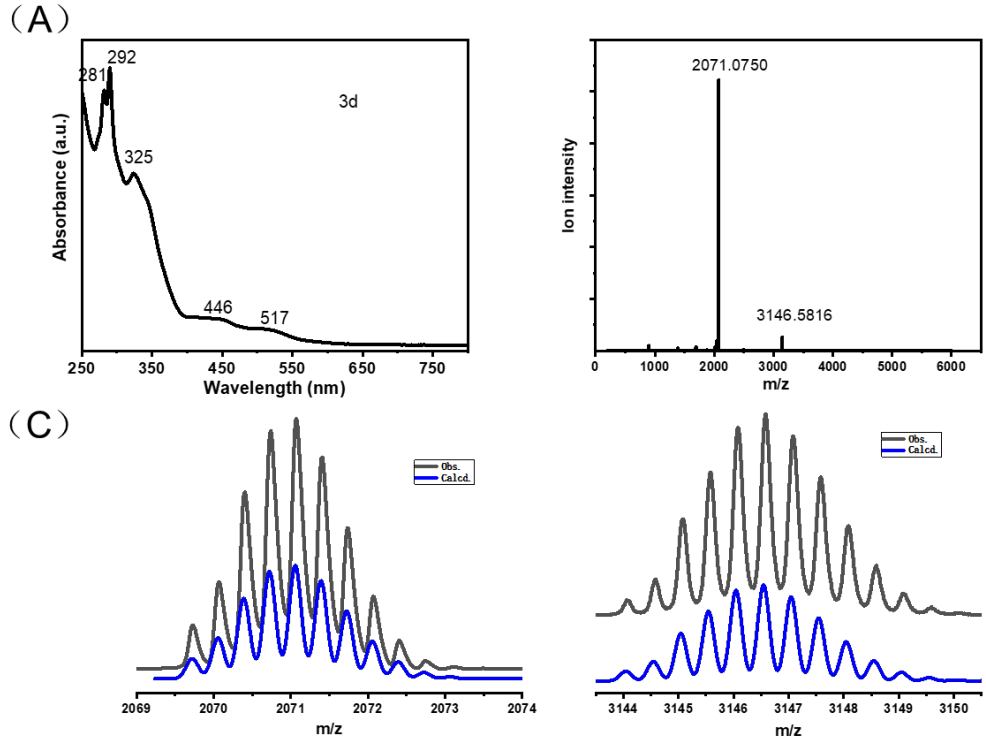

Figure S13. (A) UV-vis spectrum of cluster [**3d**]Br_3 in DCM, (B) ESI-MS of [**3d**]Br_3 and (C) expansions of the cluster peaks in the ESI-MS showing the major $[Au_{13}(C_{36}H_{20}N_4F_{20})_5Cl_2]^{3+}$ (left) and minor $[Au_{13}(C_{36}H_{20}N_4F_{20})_5Br_2]Br^{2+}$ (right) peaks (black) overlayed with their simulated isotope patterns (blue).

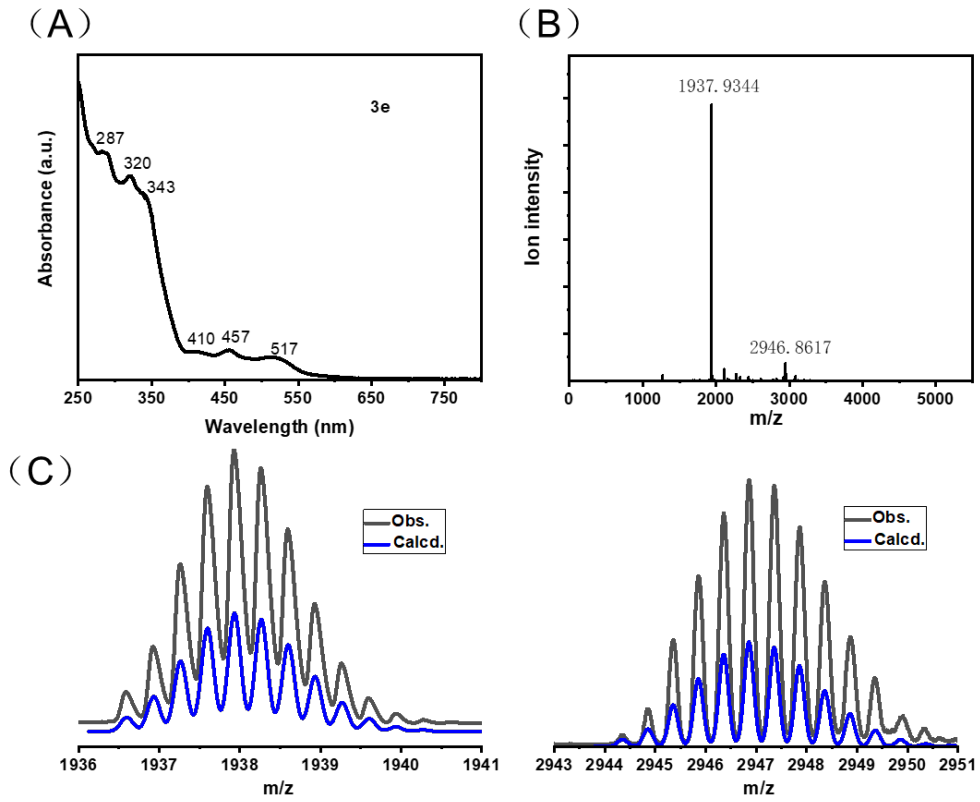

Figure S14. (A) UV-vis spectrum of cluster [**3e**]Br_3 in DCM, (B) ESI-MS of [**3e**]Br_3 and (C) expansions of the cluster peaks in the ESI-MS showing the major $[Au_{13}(C_{44}H_{34}N_4)_5Br_2]^{3+}$ (left) and minor $[Au_{13}(C_{44}H_{34}N_4)_5Br_2]Br^{2+}$ (right) peaks (black) overlayed with their simulated isotope patterns (blue).

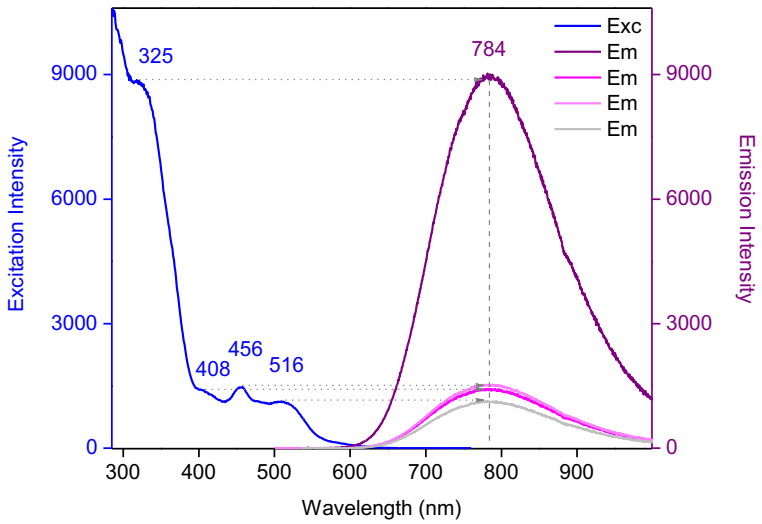

Figure S15. Excitation and fluorescence emission spectra of [**3a**]Cl_3. Excitation monitored the emission at 784 nm; emission was excited at λ_{max} of excitation bands. Spectra were recorded using excitation band pass 5 nm, emission band pass 5 nm, integration time 0.5 s, and detector accumulation 1. The emission profile and its maximum were the same for all examined excitation wavelengths.

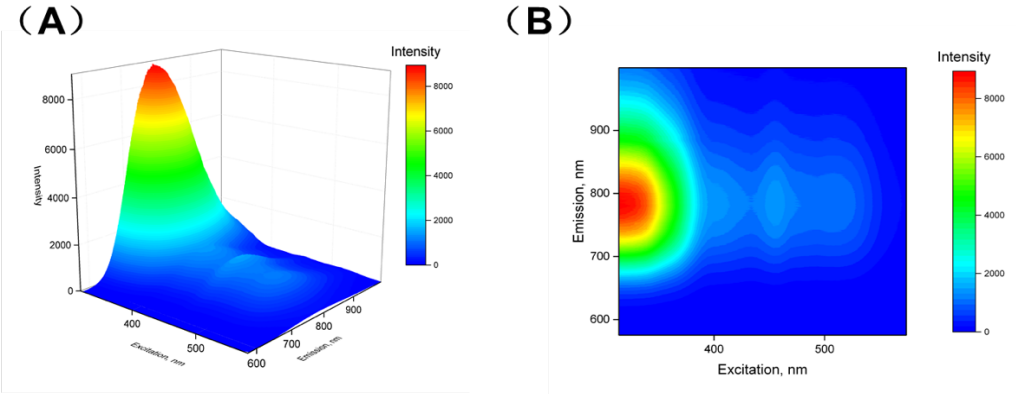

Figure S16. 3D (A) and 2D (B) plots of EEM data for [**3a**]Cl_3. Spectra were recorded using excitation band pass 5 nm, emission band pass 5 nm, integration time 0.5 s, and detector accumulation 1.

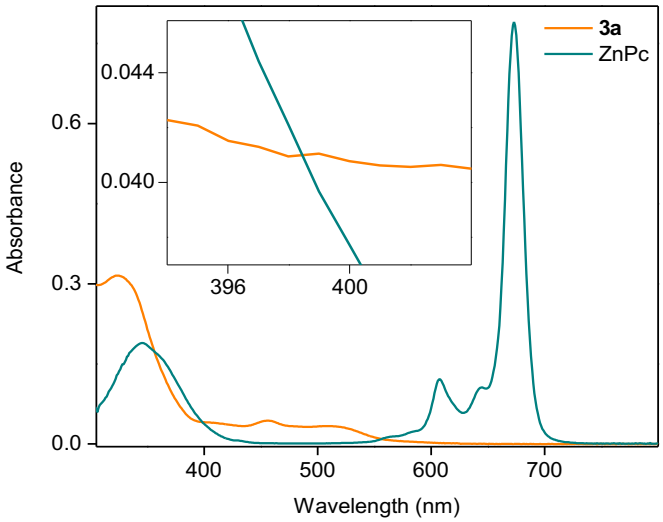

Figure S17. Absorbance spectra of reference ZnPc versus cluster [**3a**]Cl_3 samples. Inset: zoomed area showing the matched absorbance. Fixed spectral bandwidth for the instrument is 1.5 nm; signal averaging time 0.1 s.

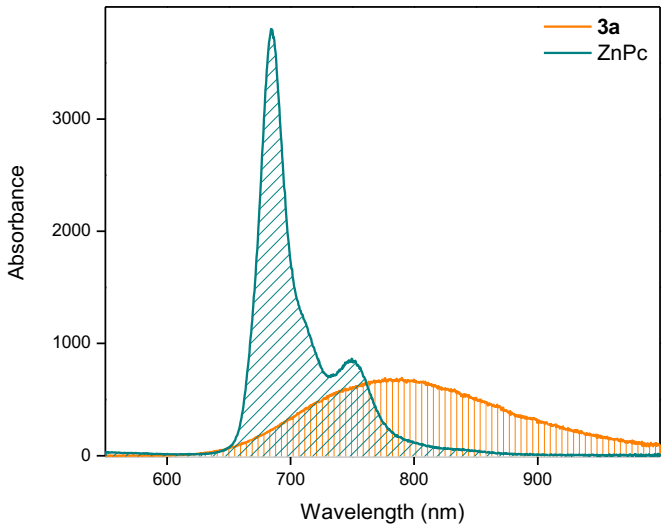

Figure S18. Emission spectra (excited at 398 nm) used to calculate fluorescence quantum yield of cluster [**3a**]Cl_3 by the comparative method. Spectra were recorded using excitation band pass 5 nm, emission band pass 5 nm, integration time 0.2 s, and detector accumulation 1.
Integrated areas: [**3a**]Cl_3 sample (*orange*) 135286; ZnPc standard (*dark cyan*) 167530.

3.2 X-ray crystallographic data

Table S1. Crystal data and structure refinement for $[3a]Cl_3$

Empirical formula	$C_{180}H_{150}Au_{13}Cl_5N_{20}$	
Formula weight	5331.01	
Temperature	123(2) K	
Wavelength	0.71073 Å	
Crystal system	*Orthorhombic*	
Space group	*P*na2_1	
Unit cell dimensions	a = 33.830(4) Å	α = 90°.
	b = 28.509(3) Å	β = 90°.
	c = 19.234(2) Å	γ = 90°.
Volume	18550(4) $Å^3$	
Z	4	
Density (calculated)	1.939 Mg/m^3	
Absorption coefficient	10.389 mm^{-1}	
F(000)	10096	
Crystal size	0.30 x 0.04 x 0.01 mm^3	
Theta range for data collection	3.1 to 27.5°.	
Index ranges	-43<=h<=43, -36<=k<=36, -24<=l<=24	
Reflections collected	181504	
Independent reflections	41330 [R(int) = 0.0637]	
Completeness to theta = 27.5°	0.949	
Absorption correction	Numerical (Multi-scan)	
Refinement method	Full-matrix least-squares on F^2 (SHELX-2018/3)	
Data / restraints / parameters	41330 / 1410 / 1955	
Goodness-of-fit on F^2	1.137	
Final R indices [I>2sigma(I)]	R_1 = 0.0531, wR_2 = 0.1123	
R indices (all data)	R_1 = 0.0952, wR_2 = 0.1420	
Extinction coefficient	n/a	
Largest diff. peak and hole	4.056 and -1.870 e.$Å^{-3}$	

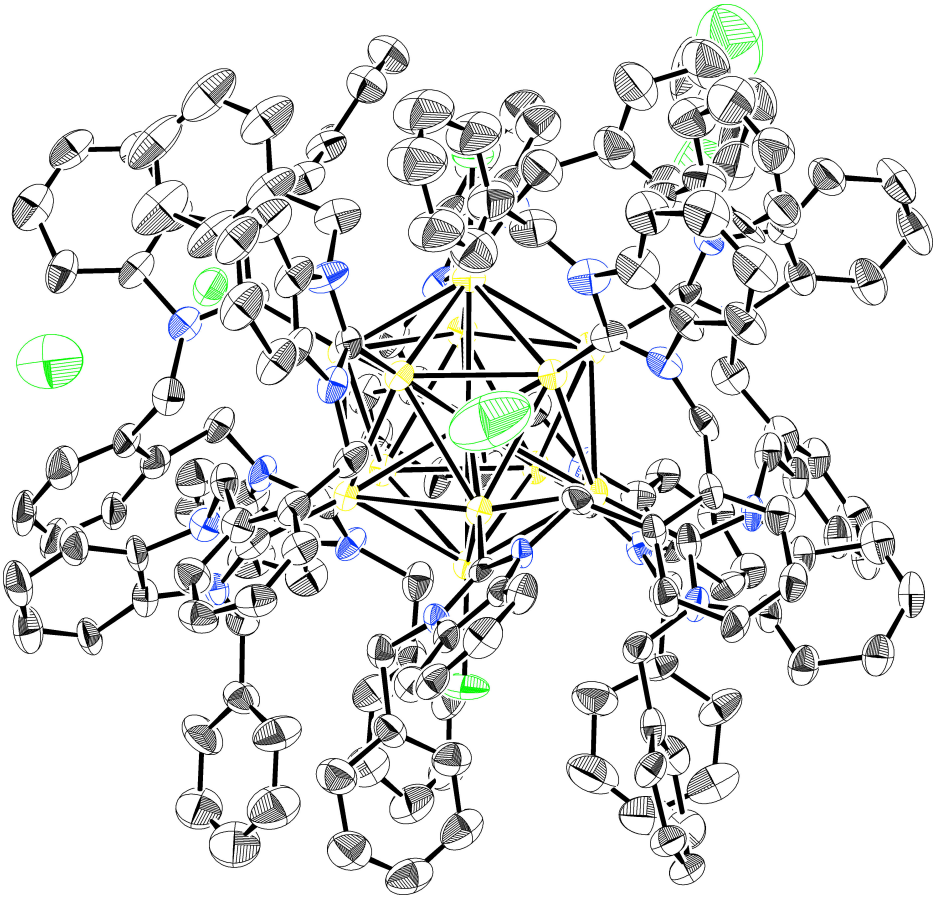

Figure S19. Full ORTEP diagram showing the X-ray structure of [**3a**]Cl_3 with thermal ellipsoids at 50% probability. H atoms have been omitted for clarity (legend: Au - yellow; Cl - green; C – grey; N - blue).

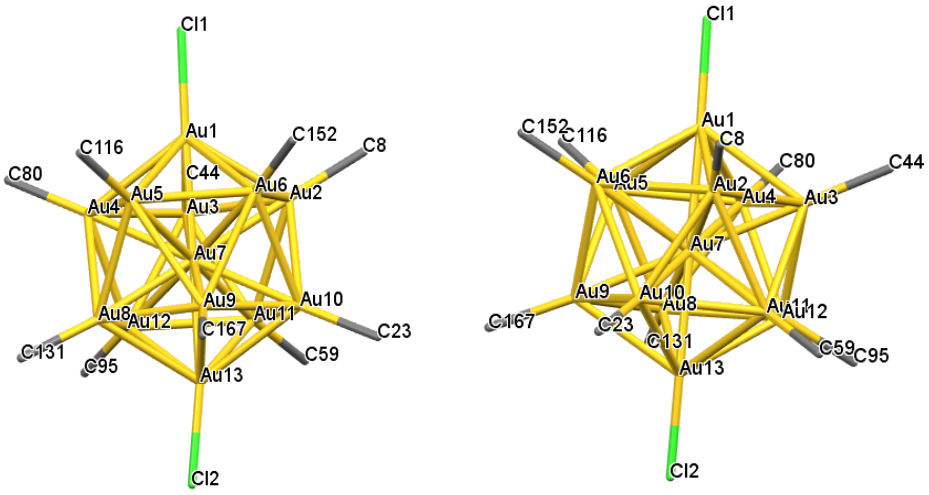

Figure S20. Alternative views of the X-ray structure of [**3a**]Cl_3 highlighting the central Au_{13} core and atoms directly attached to Au; all other atoms are removed for clarity (legend: Au - yellow; Cl - green; C – grey).

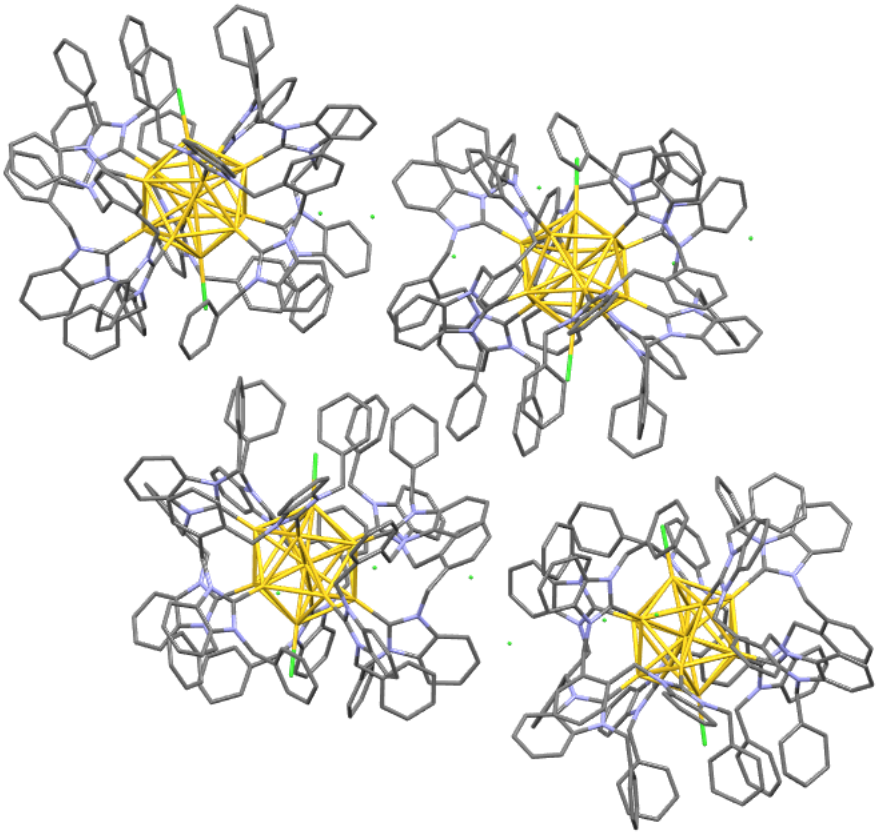

Figure S21. Unit cell of the X-ray structure of [**3a**]Cl_3 showing four cluster molecules as two pairs of enantiomers.

Table S2. Summary of important bond lengths for [**3a**]Cl_3

Atom 1	Atom 2	Length	Atom 1	Atom 2	Length	Atom 1	Atom 2	Length
Au1	Au2	2.860(1)	Au4	Au5	2.889(1)	Au7	Au12	2.788(1)
Au1	Au3	2.884(1)	Au4	Au7	2.758(1)	Au7	Au13	2.731(1)
Au1	Au4	2.888(1)	Au4	Au8	2.953(1)	Au8	Au9	2.894(1)
Au1	Au5	2.894(1)	Au4	Au12	2.893(1)	Au8	Au12	2.901(1)
Au1	Au6	2.883(1)	Au4	C80	2.05(2)	Au8	Au13	2.865(1)
Au1	Au7	2.747(1)	Au5	Au6	2.894(1)	Au8	C131	2.09(2)
Au1	Cl1	2.362(5)	Au5	Au7	2.776(1)	Au9	Au10	2.914(1)
Au2	Au3	2.907(1)	Au5	Au8	2.919(1)	Au9	Au13	2.876(1)
Au2	Au6	2.891(1)	Au5	Au9	2.954(1)	Au9	C167	2.04(2)
Au2	Au7	2.777(1)	Au5	C116	2.08(2)	Au10	Au11	2.894(1)
Au2	Au10	2.908(1)	Au6	Au7	2.778(1)	Au10	Au13	2.910(1)
Au2	Au11	3.007(1)	Au6	Au9	2.913(1)	Au10	C23	2.03(2)
Au2	C8	2.06(2)	Au6	Au10	2.973(1)	Au11	Au12	2.935(1)
Au3	Au4	2.921(1)	Au6	C152	2.07(2)	Au11	Au13	2.871(1)
Au3	Au7	2.757(1)	Au7	Au8	2.785(1)	Au11	C59	2.05(2)
Au3	Au11	2.897(1)	Au7	Au9	2.762(1)	Au12	Au13	2.883(1)
Au3	Au12	2.975(1)	Au7	Au10	2.768(1)	Au12	C95	2.01(2)
Au3	C44	2.07(2)	Au7	Au11	2.762(1)	Au13	Cl2	2.300(6)

3.3 NMR spectra

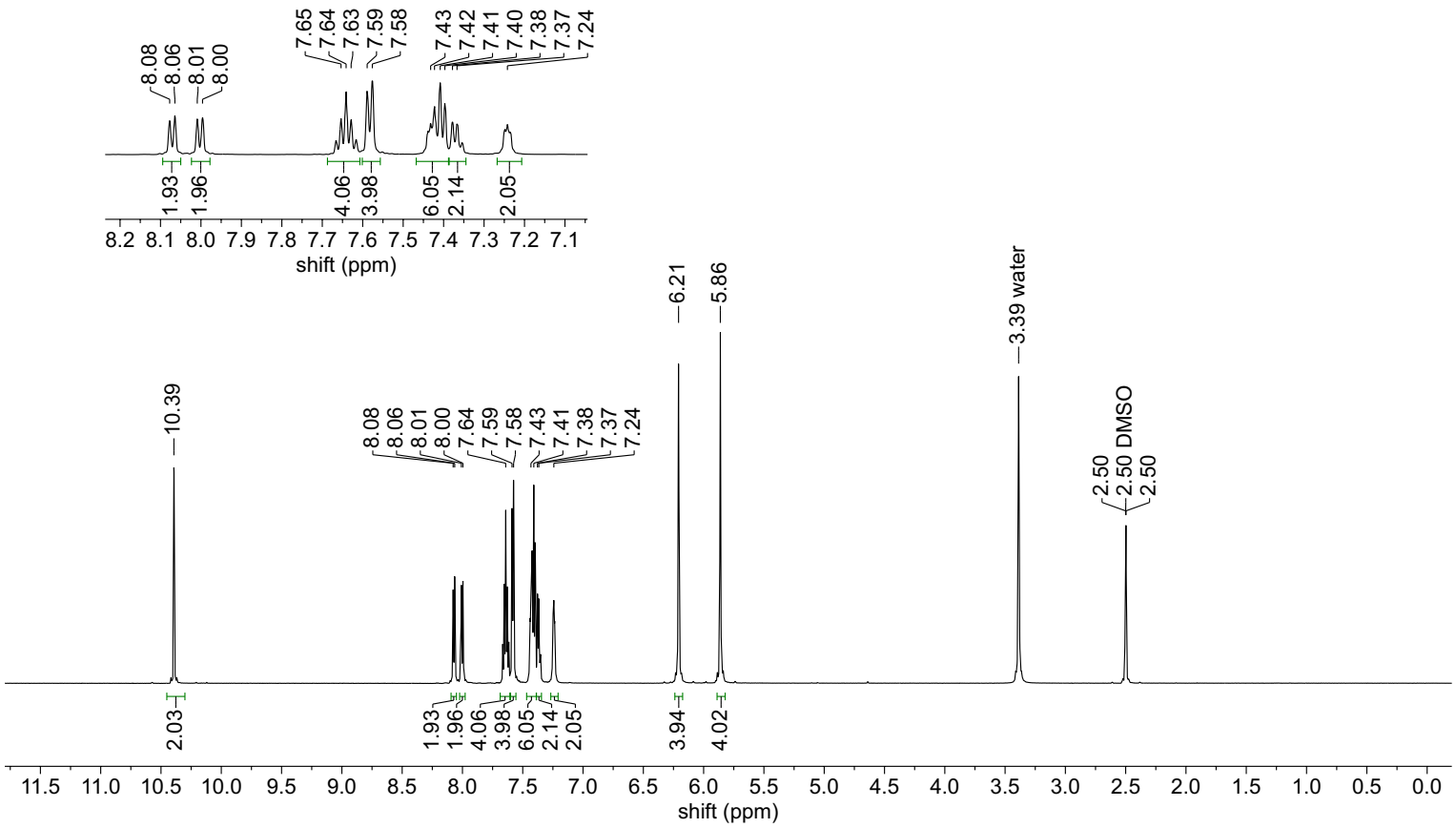

Figure S22. ^{1}H NMR spectrum (DMSO-d_6, 600 MHz) of **1a**.

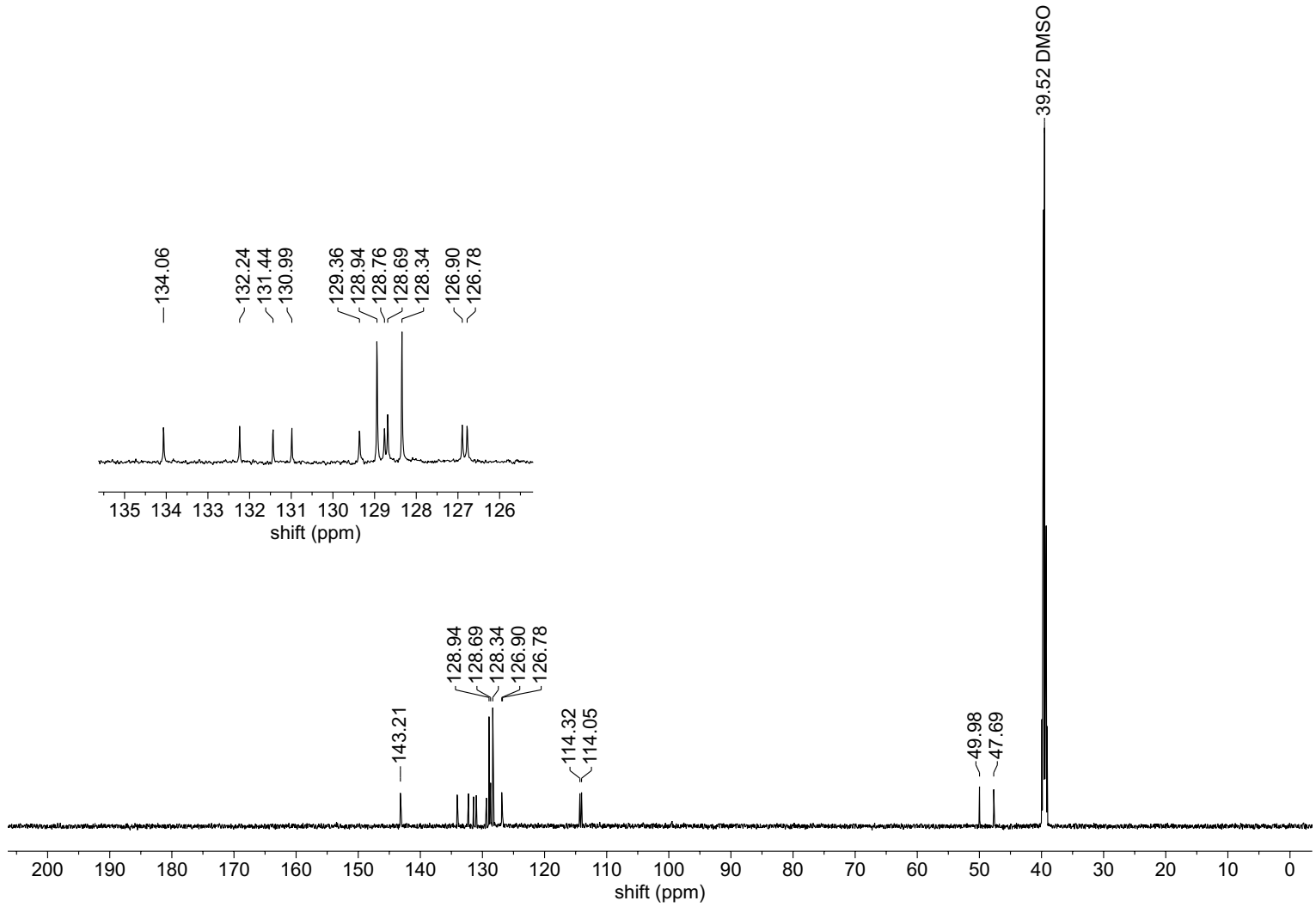

Figure S23. $^{13}C\{^{1}H\}$ NMR spectrum (DMSO- d_6, 151 MHz) of **1a**.

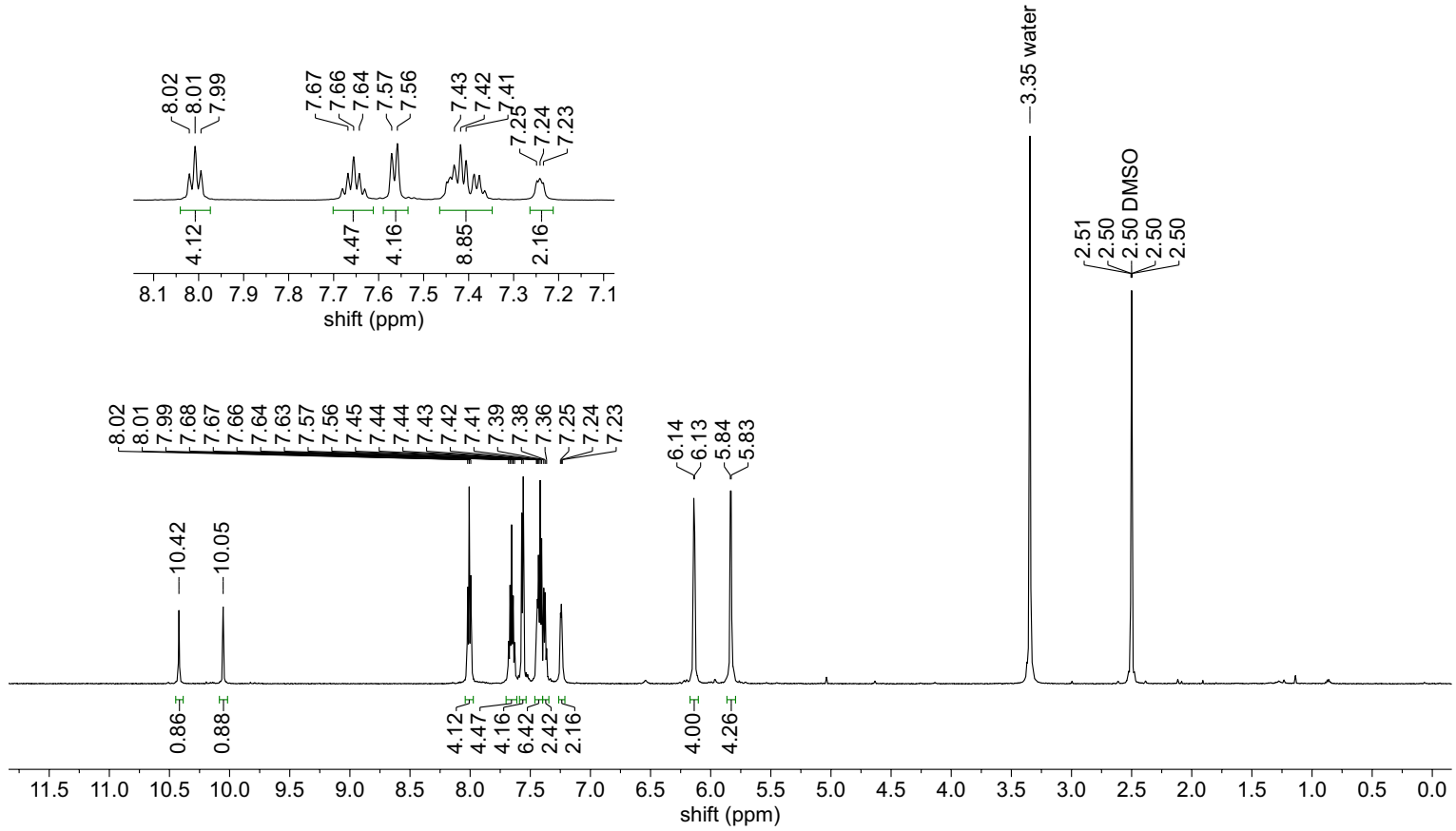

Figure S24. ^{1}H NMR spectrum (DMSO- d_6, 600 MHz) of **^{13}C-1a**.

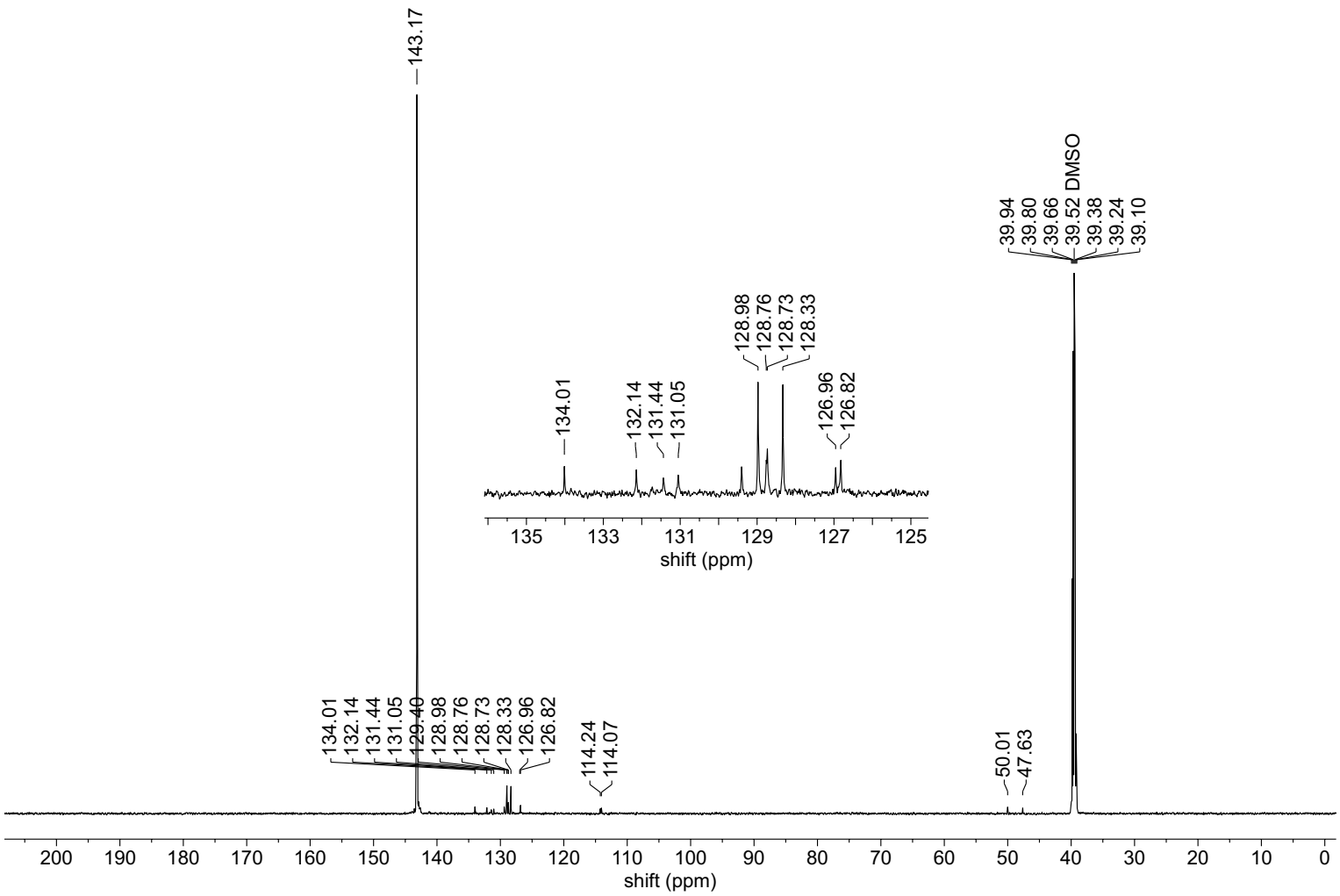

Figure S25. $^{13}C\{^{1}H\}$ NMR spectrum (DMSO- d_6, 151 MHz) of **^{13}C-1a**.

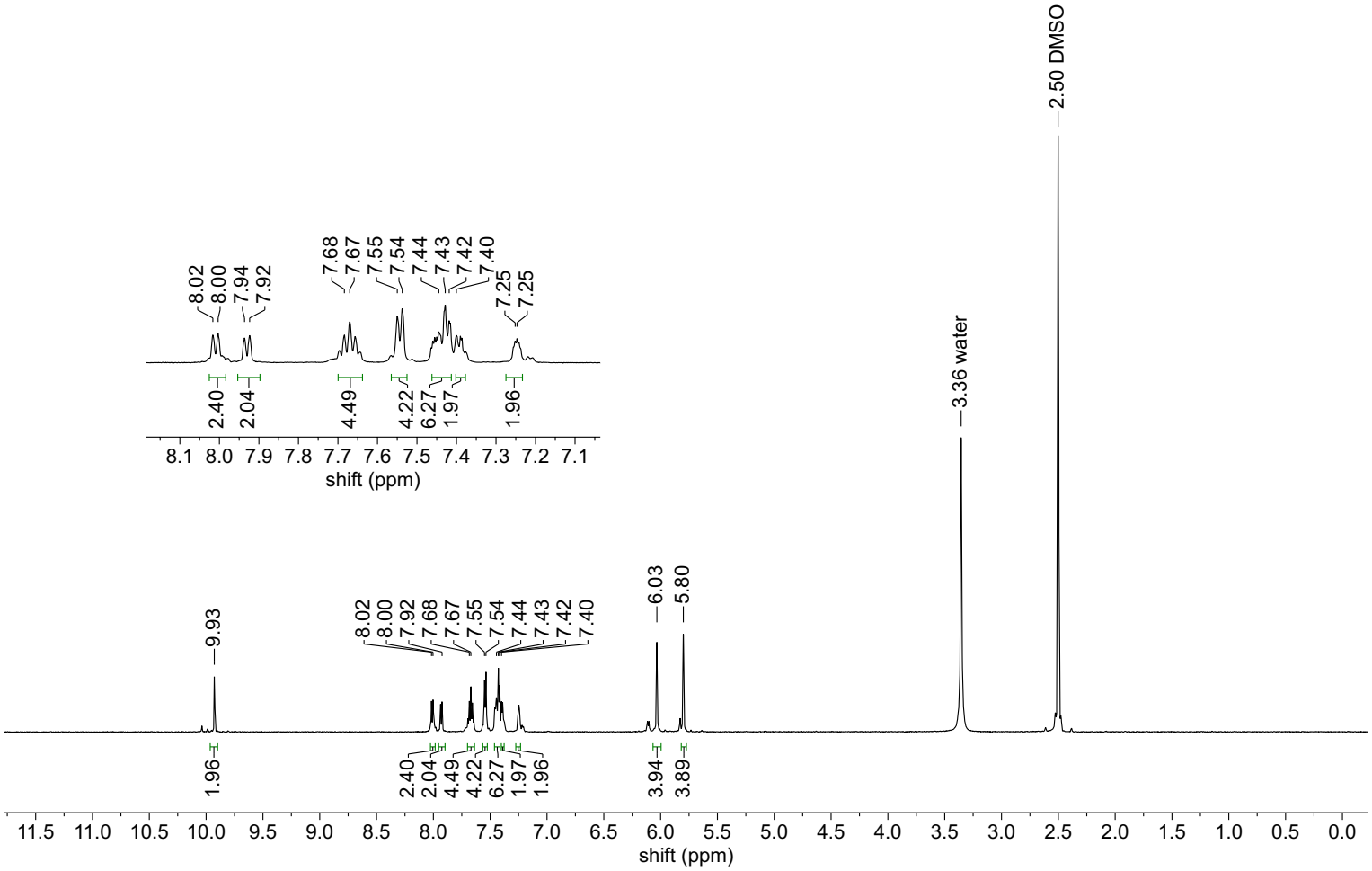

Figure S26. ^{1}H NMR spectrum (DMSO- d_6, 600 MHz) of **1b**.

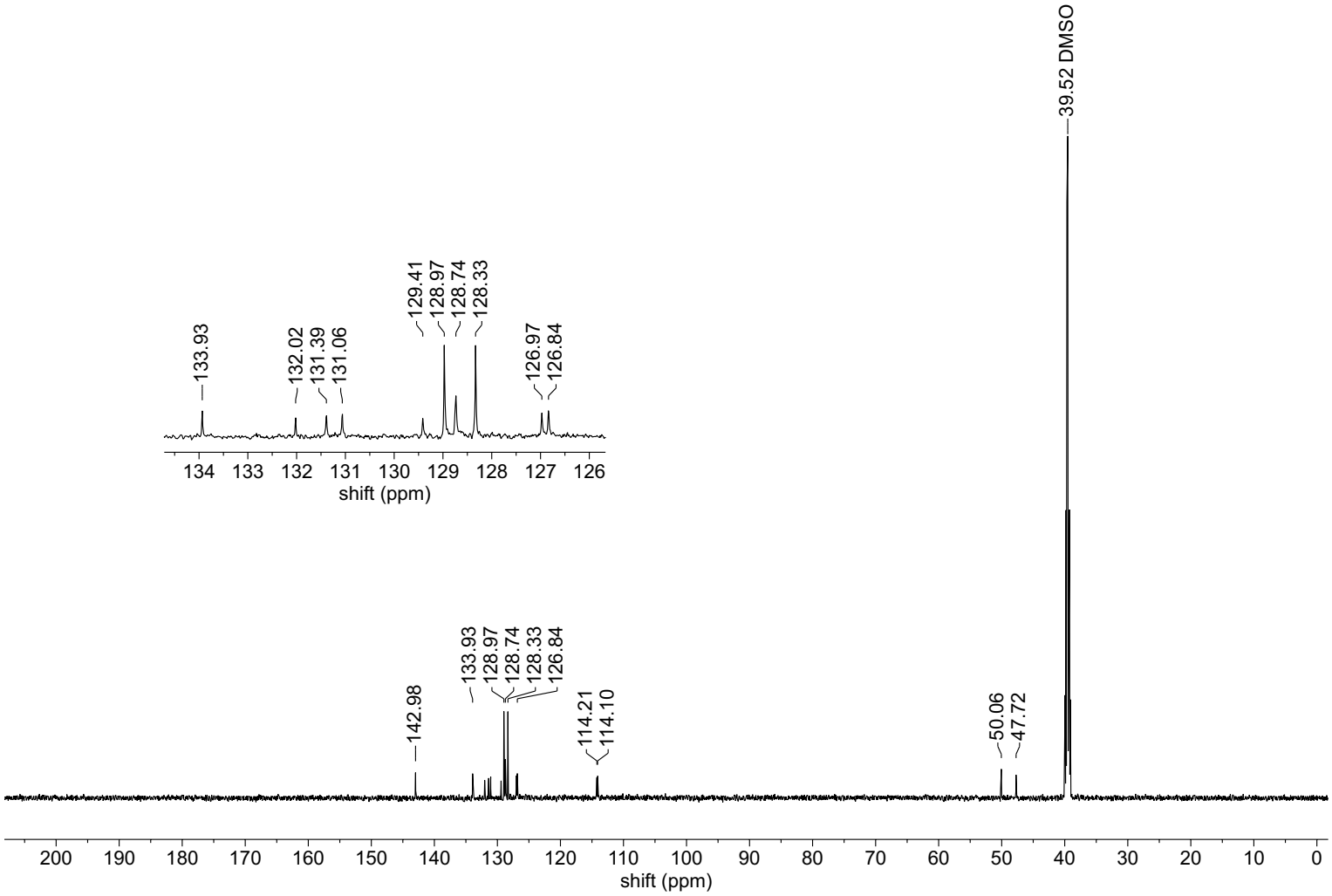

Figure S27. $^{13}C\{^{1}H\}$ NMR spectrum (DMSO- d_6, 151 MHz) of **1b**.

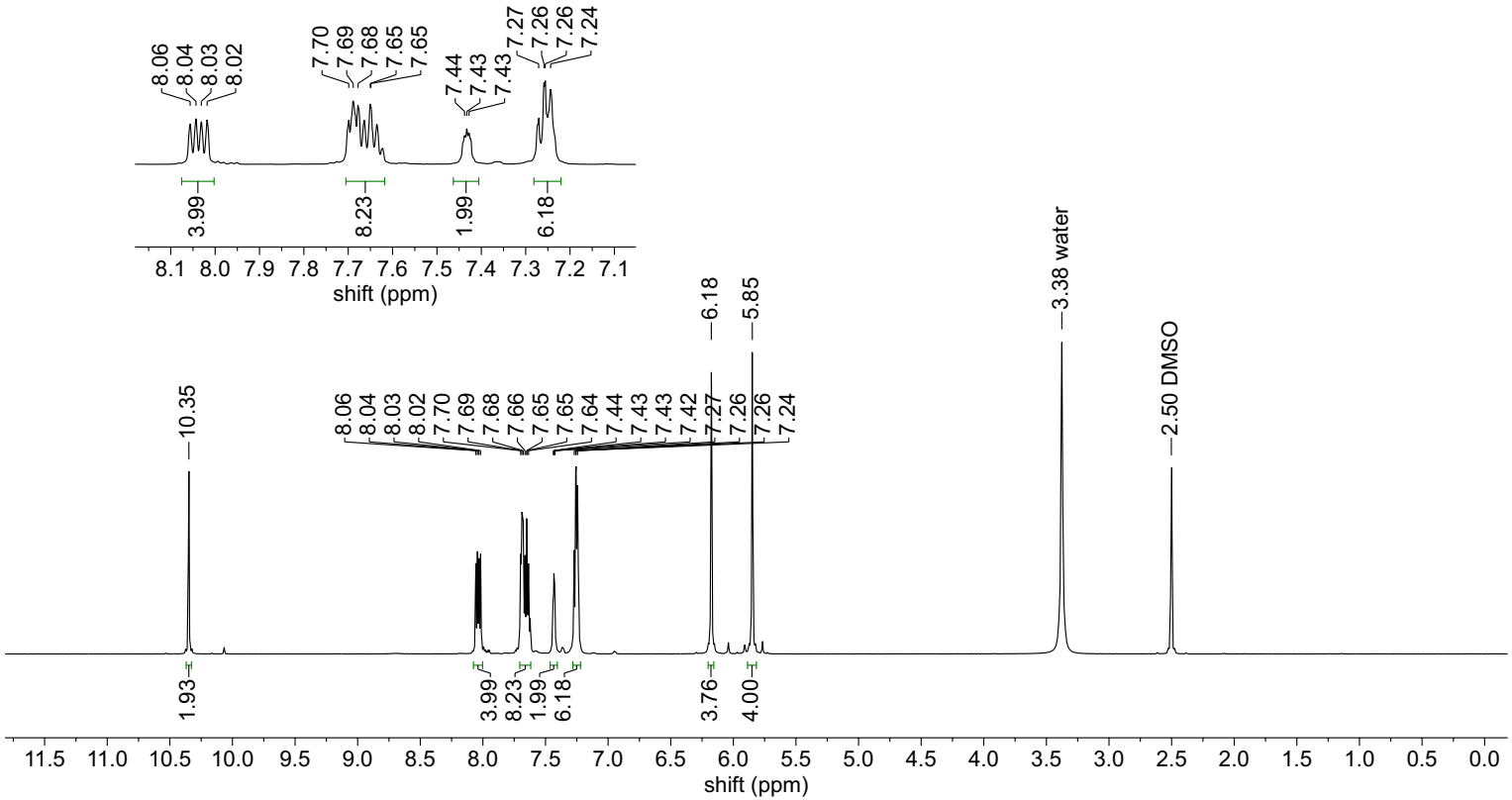

Figure S28. ^{1}H NMR spectrum (DMSO- d_6, 600 MHz) of **1c**.

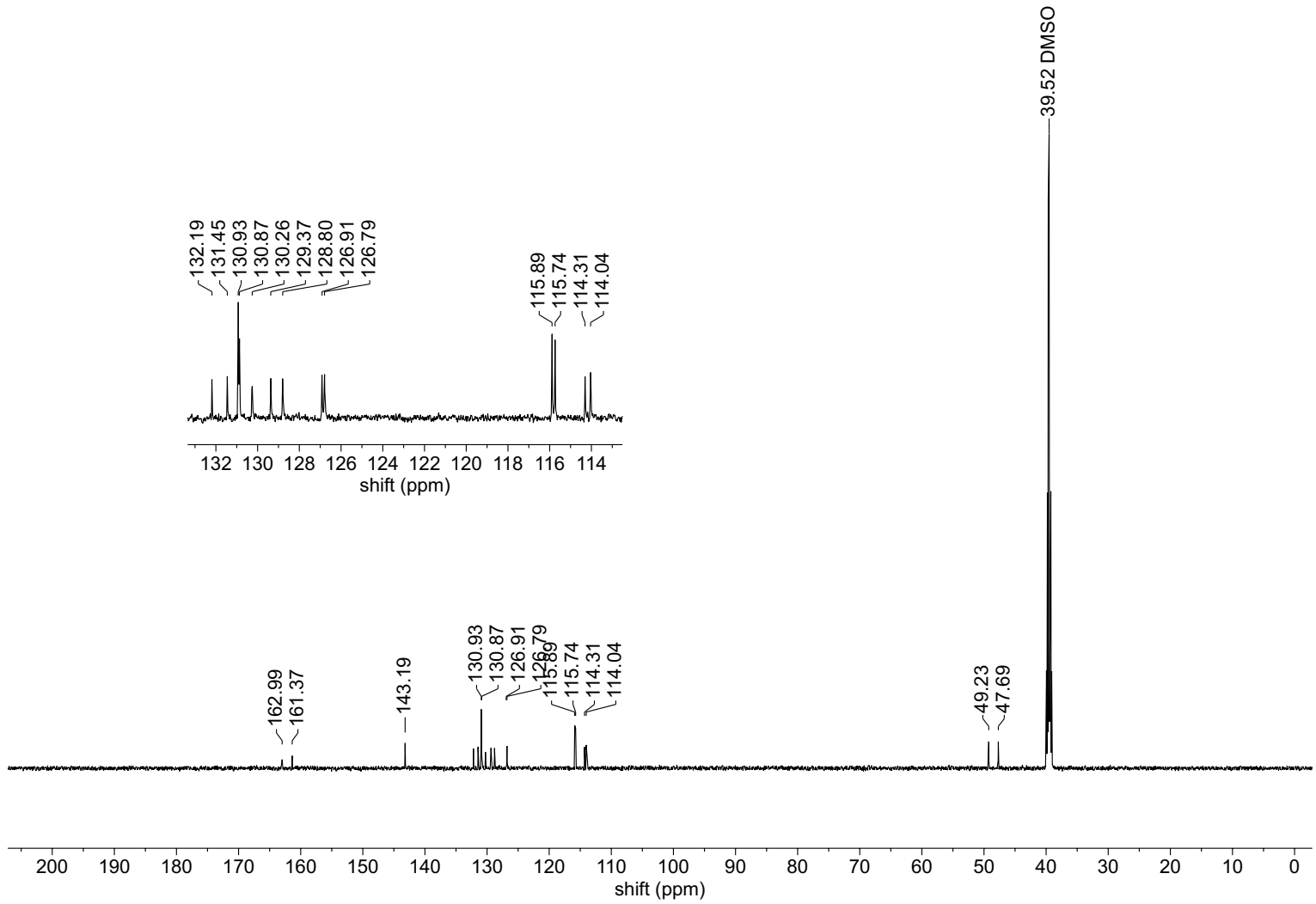

Figure S29. $^{13}C\{^{1}H\}$ NMR spectrum (DMSO- d_6, 151 MHz) of **1c**.

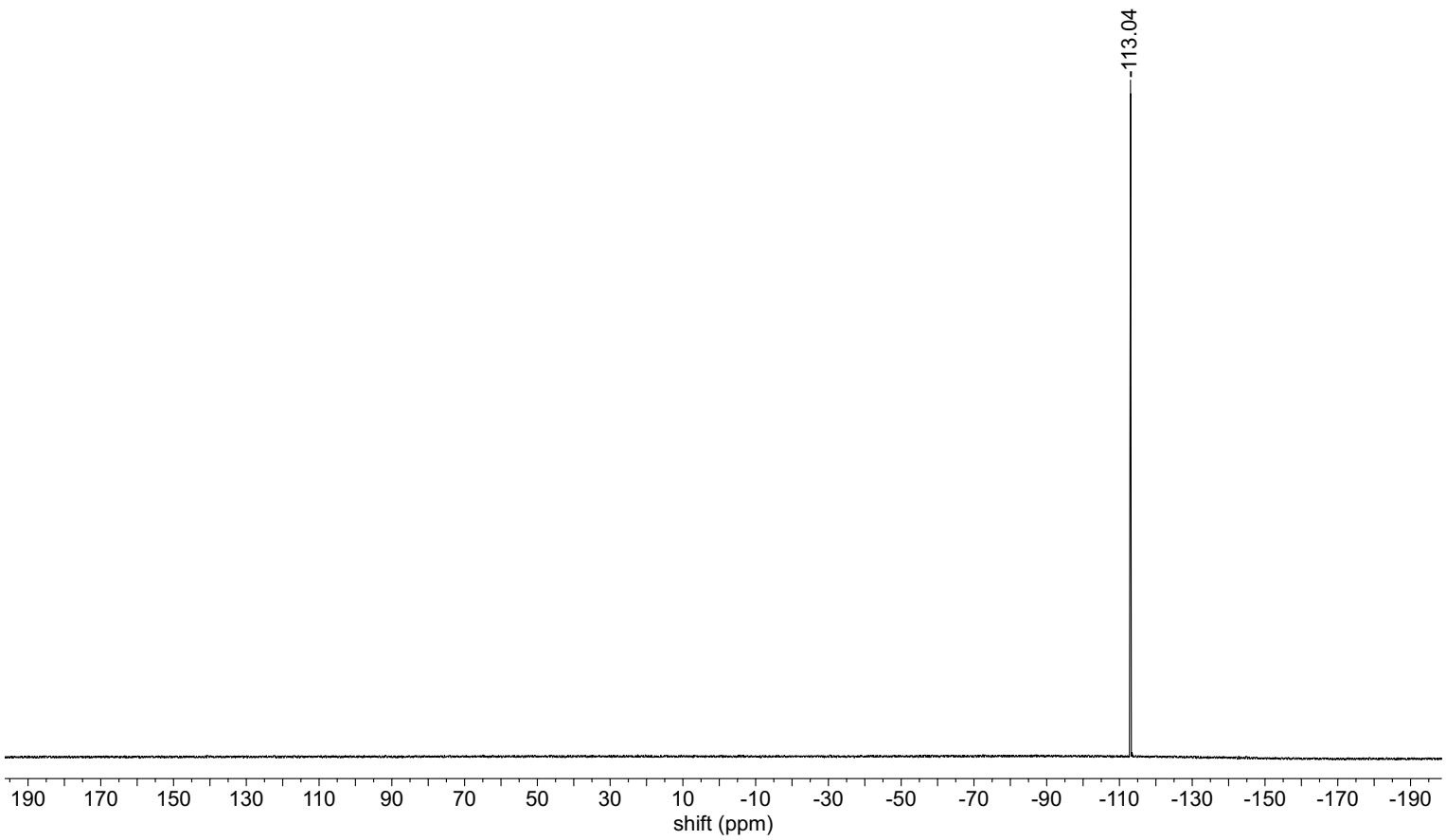

Figure S30. ^{19}F NMR spectrum (DMSO- d_6, 376 MHz) of **1c**.

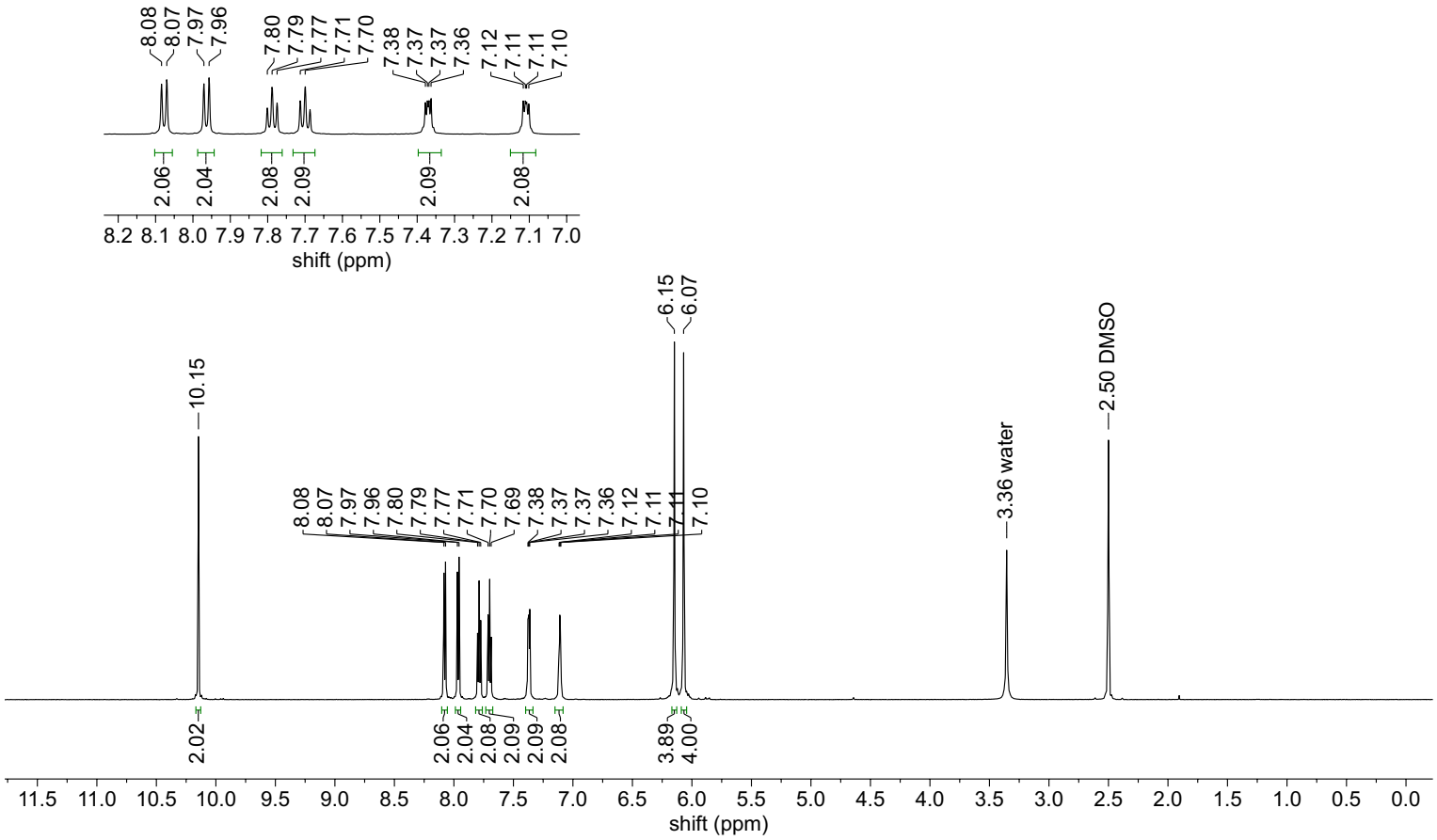

Figure S31. ^{1}H NMR spectrum (DMSO- d_6, 600 MHz) of **1d**.

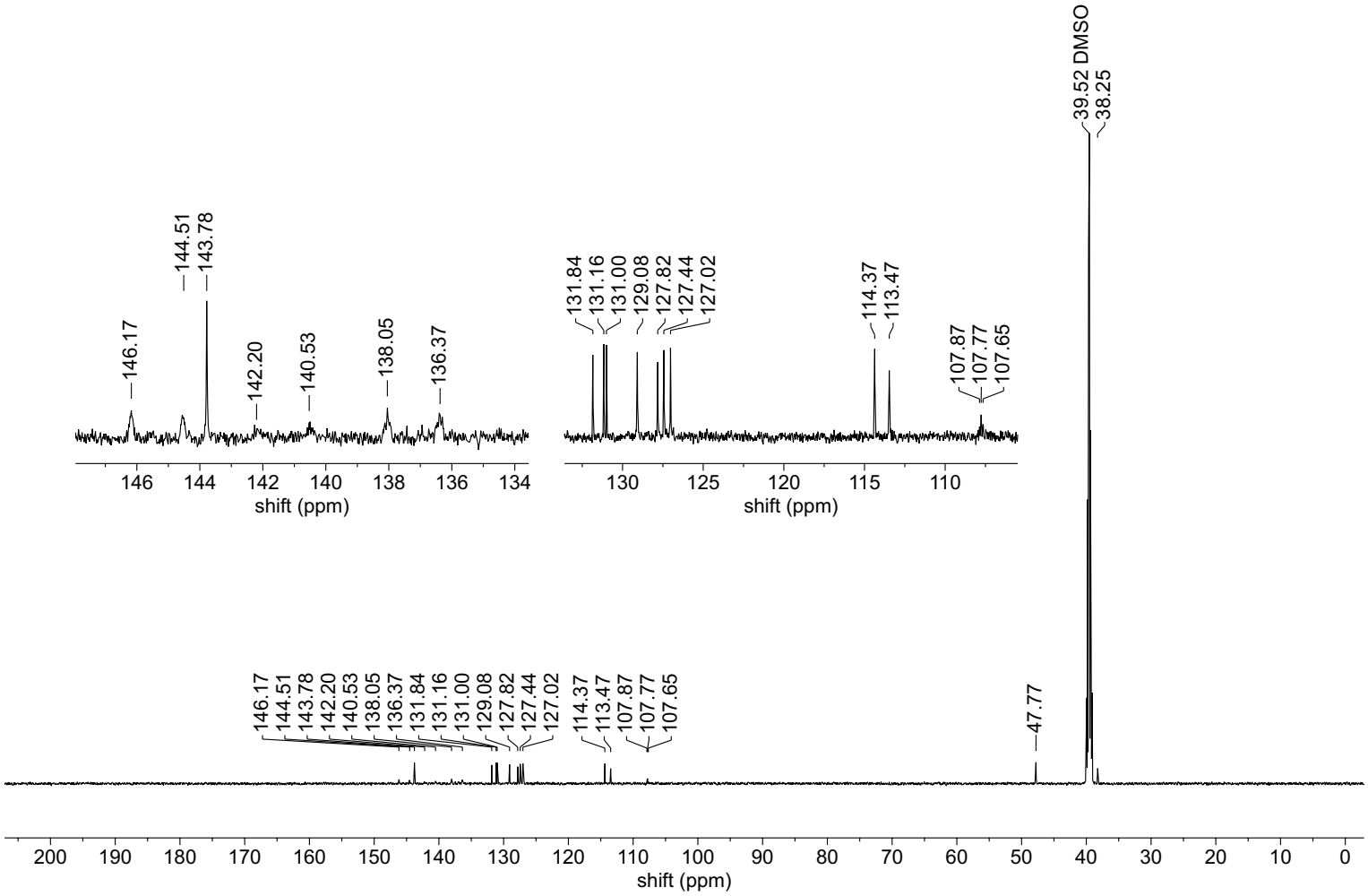

Figure S32. $^{13}C\{^{1}H\}$ NMR spectrum (DMSO- d_6, 151 MHz) of **1d**.

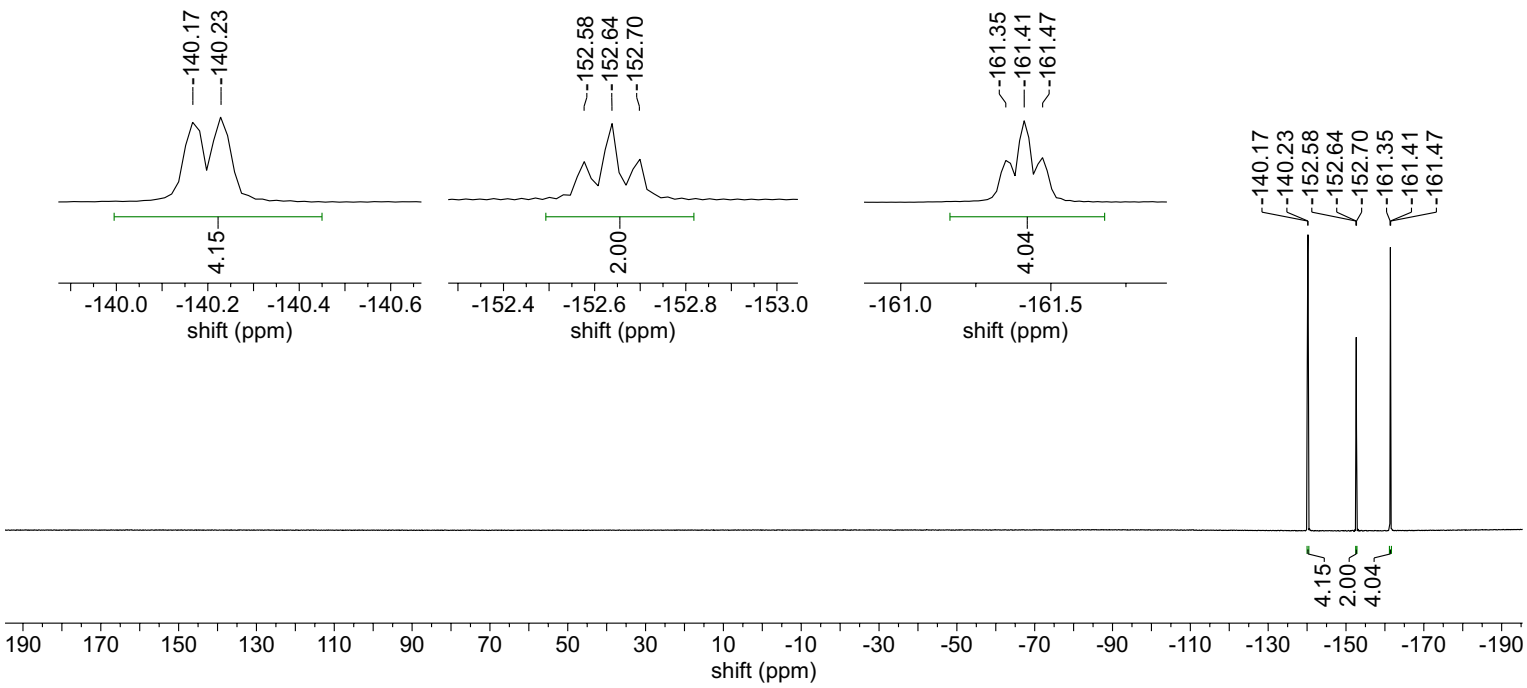

Figure S33. ^{19}F NMR spectrum (DMSO- d_6, 376 MHz) of **1d**.

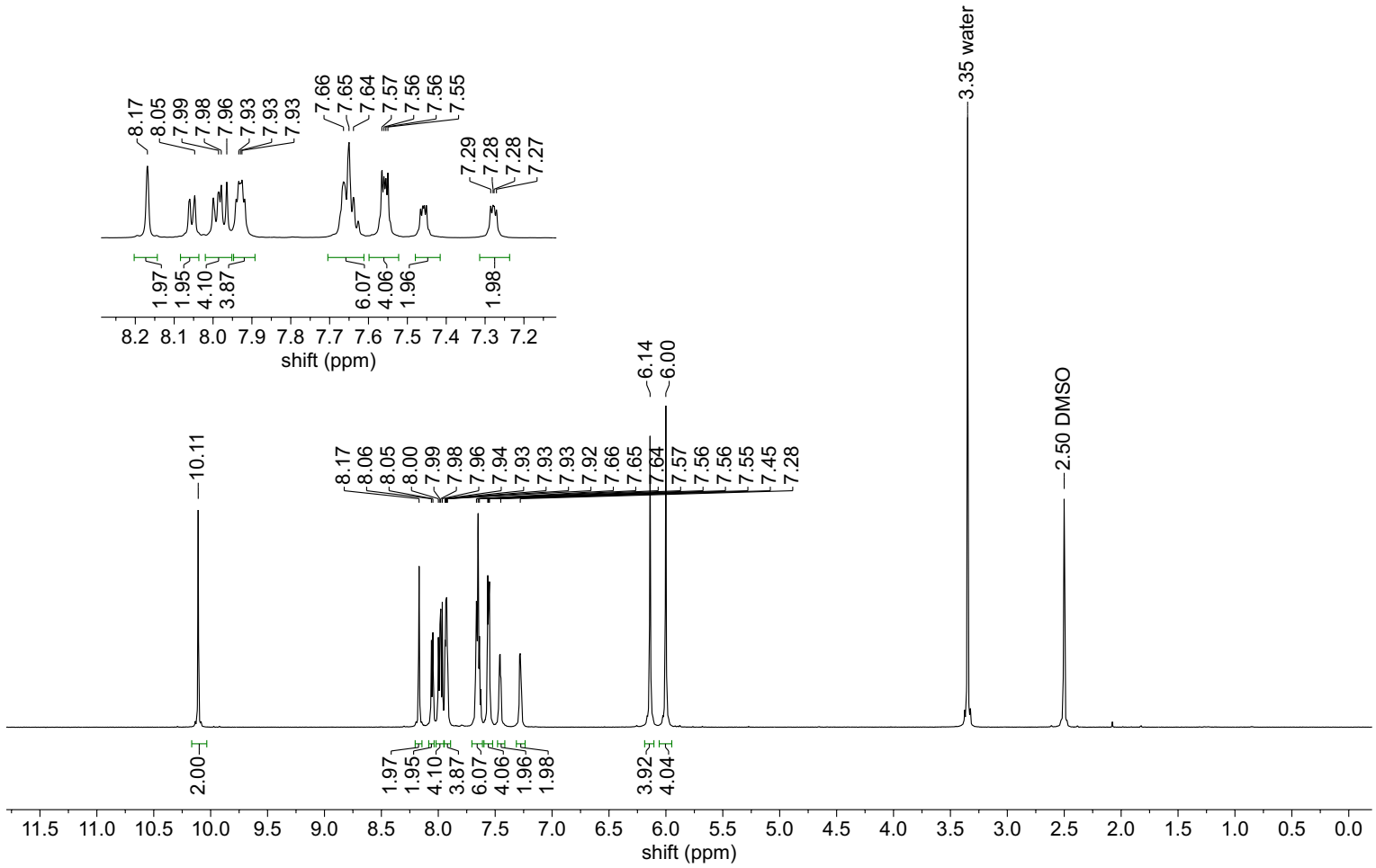

Figure S34. ^{1}H NMR spectrum (DMSO- d_6, 600 MHz) of **1e**.

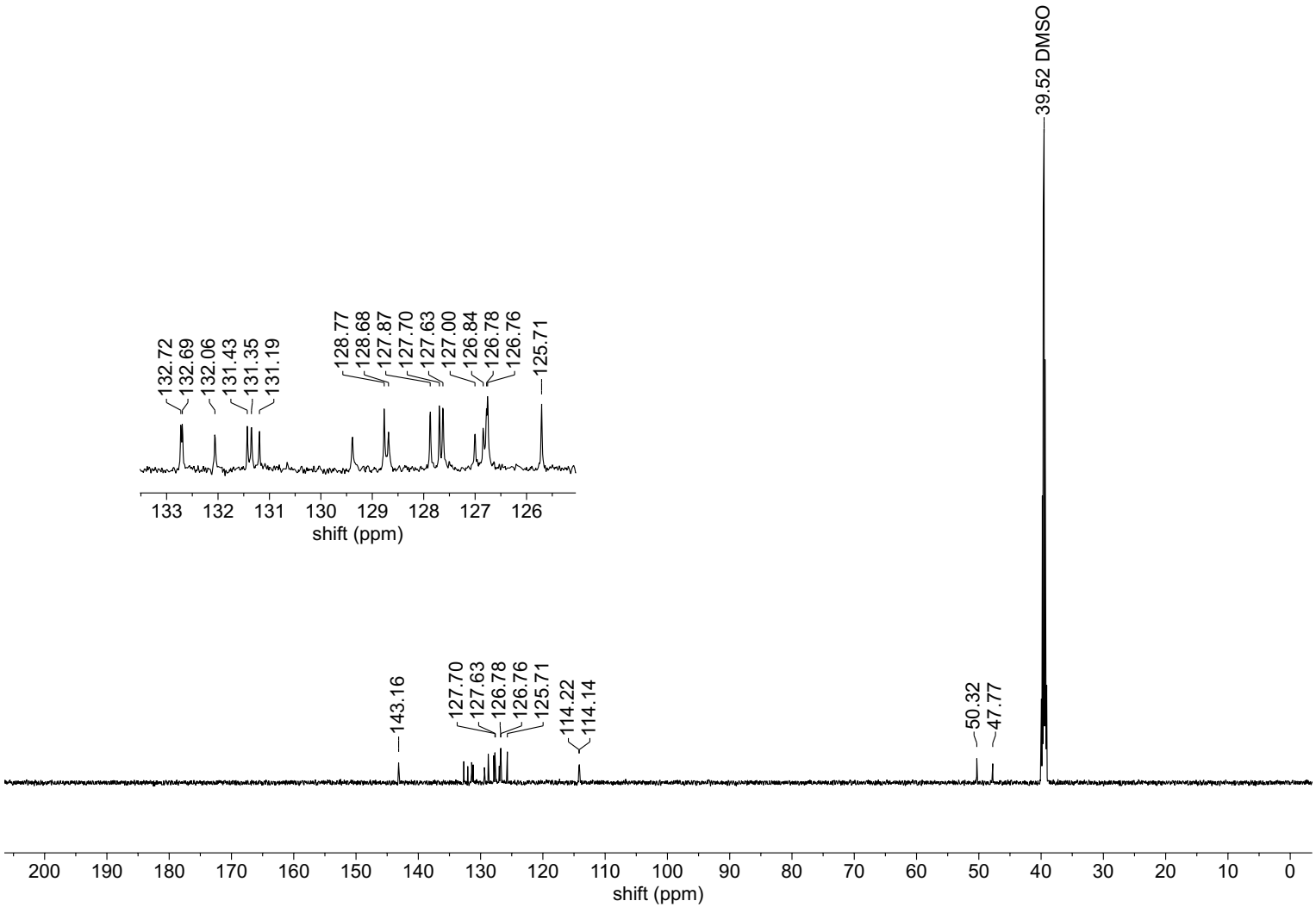

Figure S35. $^{13}C\{^{1}H\}$ NMR spectrum (DMSO- d_6, 151 MHz) of **1e**.

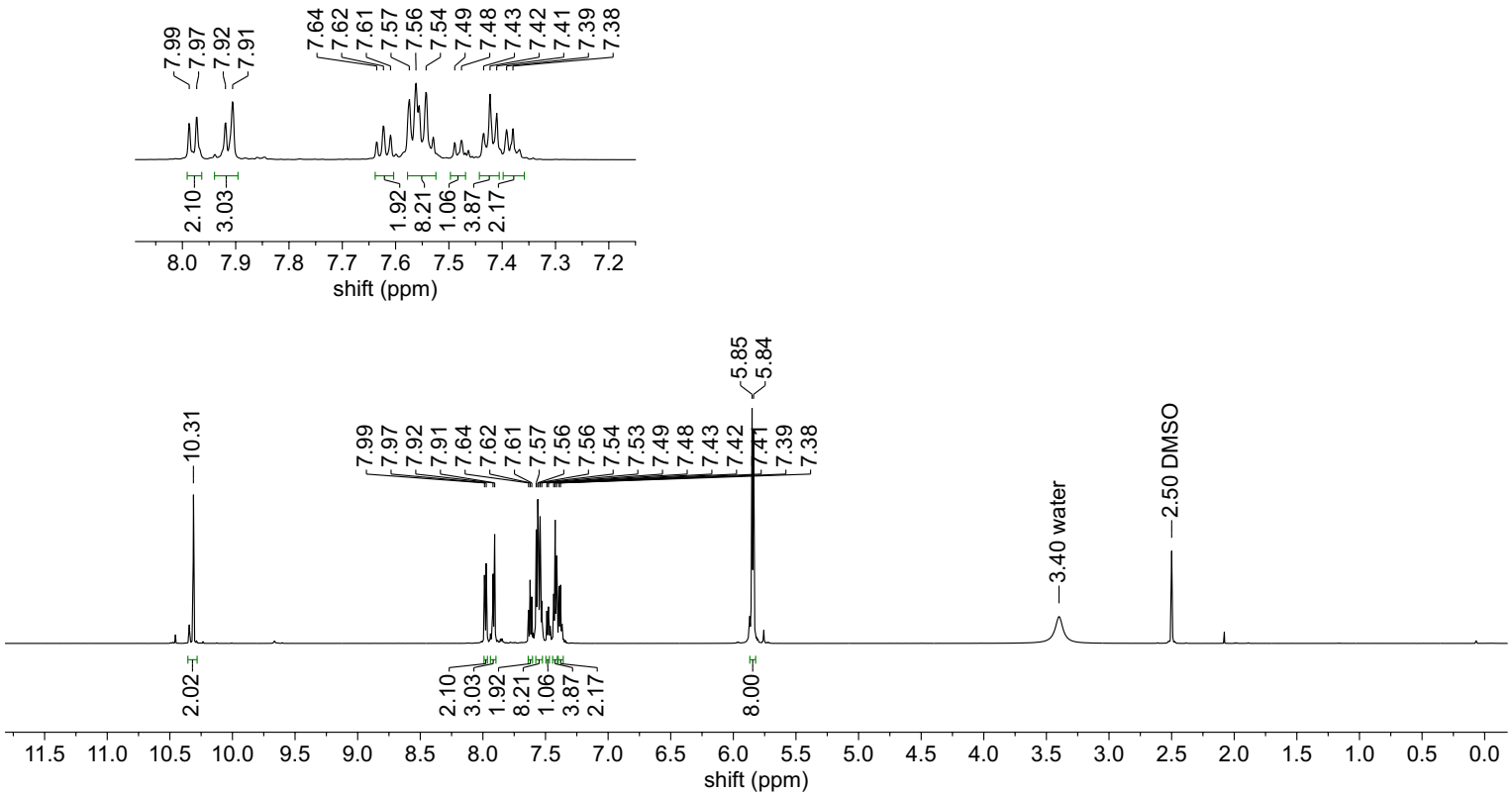

Figure S36. ^{1}H NMR spectrum (DMSO- d_6, 600 MHz) of **1f**.

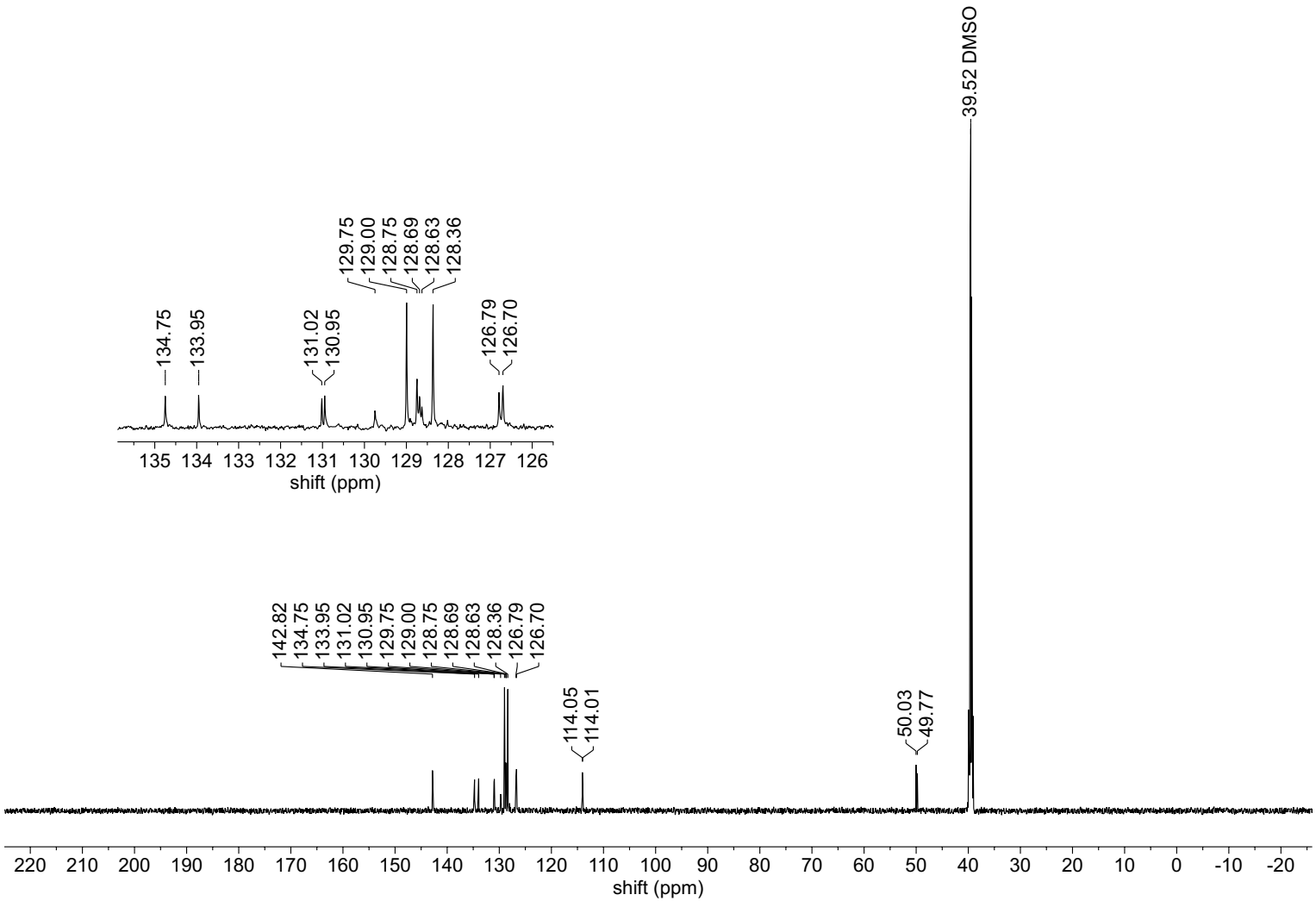

Figure S37. $^{13}C\{^{1}H\}$ NMR spectrum (DMSO- d_6, 151 MHz) of **1f**.

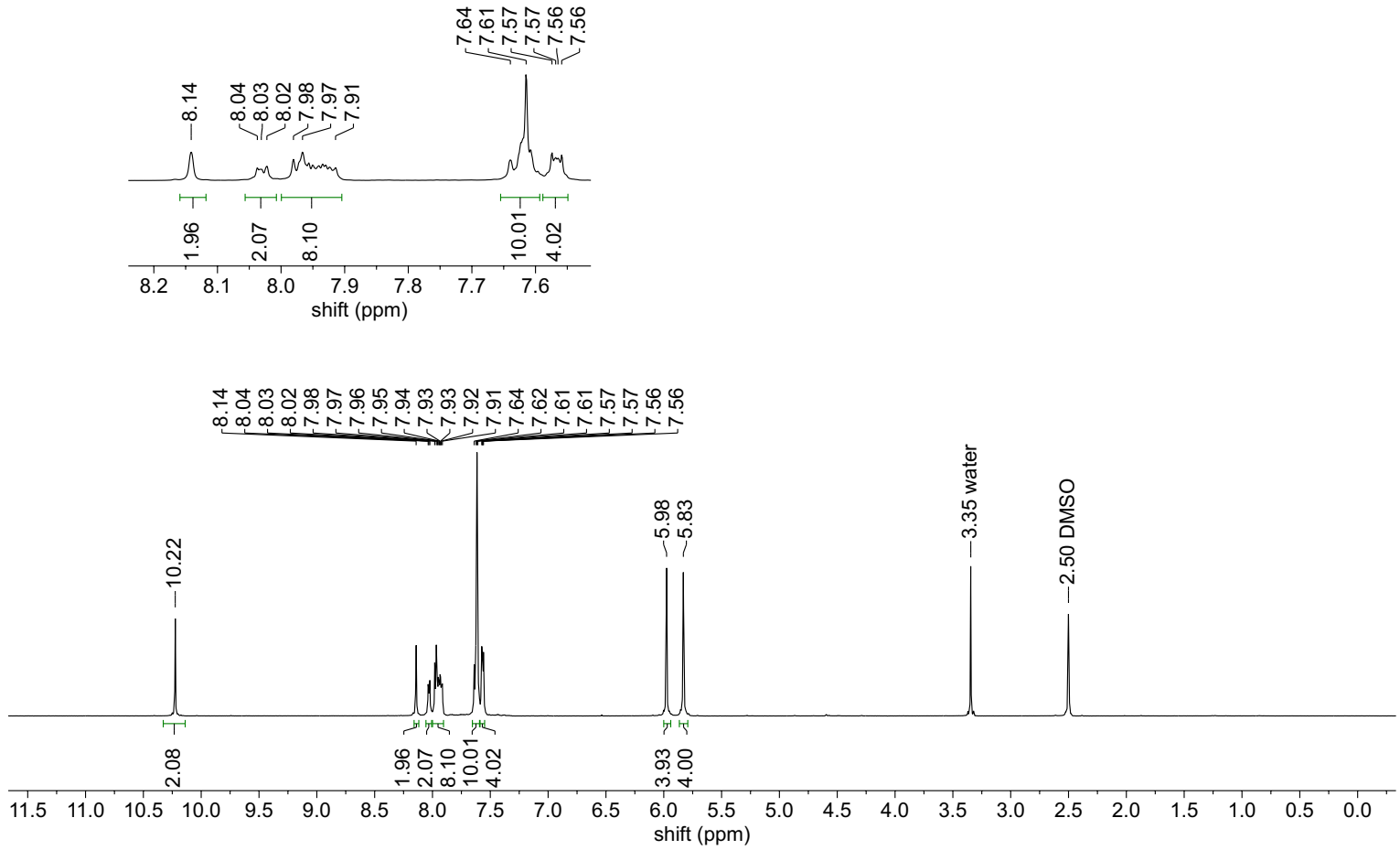

Figure S38. ^{1}H NMR spectrum (DMSO- d_6, 600 MHz) of **1g**.

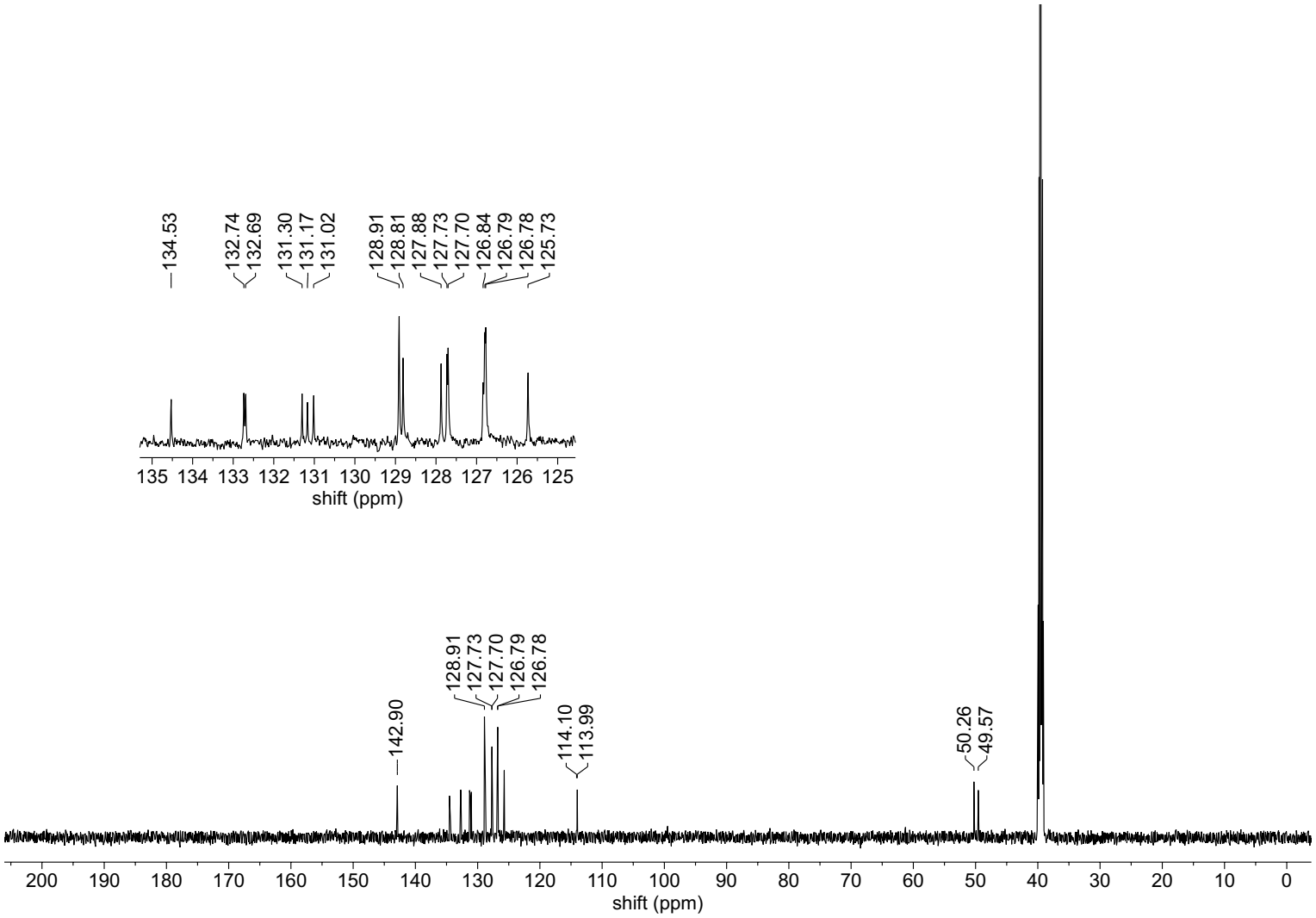

Figure S39. $^{13}C\{^{1}H\}$ NMR spectrum (DMSO- d_6, 151 MHz) of **1g**.

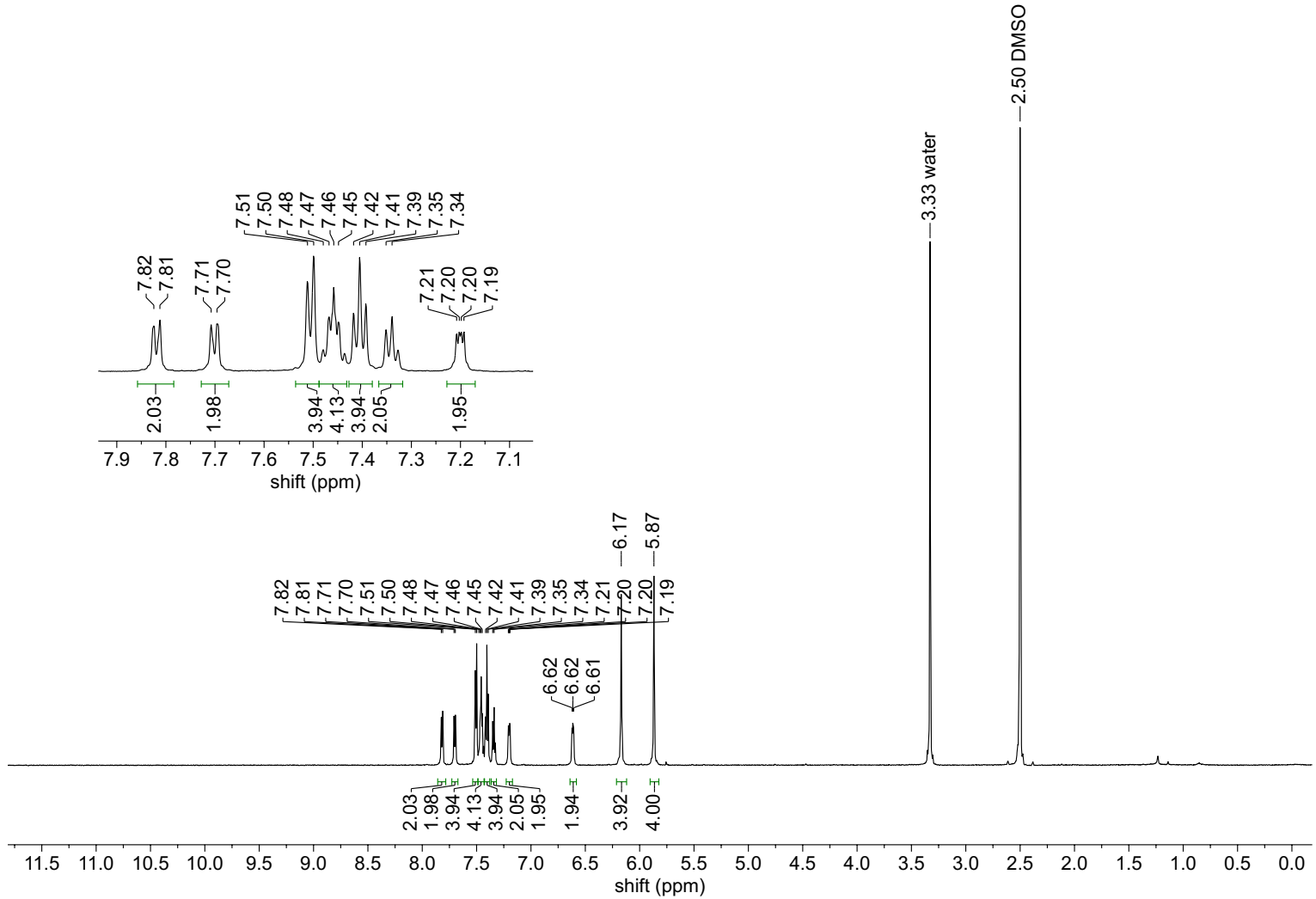

Figure S40. [1]H NMR spectrum (DMSO- d_6, 600 MHz) of **2a**.

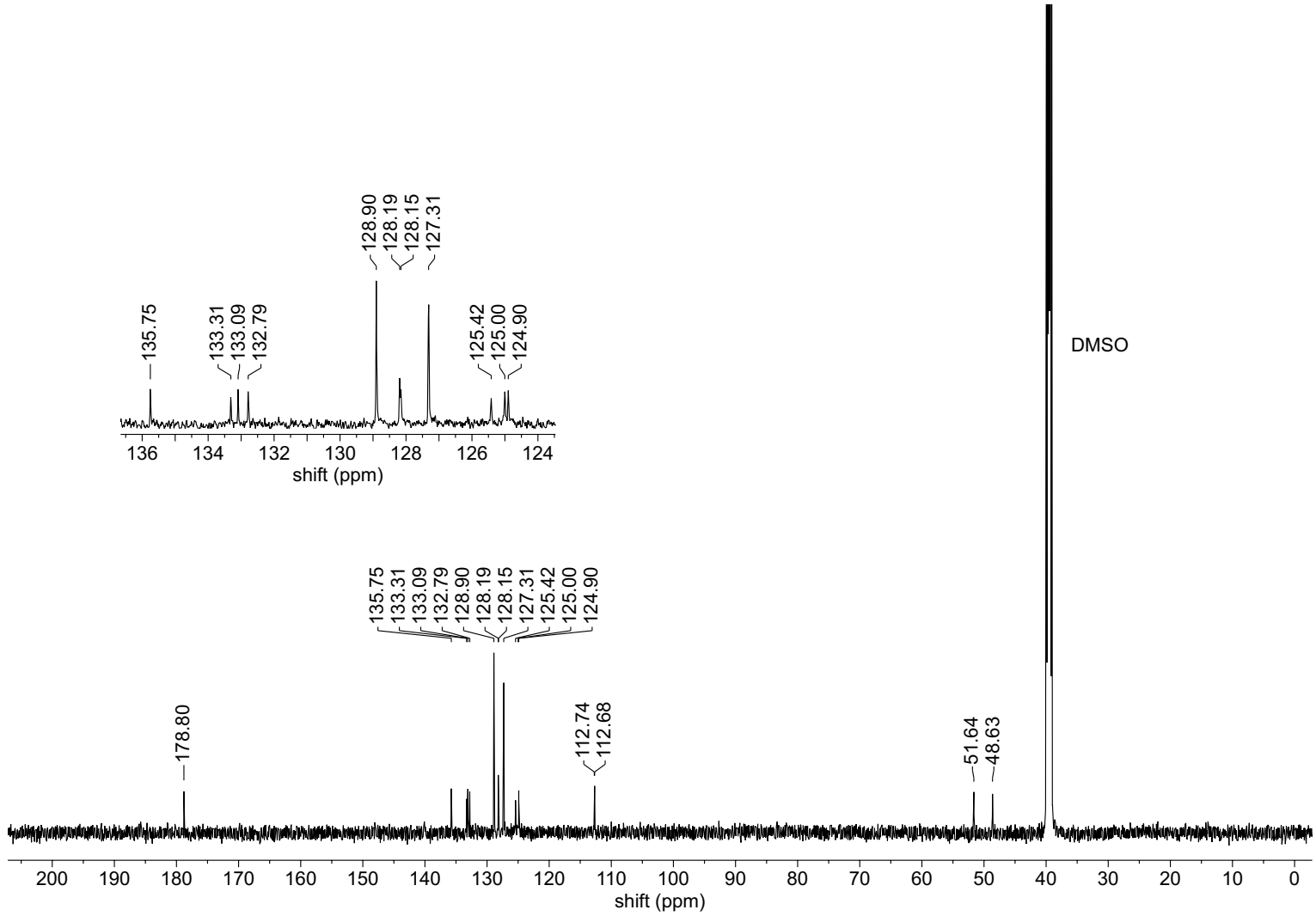

Figure S41. $^{13}C\{^{1}H\}$ NMR spectrum (DMSO- d_6, 151 MHz) of **2a**.

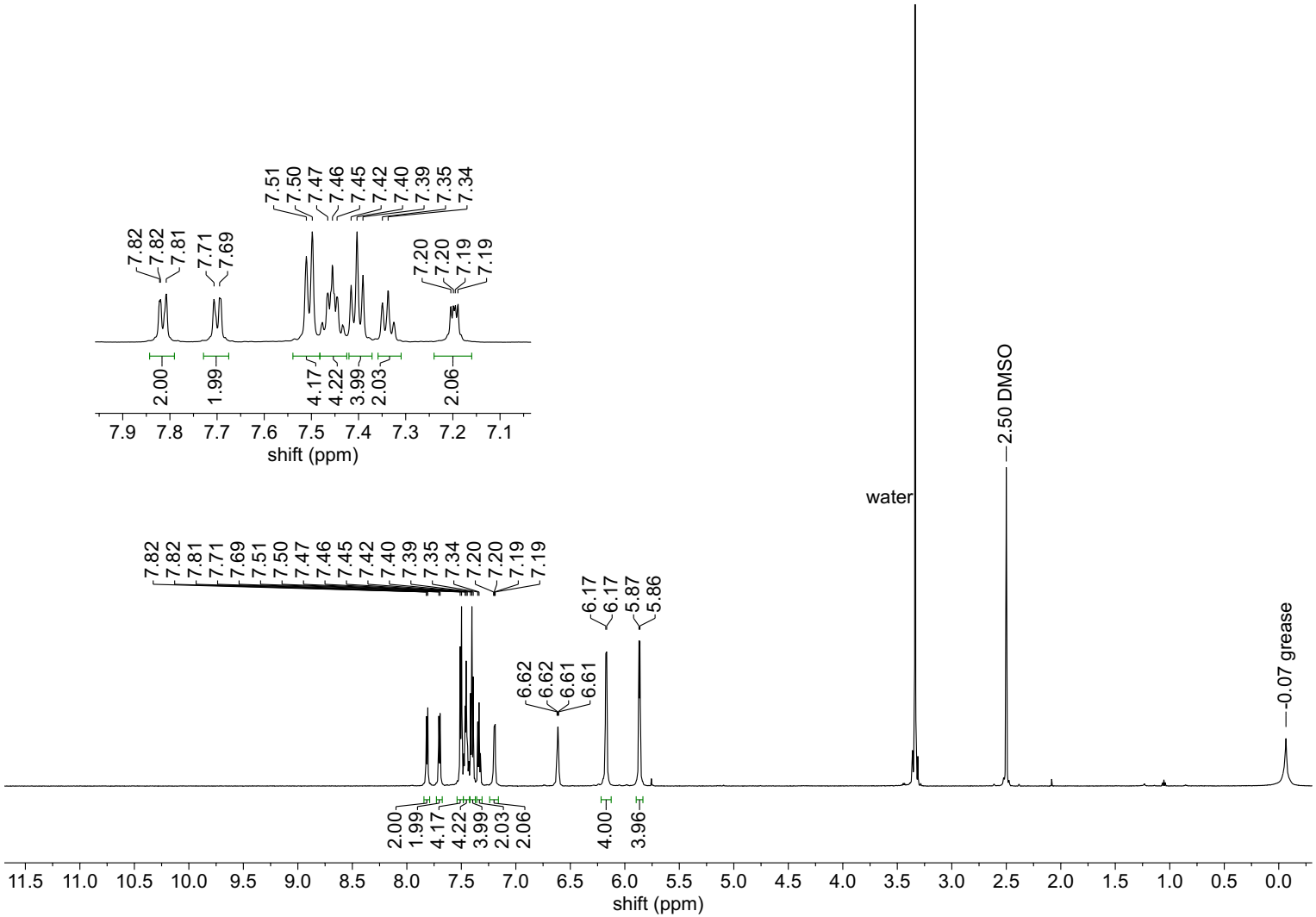

Figure S42. ^{1}H NMR spectrum (DMSO- d_6, 600 MHz) of **^{13}C-2a**.

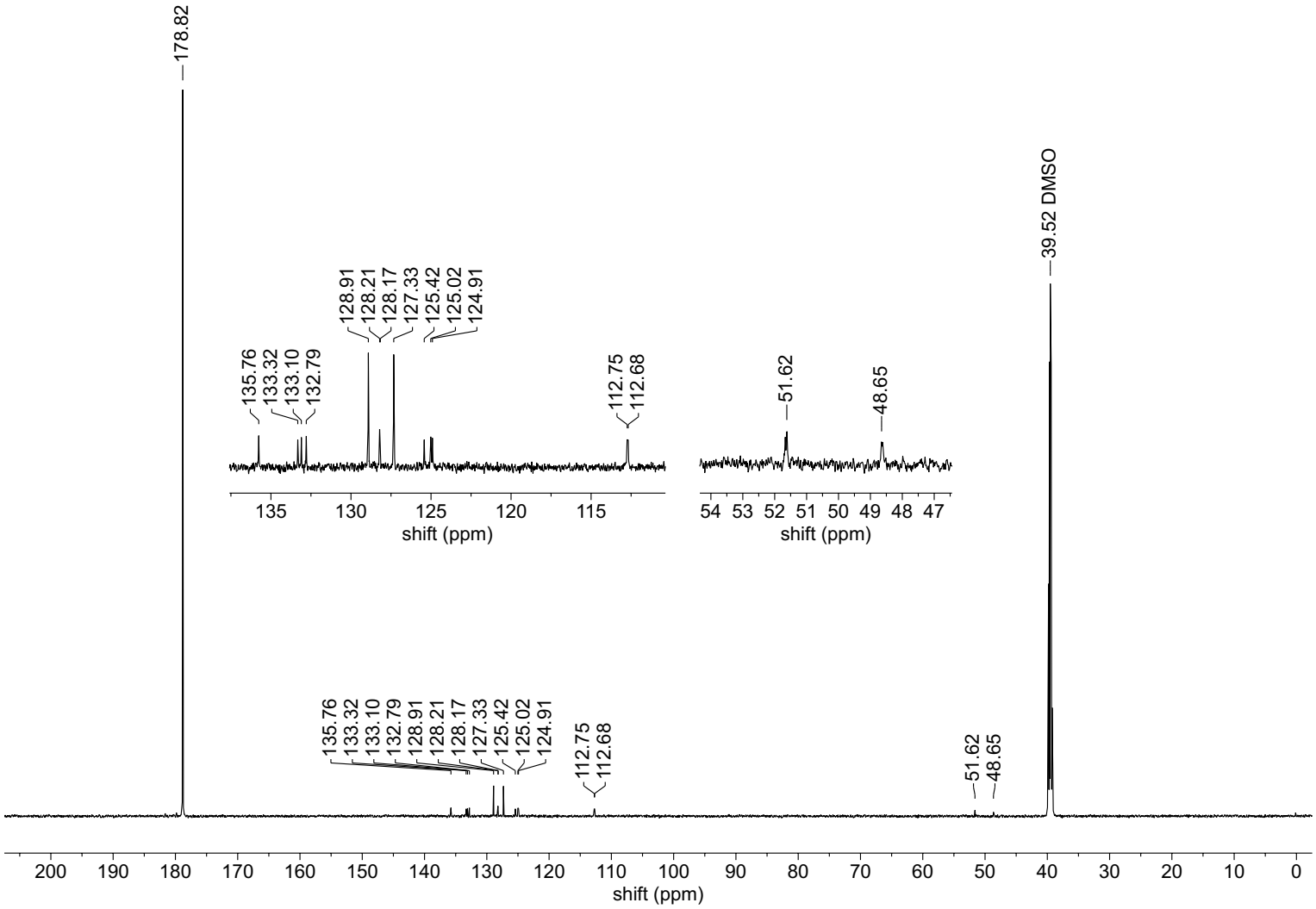

Figure S43. $^{13}C\{^{1}H\}$ NMR spectrum (DMSO- d_6, 151 MHz) of **^{13}C-2a**.

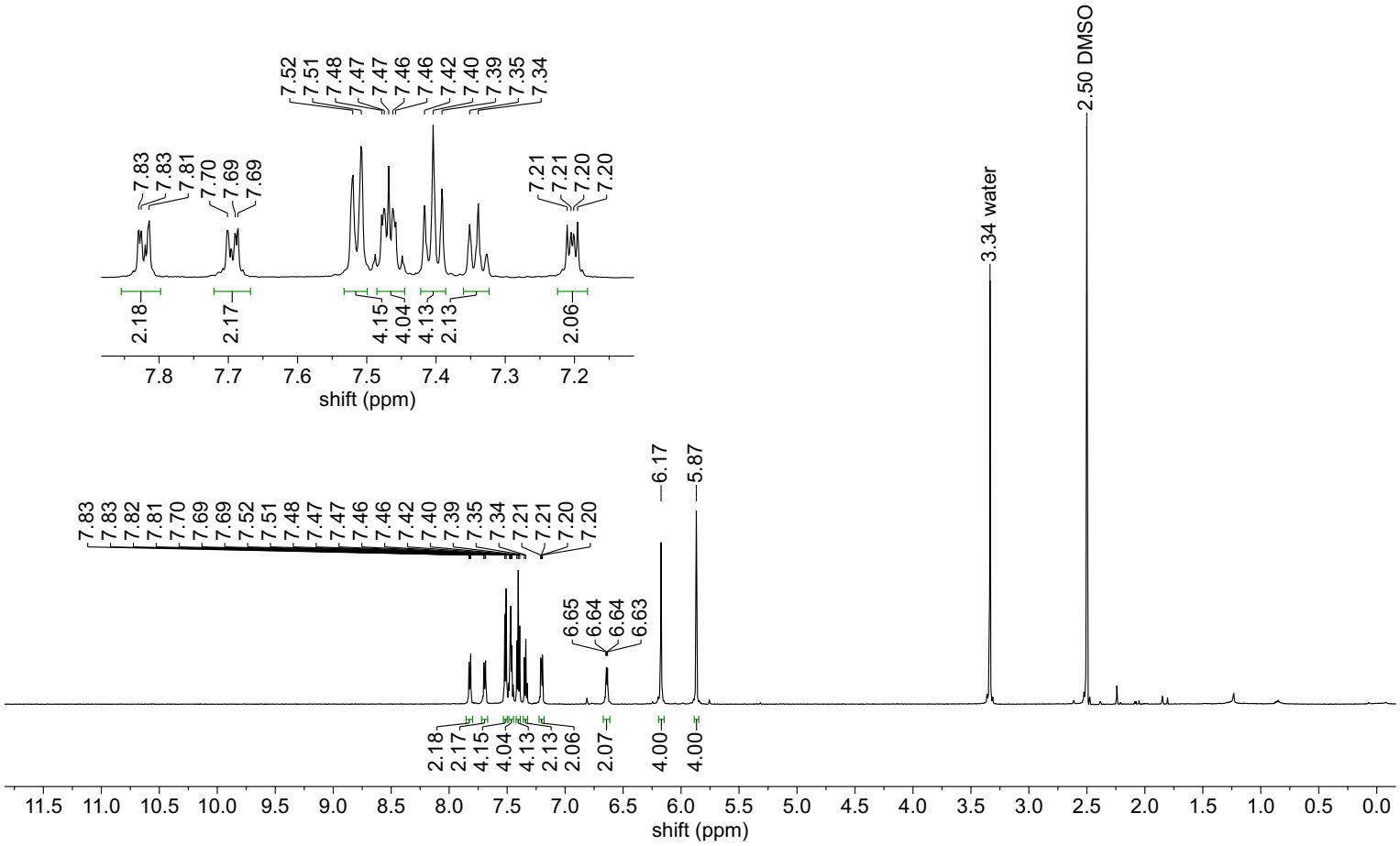

Figure S44. ^{1}H NMR spectrum (DMSO- d_6, 600 MHz) of **2b**.

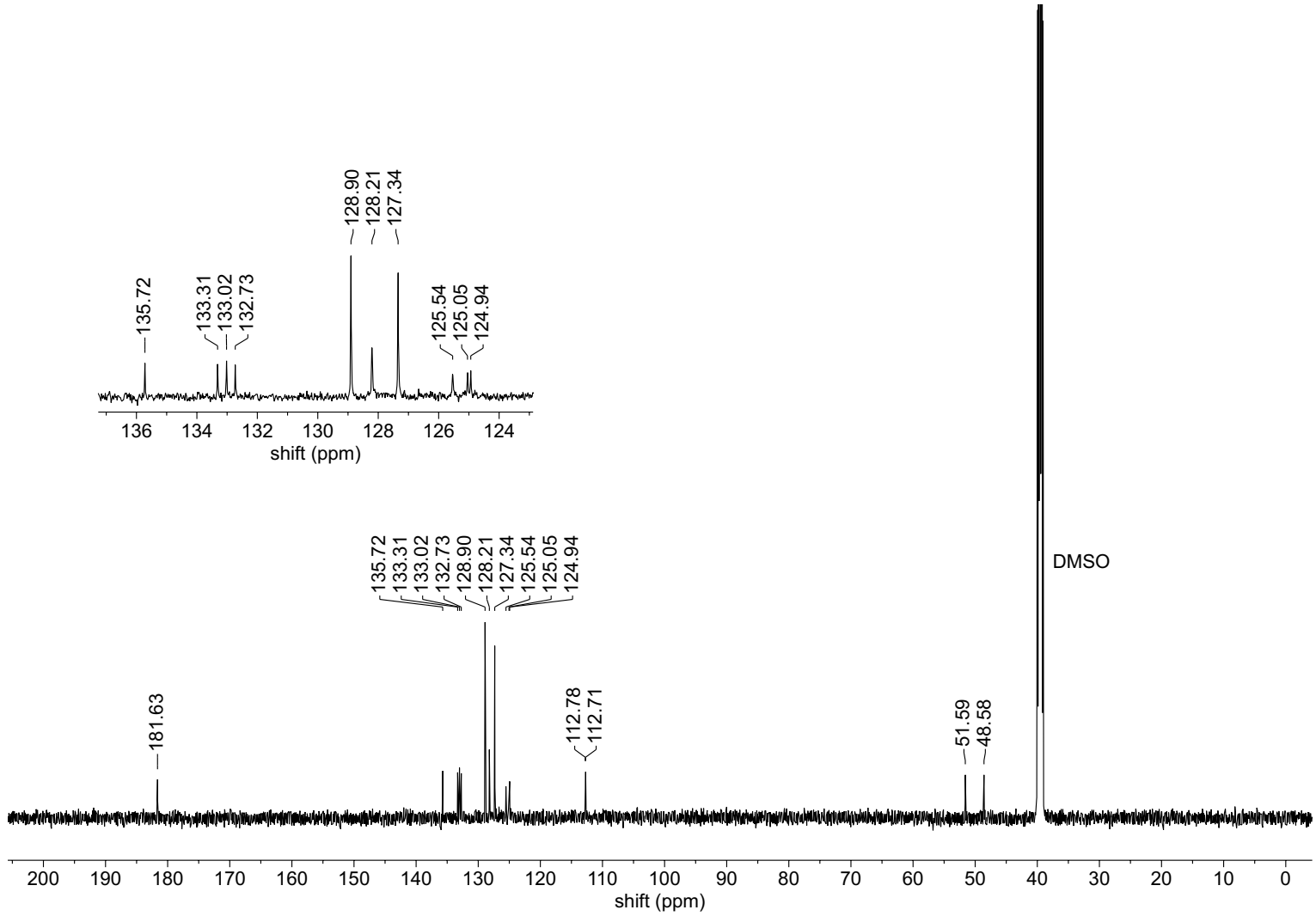

Figure S45. $^{13}C\{^{1}H\}$ NMR spectrum (DMSO- d_6, 151 MHz) of **2b**.

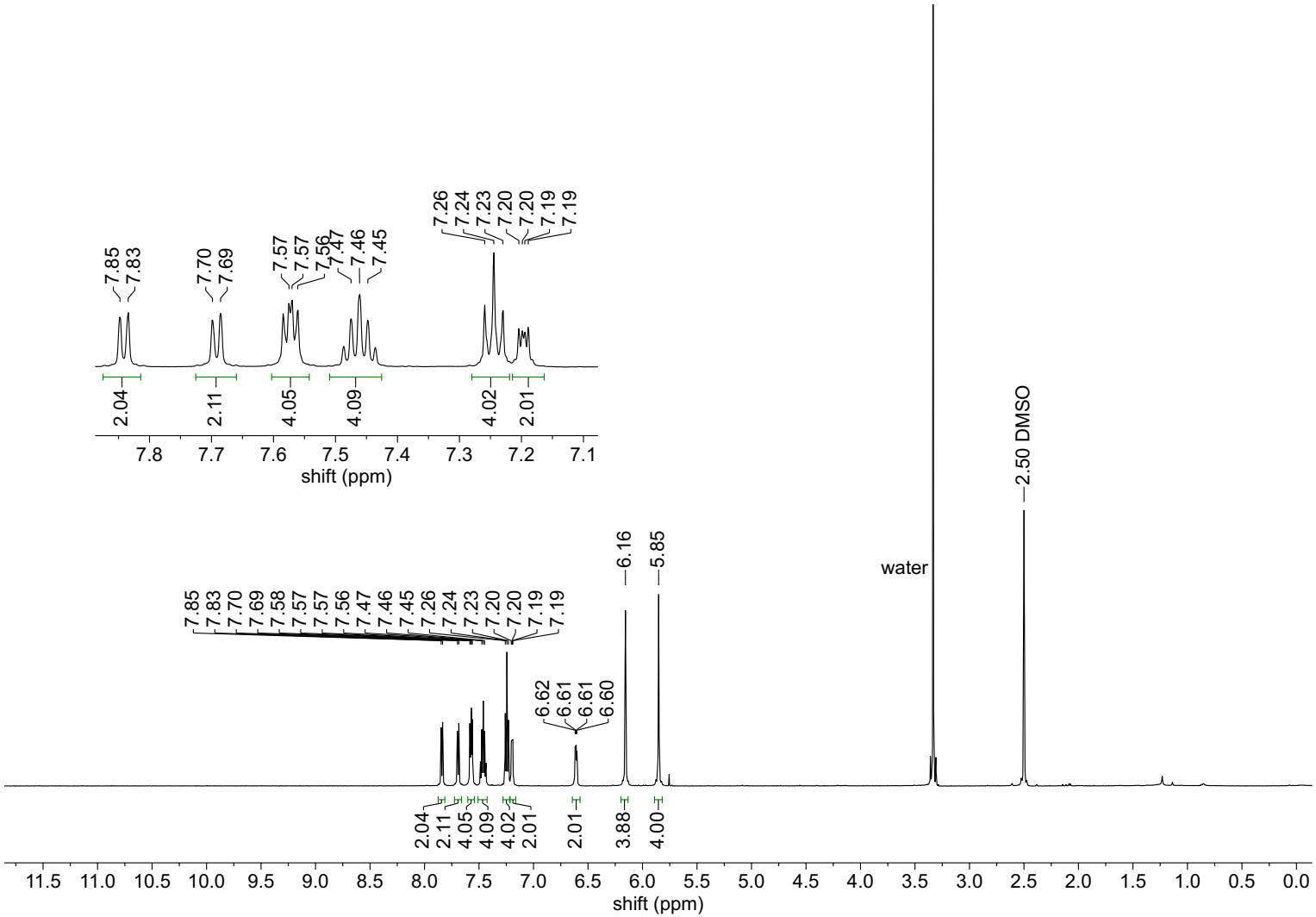

Figure S46. ^{1}H NMR spectrum (DMSO- d_6, 600 MHz) of **2c**.

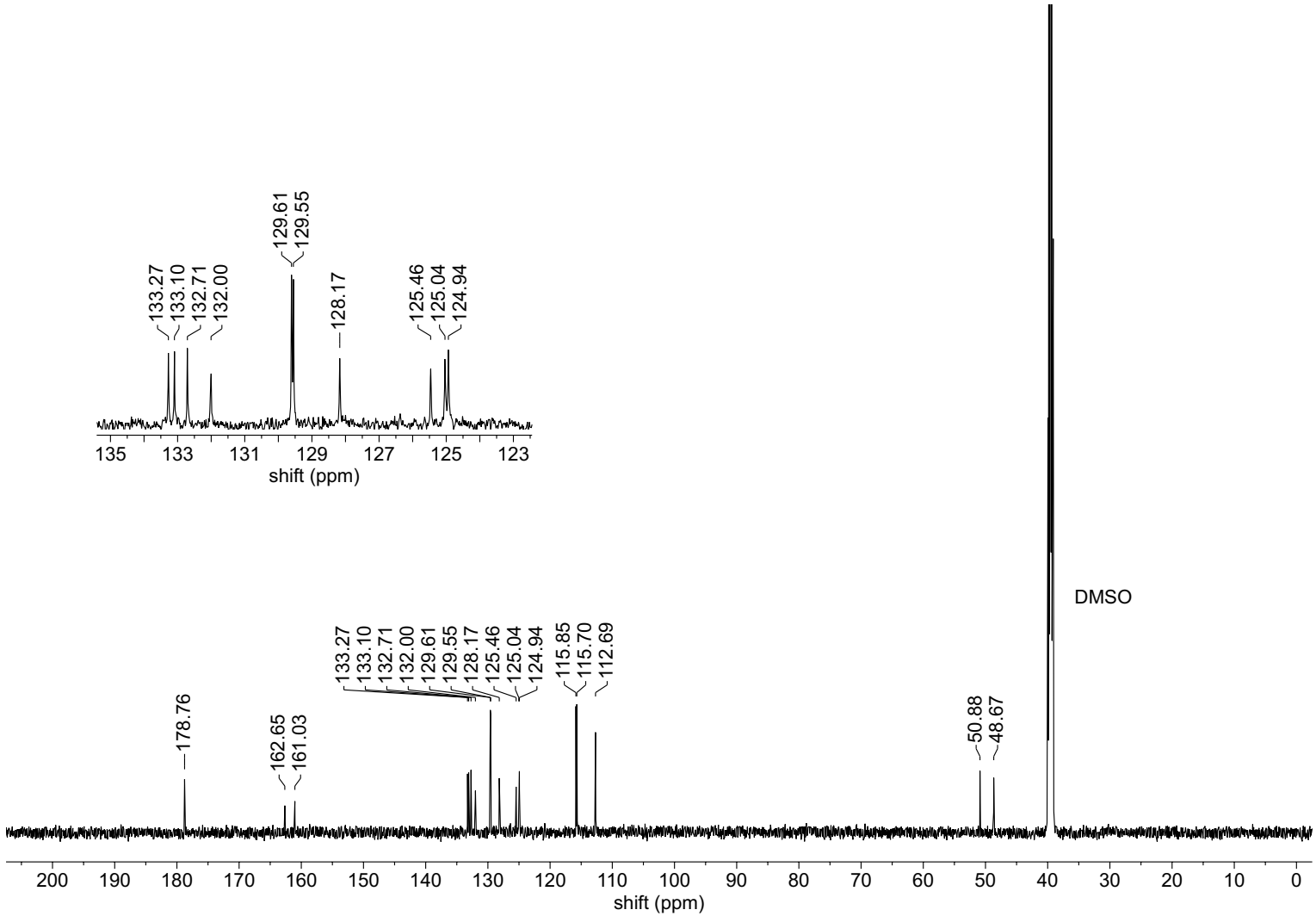

Figure S47. $^{13}C\{^{1}H\}$ NMR spectrum (DMSO-d_6, 151 MHz) of **2c**.

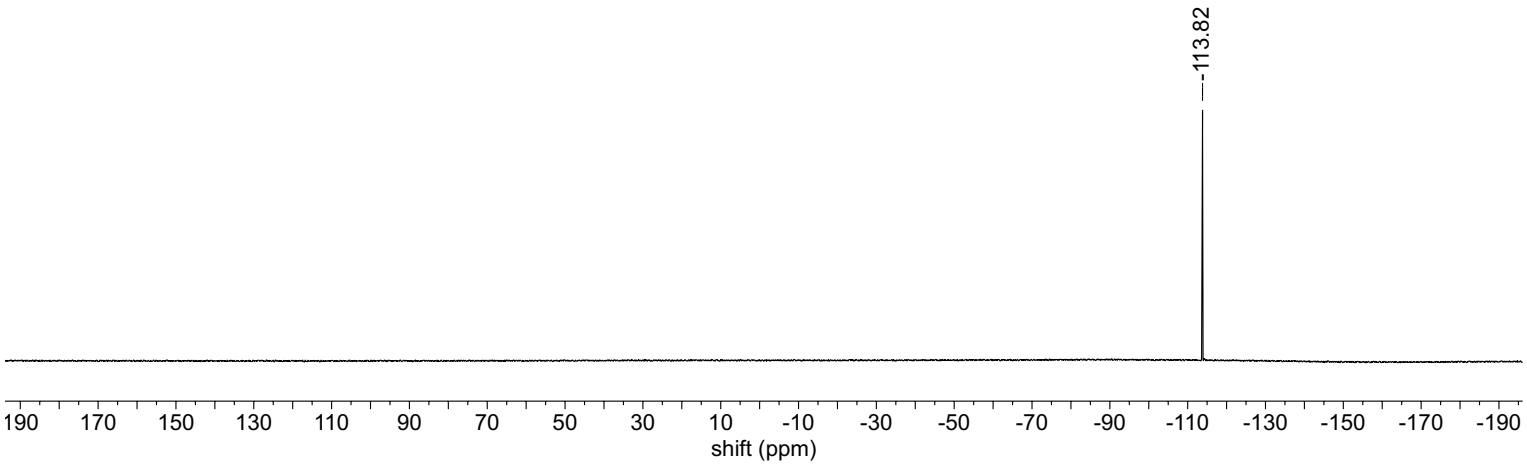

Figure S48. ^{19}F NMR spectrum (DMSO- d_6, 376 MHz) of **2c**.

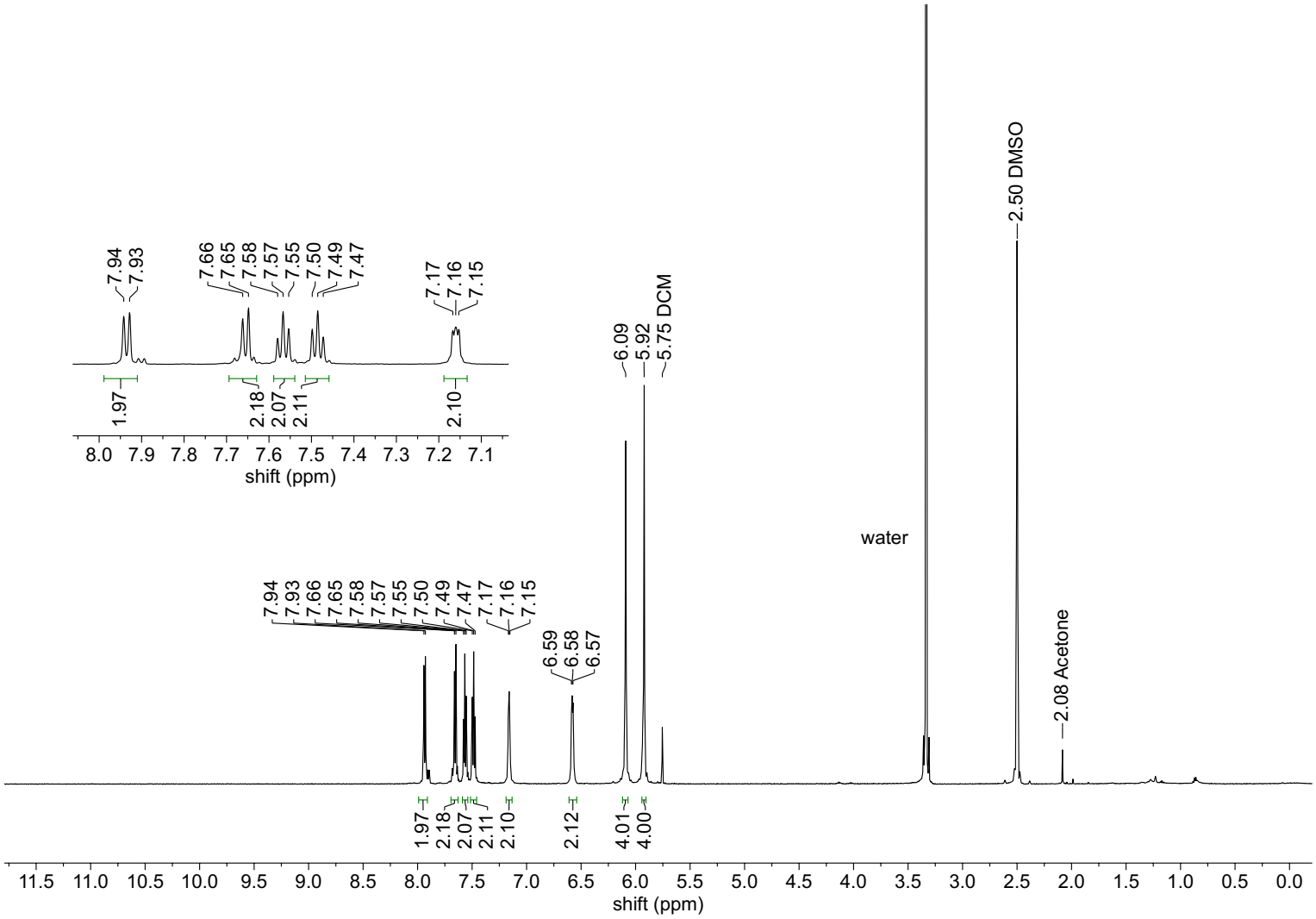

Figure S49. ^{1}H NMR spectrum (DMSO- d_6, 600 MHz) of **2d**.

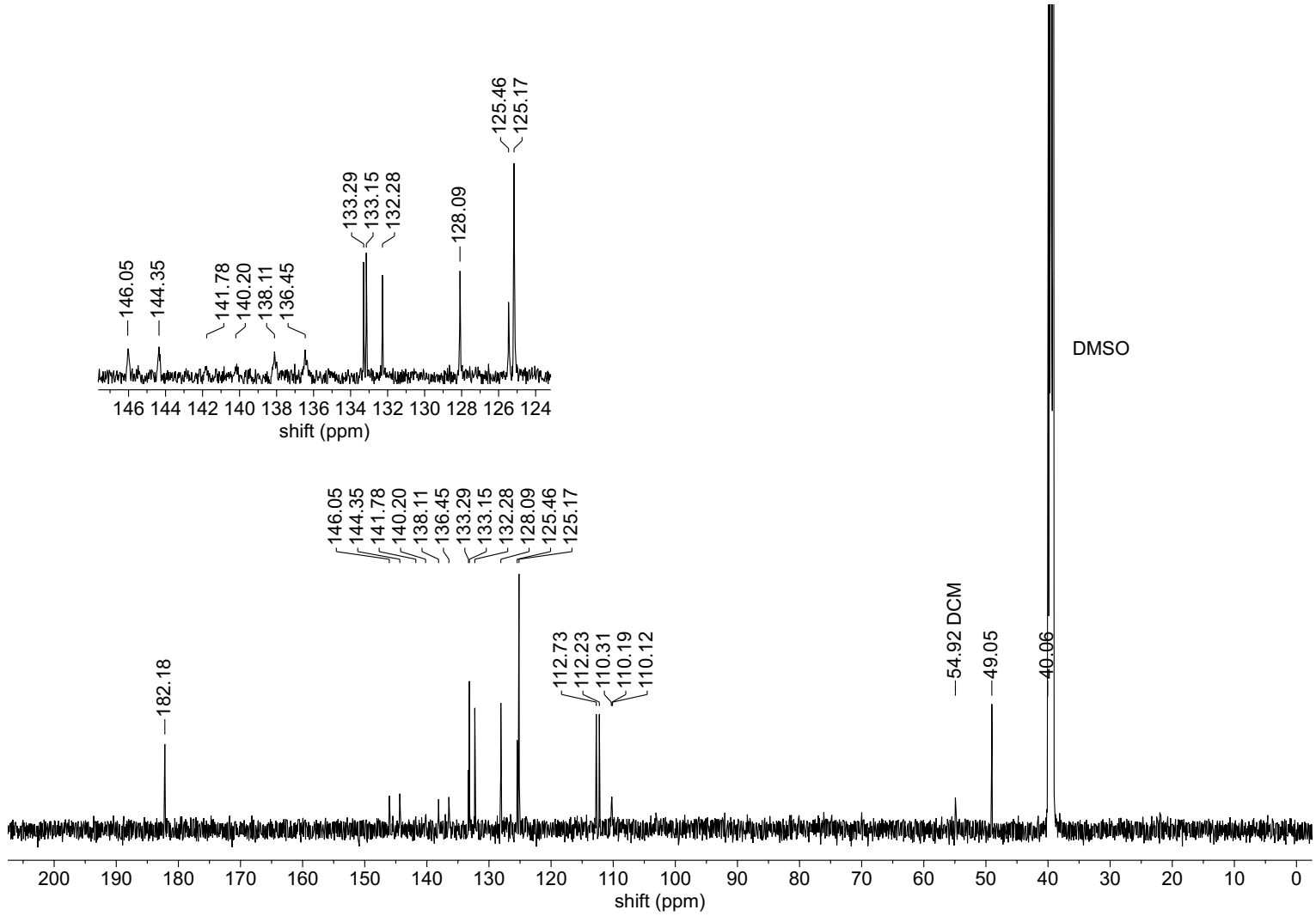

Figure S50. $^{13}C\{^{1}H\}$ NMR spectrum (DMSO- d_6, 151 MHz) of **2d**.

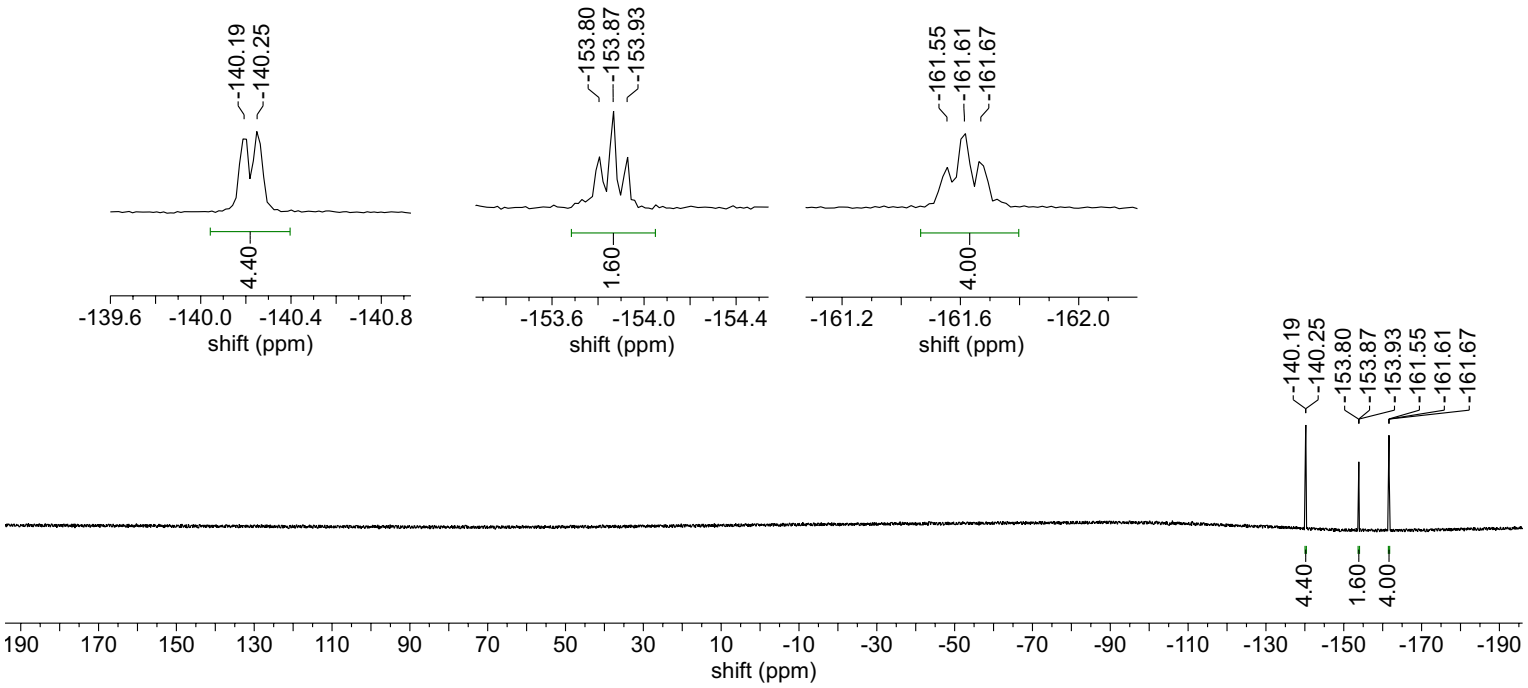

Figure S51. ^{19}F NMR spectrum (DMSO- d_6, 376 MHz) of **2d**.

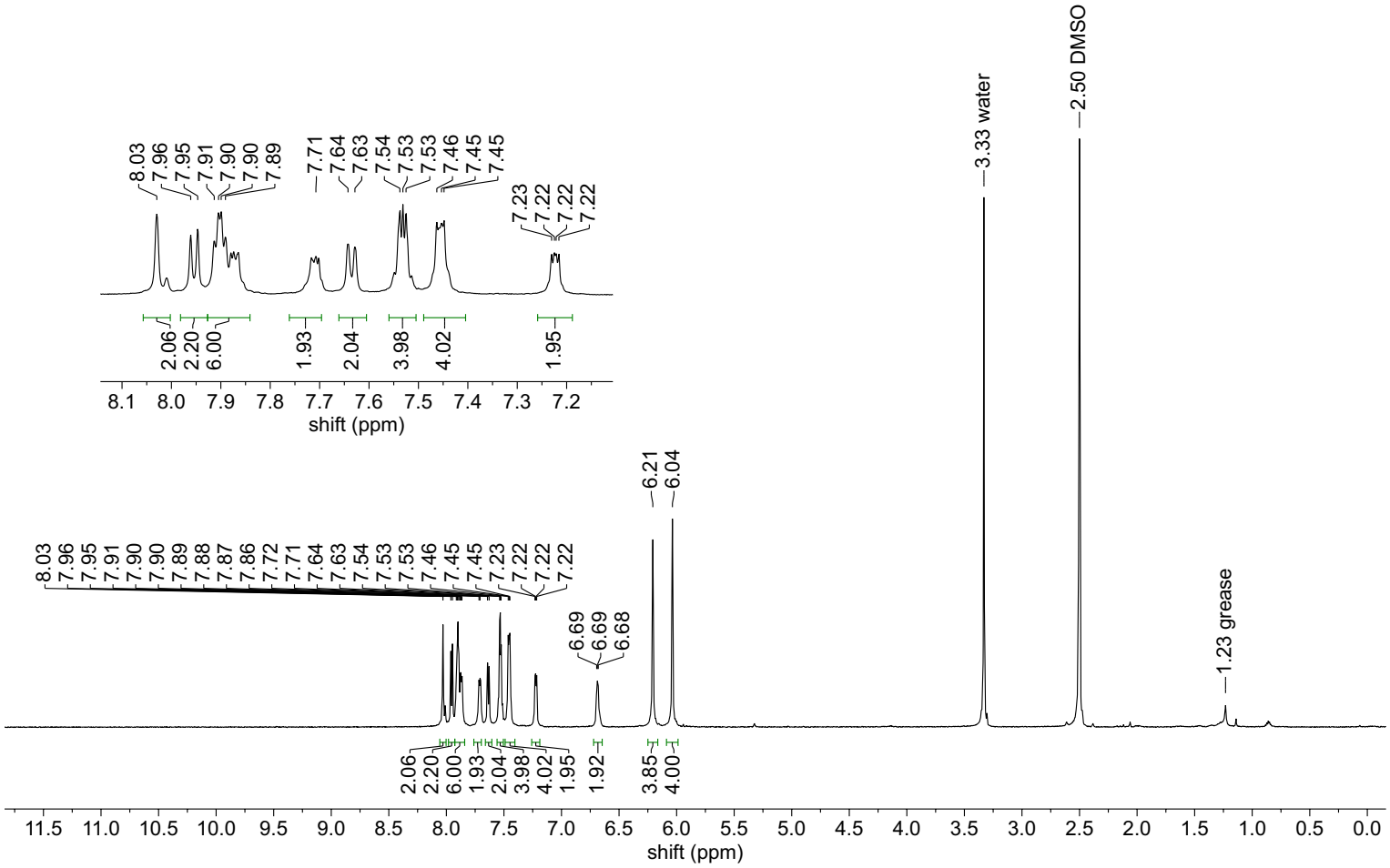

Figure S52. ^{1}H NMR spectrum (DMSO- d_6, 600 MHz) of **2e**.

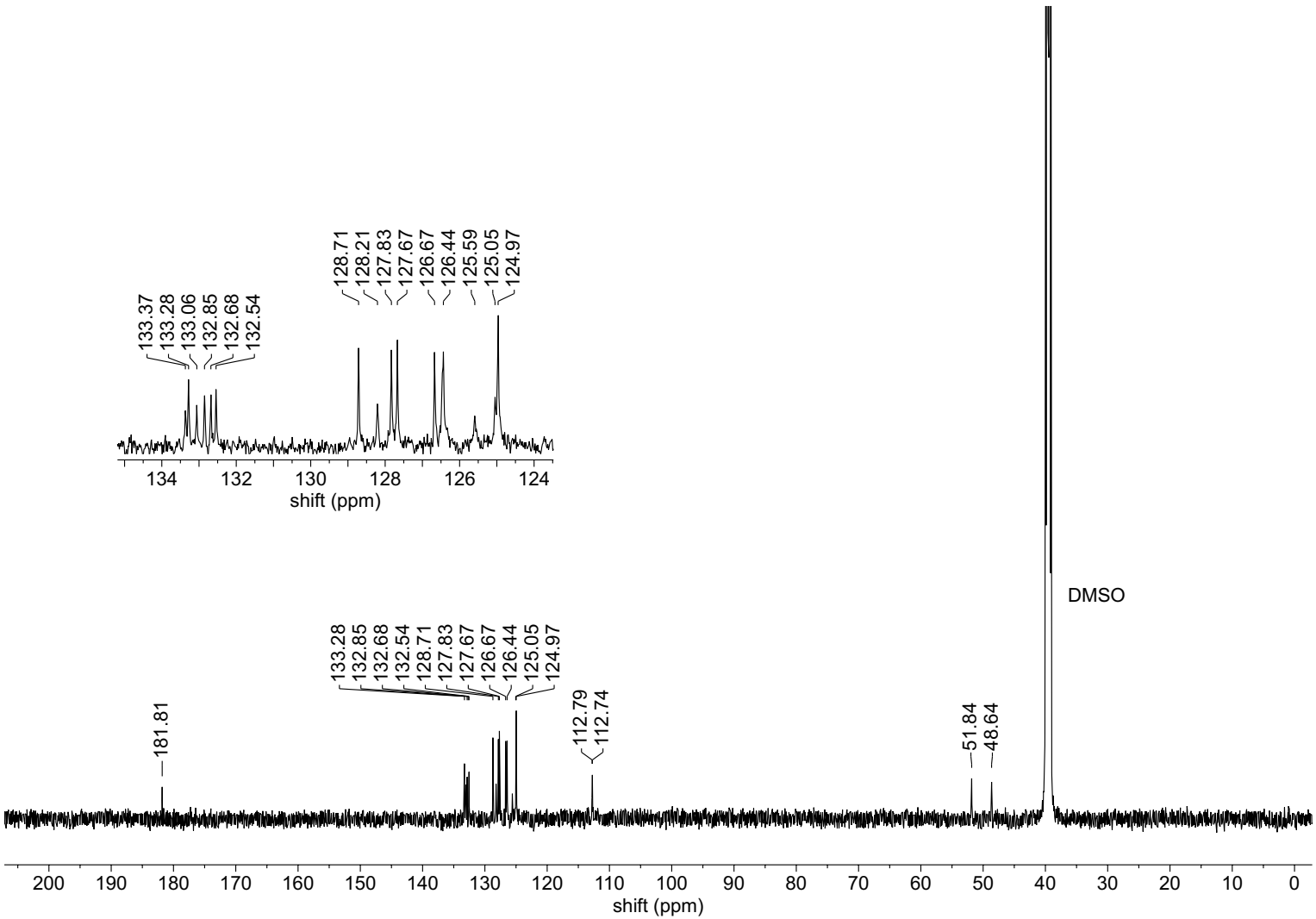

Figure S53. $^{13}C\{^{1}H\}$ NMR spectrum (DMSO- d_6, 151 MHz) of **2e**.

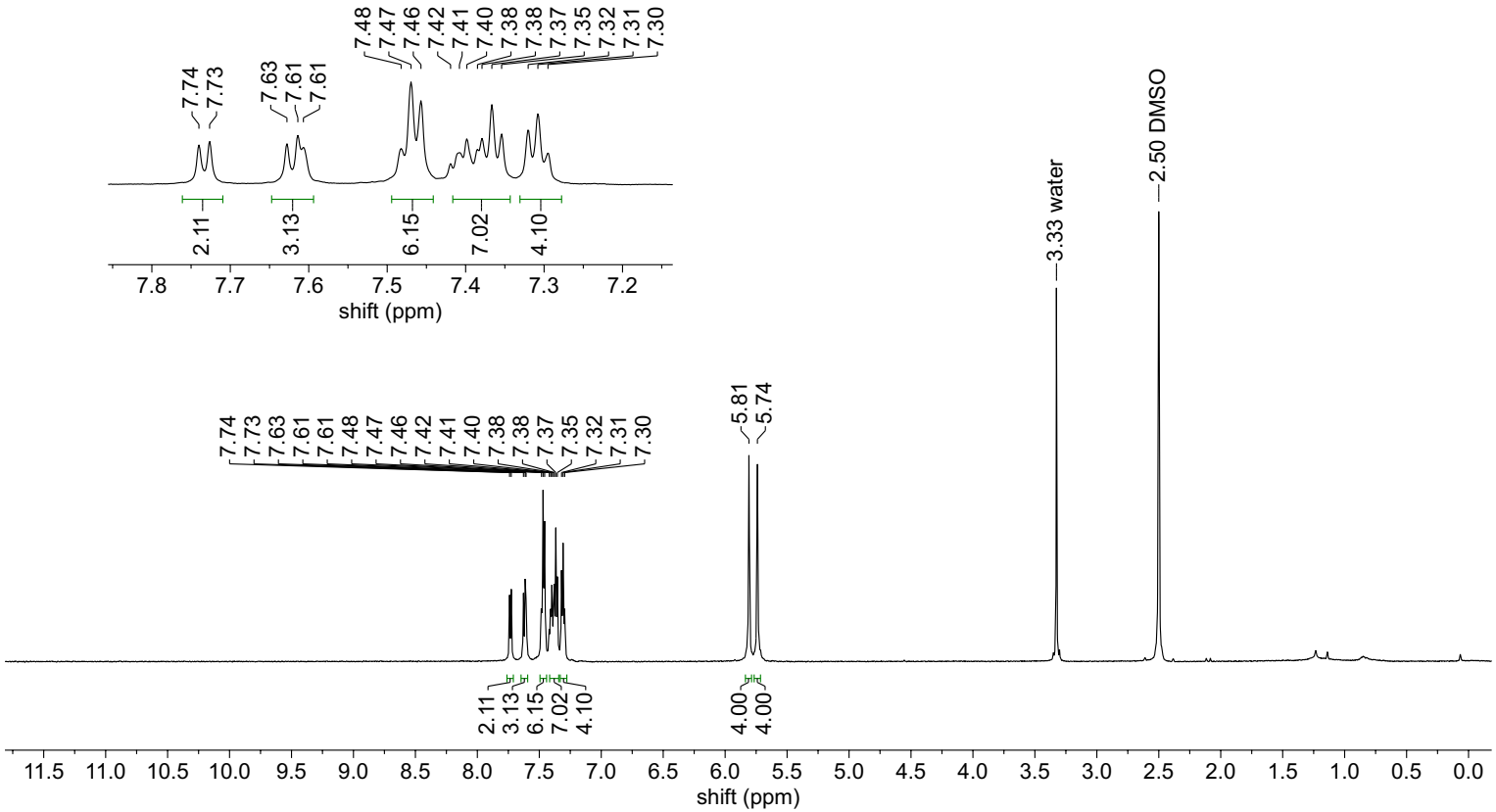

Figure S54. ^{1}H NMR spectrum (DMSO- d_6, 600 MHz) of **2f**.

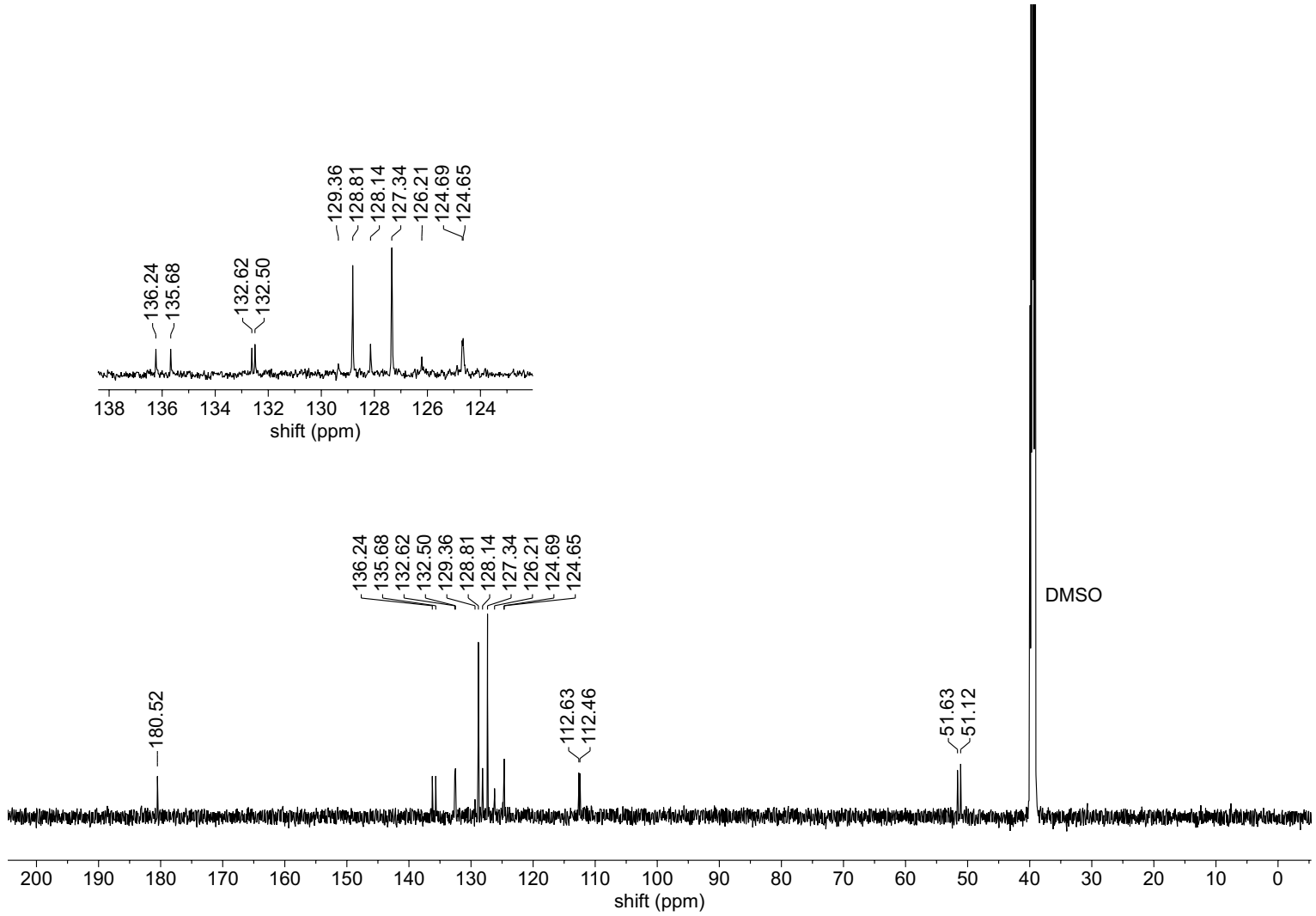

Figure S55. $^{13}C\{^{1}H\}$ NMR spectrum (DMSO- d_6, 151 MHz) of **2f**.

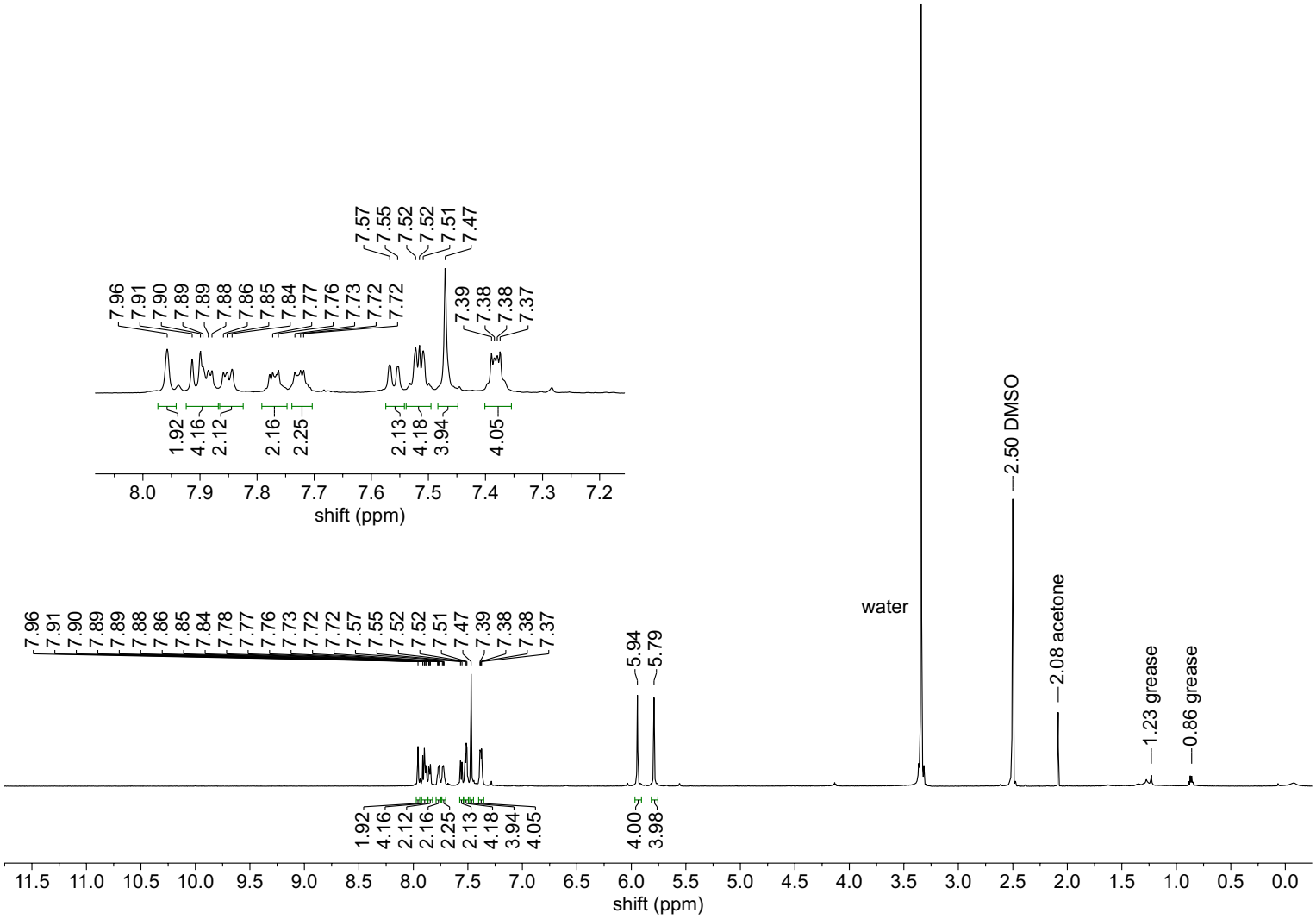

Figure S56. ^{1}H NMR spectrum (DMSO- d_6, 600 MHz) of **2g**.

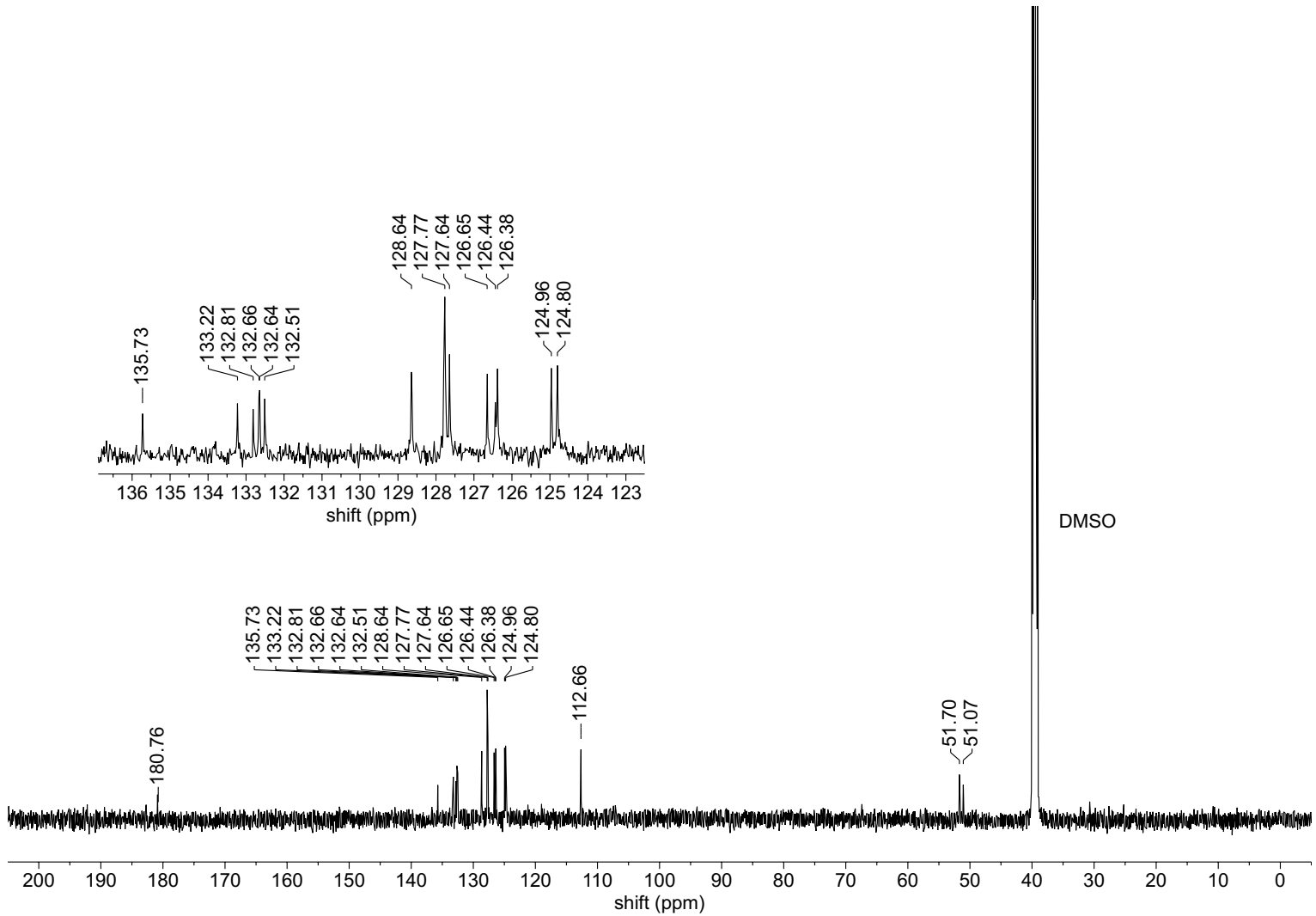

Figure S57. $^{13}C\{^{1}H\}$ NMR spectrum (DMSO- d_6, 151 MHz) of **2g**.

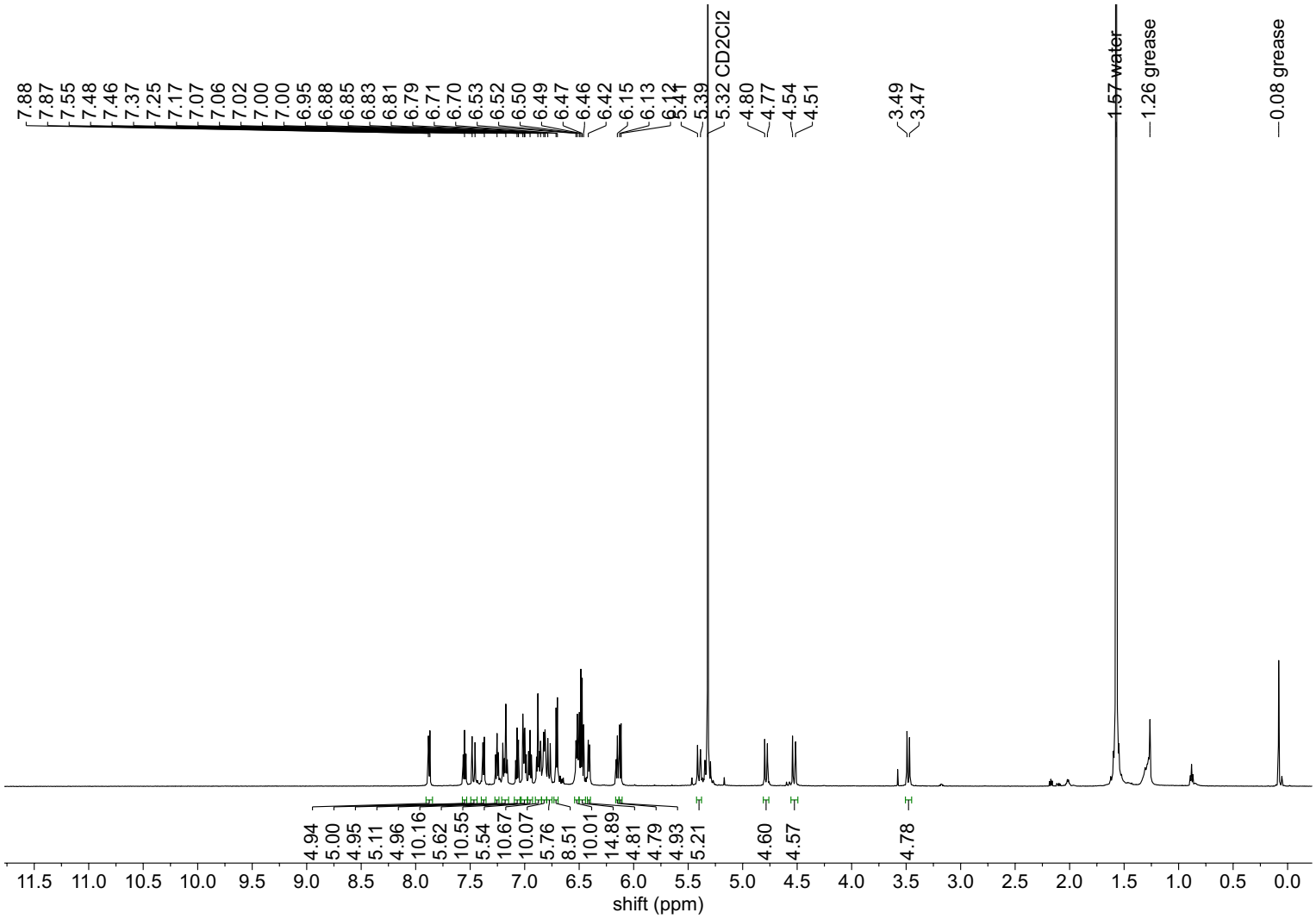

Figure S58. ^{1}H NMR spectrum (CD_2Cl_2, 600 MHz) of [**3a**]Cl_3.

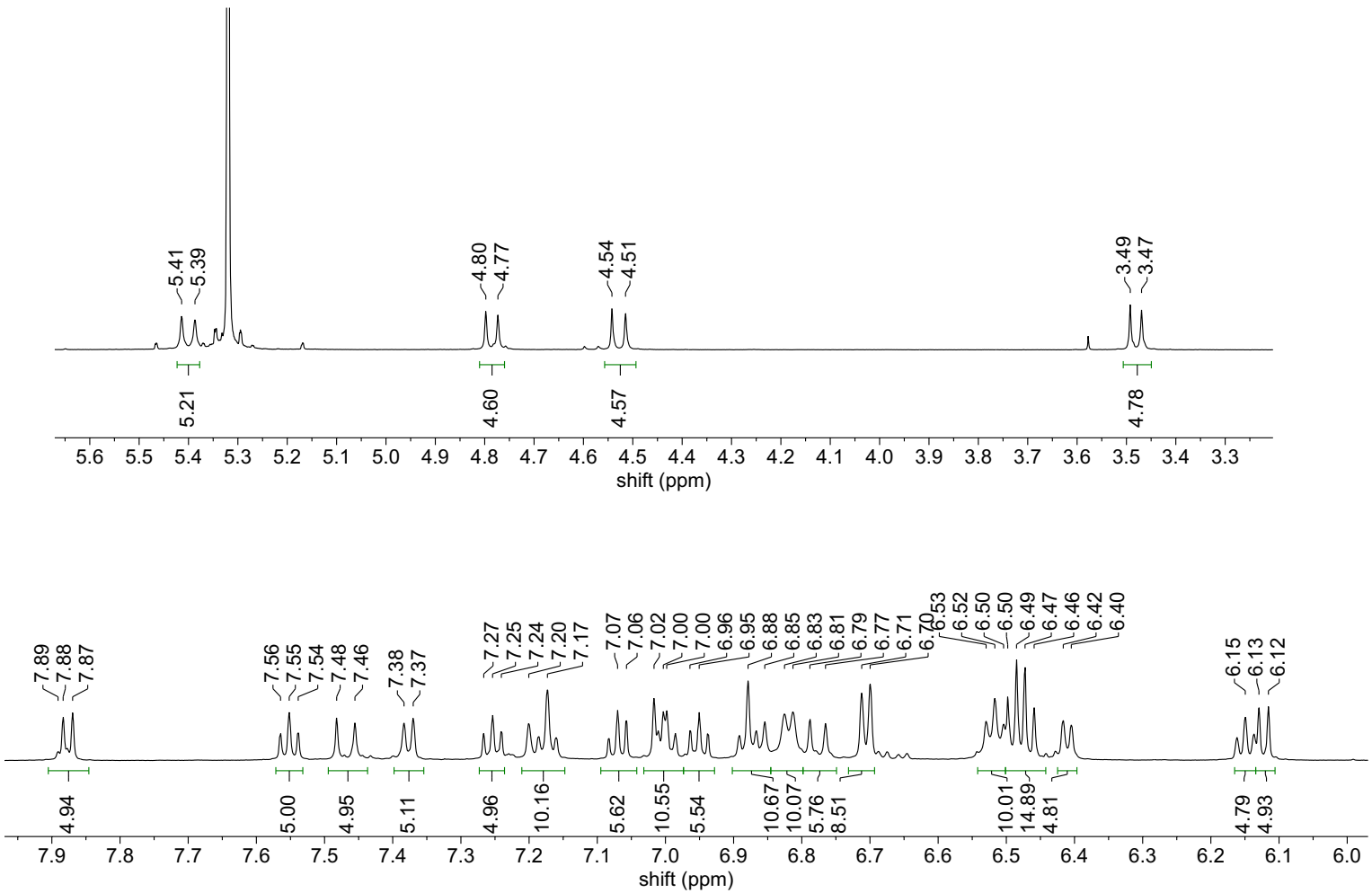

Figure S59. ^{1}H NMR spectrum (CD_2Cl_2, 600 MHz) of [**3a**]Cl_3 showing expanded aryl and alkyl regions.

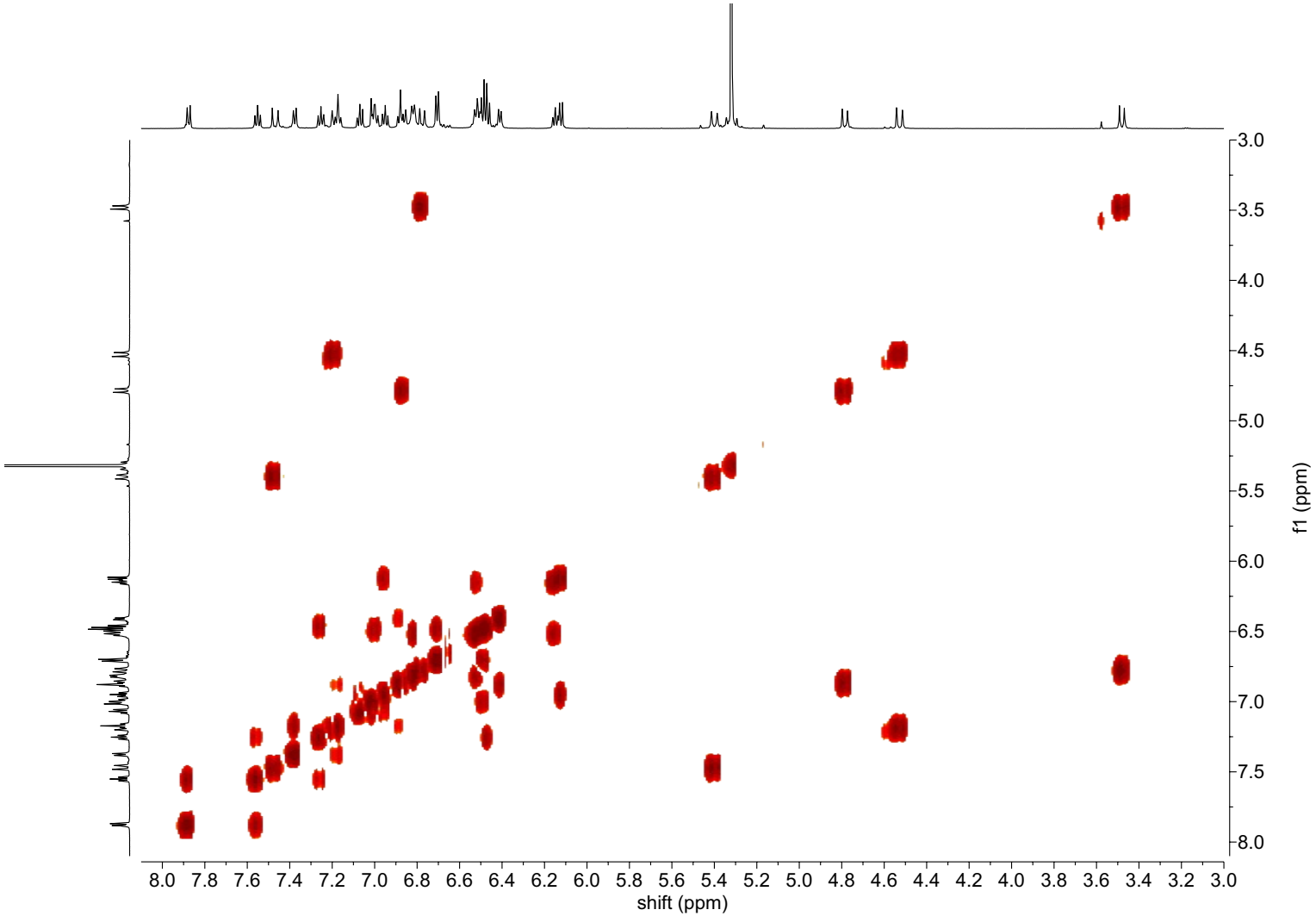

Figure S60. ^{1}H-^{1}H COSY NMR spectrum (CD_2Cl_2, 600 MHz) of [**3a**]Cl_3.

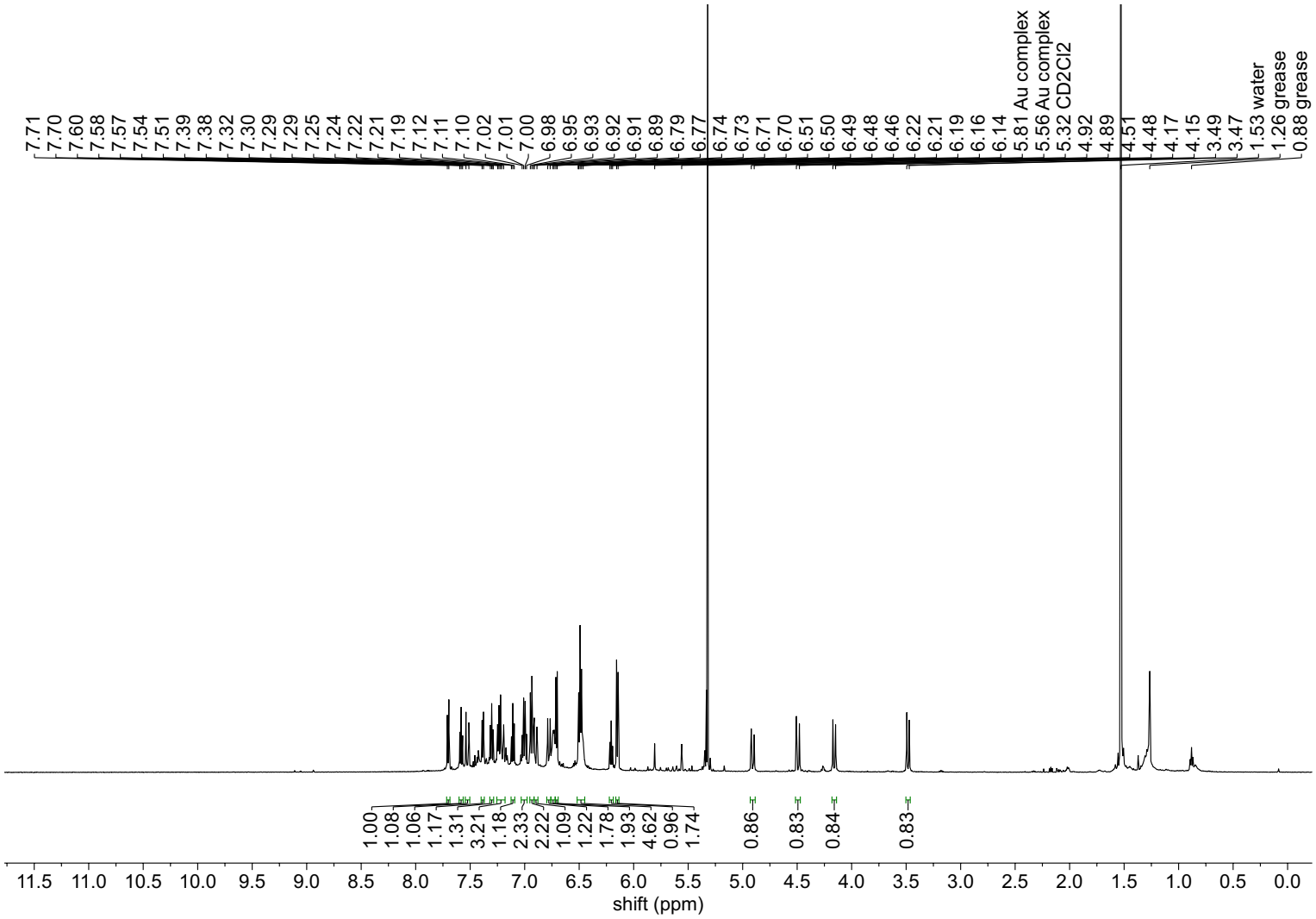

Figure S61. ^{1}H NMR spectrum (CD_2Cl_2, 600 MHz) of [**3a**][PF_6]$_3$.

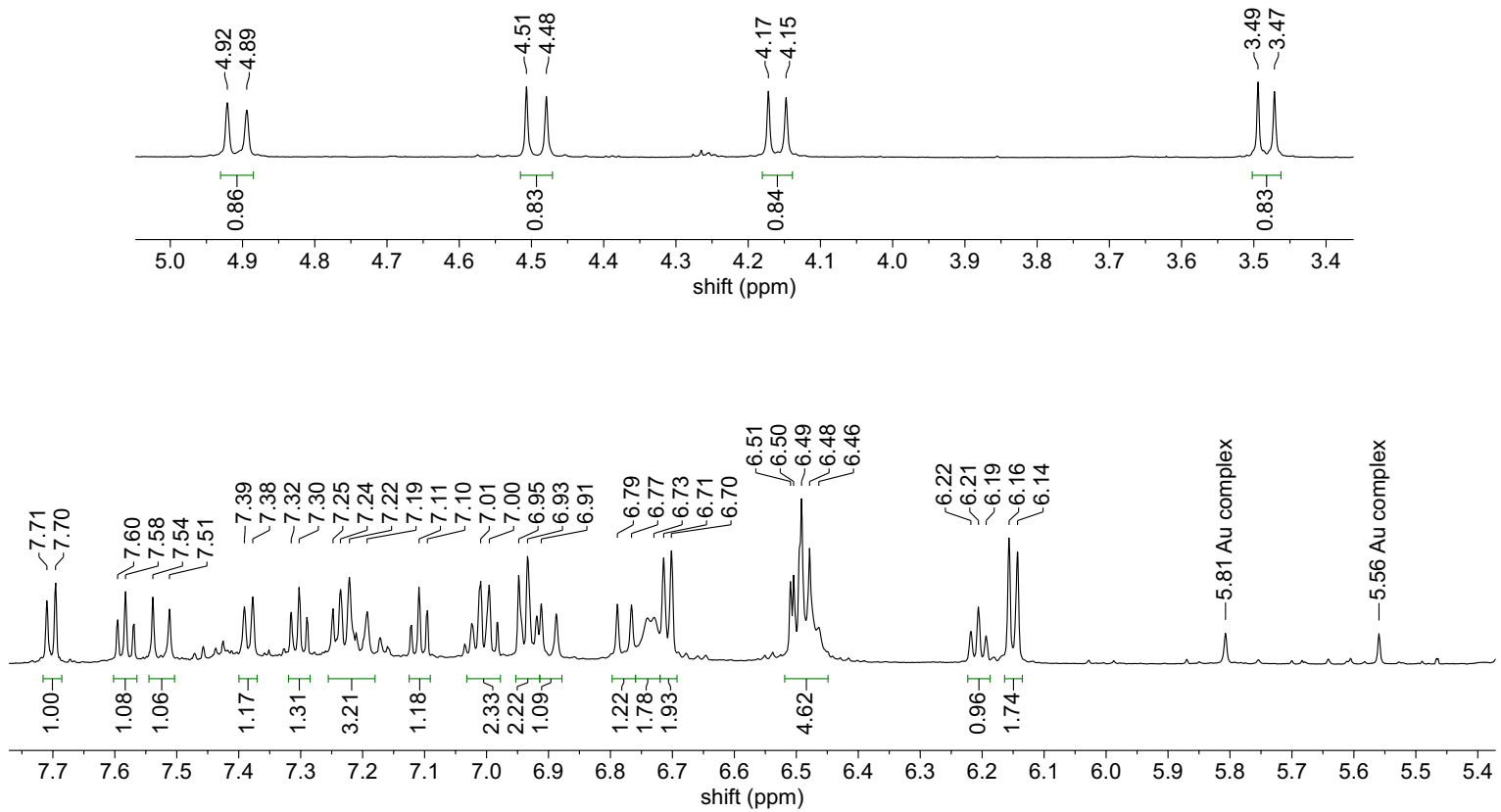

Figure S62. ^{1}H NMR spectrum (CD_2Cl_2, 600 MHz) of [**3a**][PF_6]$_3$ showing expanded aryl and alkyl regions. ESI-MS suggests the Au complex is $[L_2Au_2]Cl_2$.

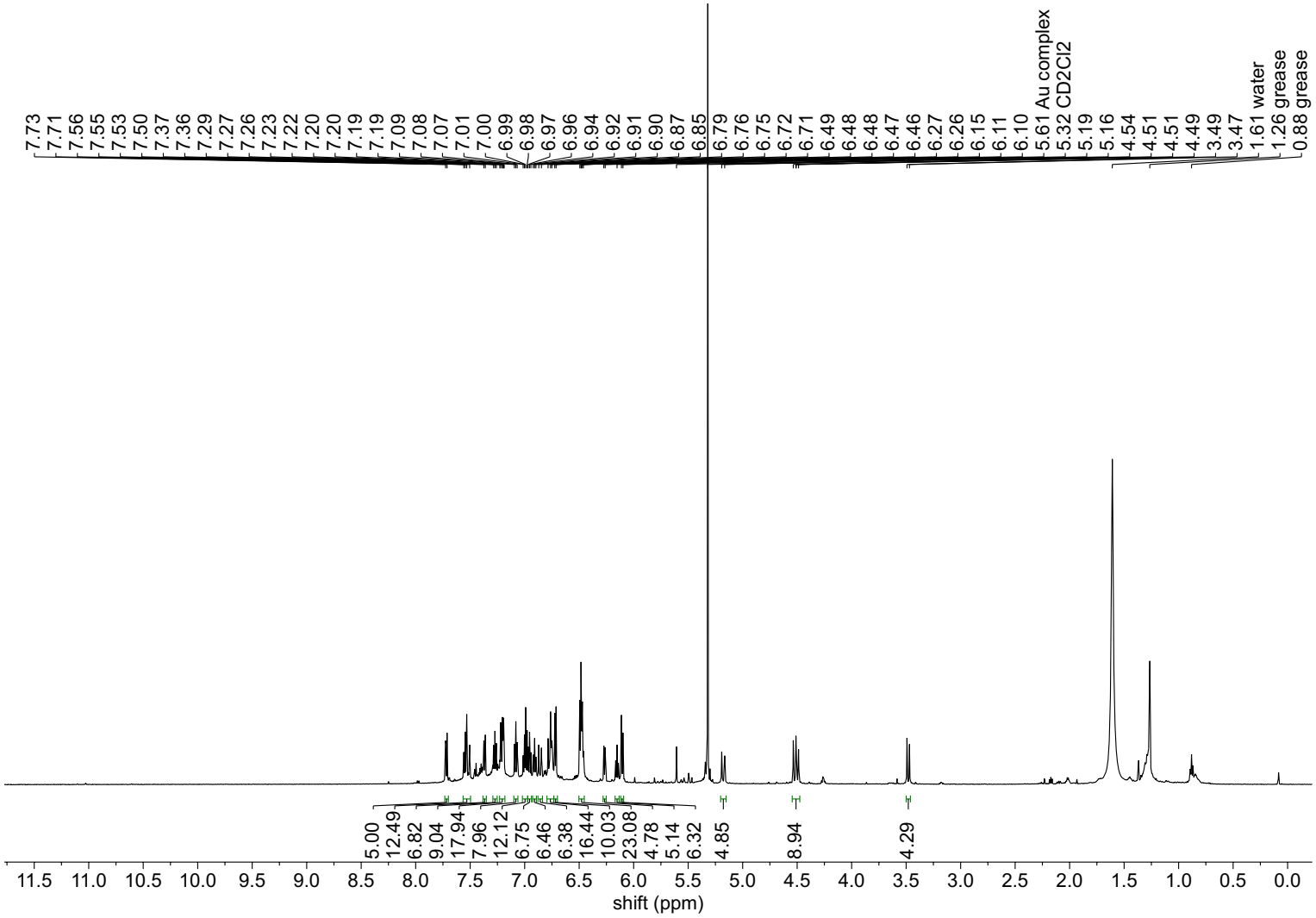

Figure S63. ^{1}H NMR spectrum (CD_2Cl_2, 600 MHz) of [**3a**][CO_2CF_3]$_3$.

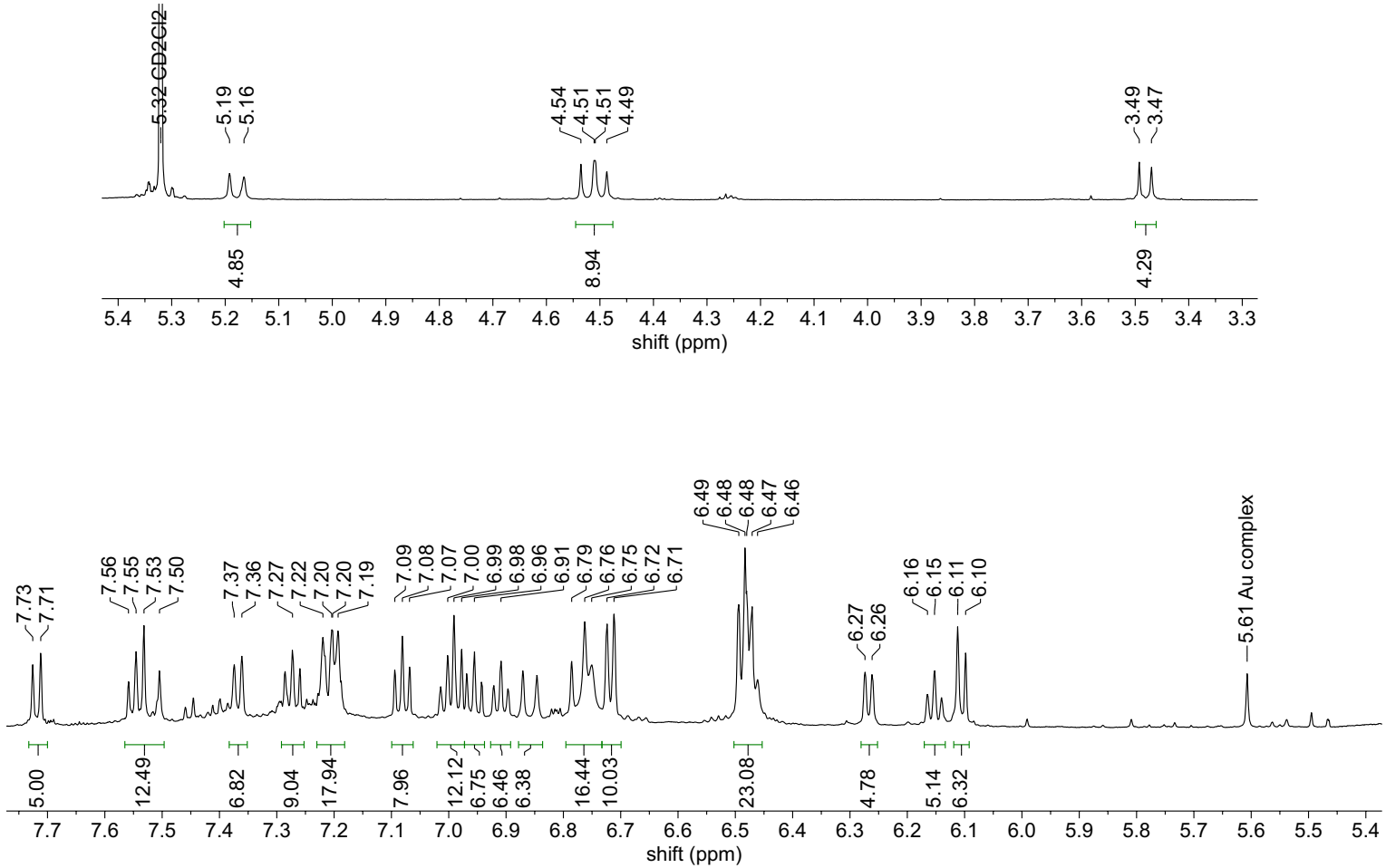

Figure S64. ^{1}H NMR spectrum (CD_2Cl_2, 600 MHz) of [**3a**][CO_2CF_3]$_3$ showing expanded aryl and alkyl regions. ESI-MS suggests the Au complex is [L_2Au_2]Cl_2.

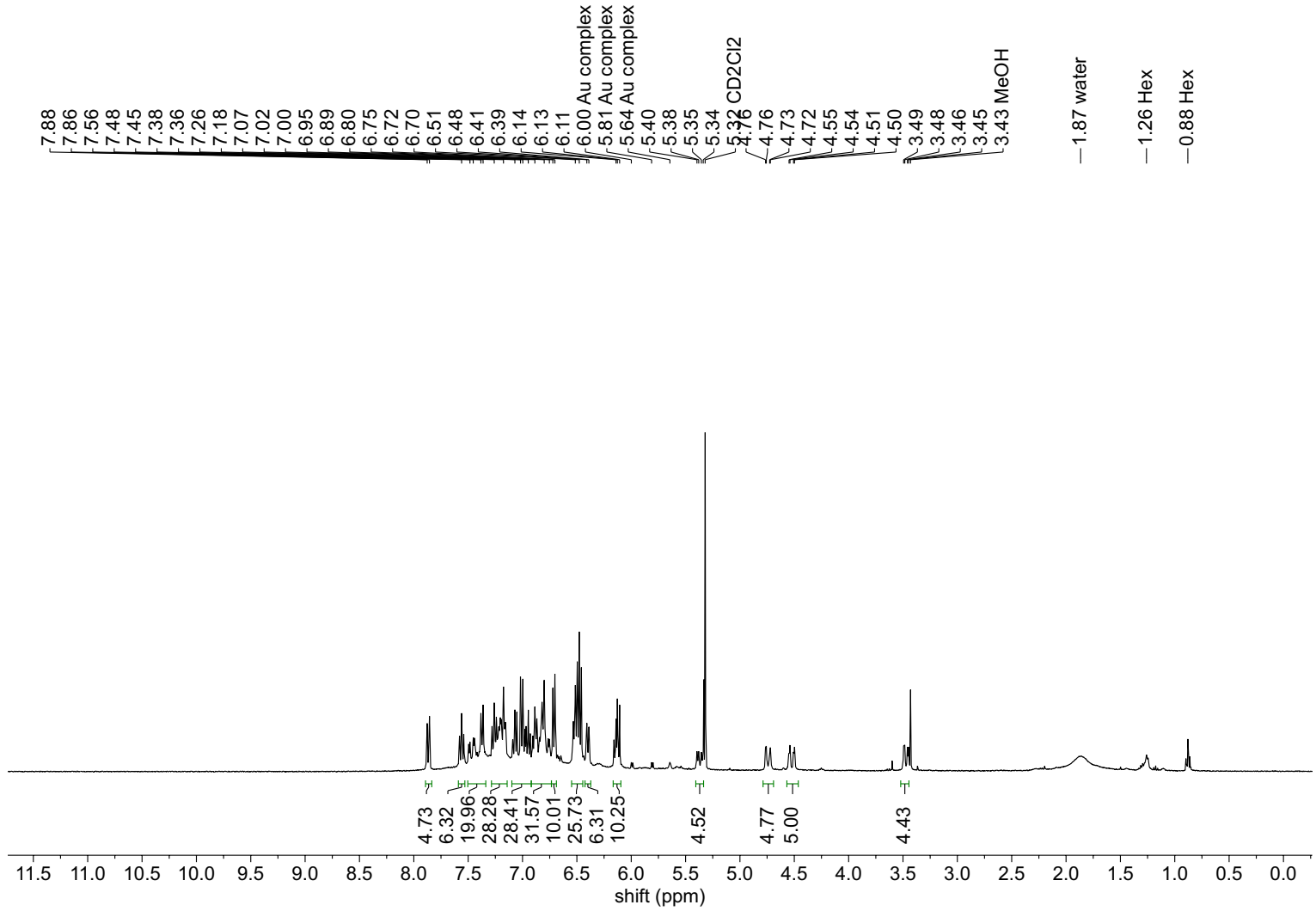

Figure S65. ^{1}H NMR spectrum (CD_2Cl_2, 600 MHz) of **^{13}C-[3a]**Cl_3.

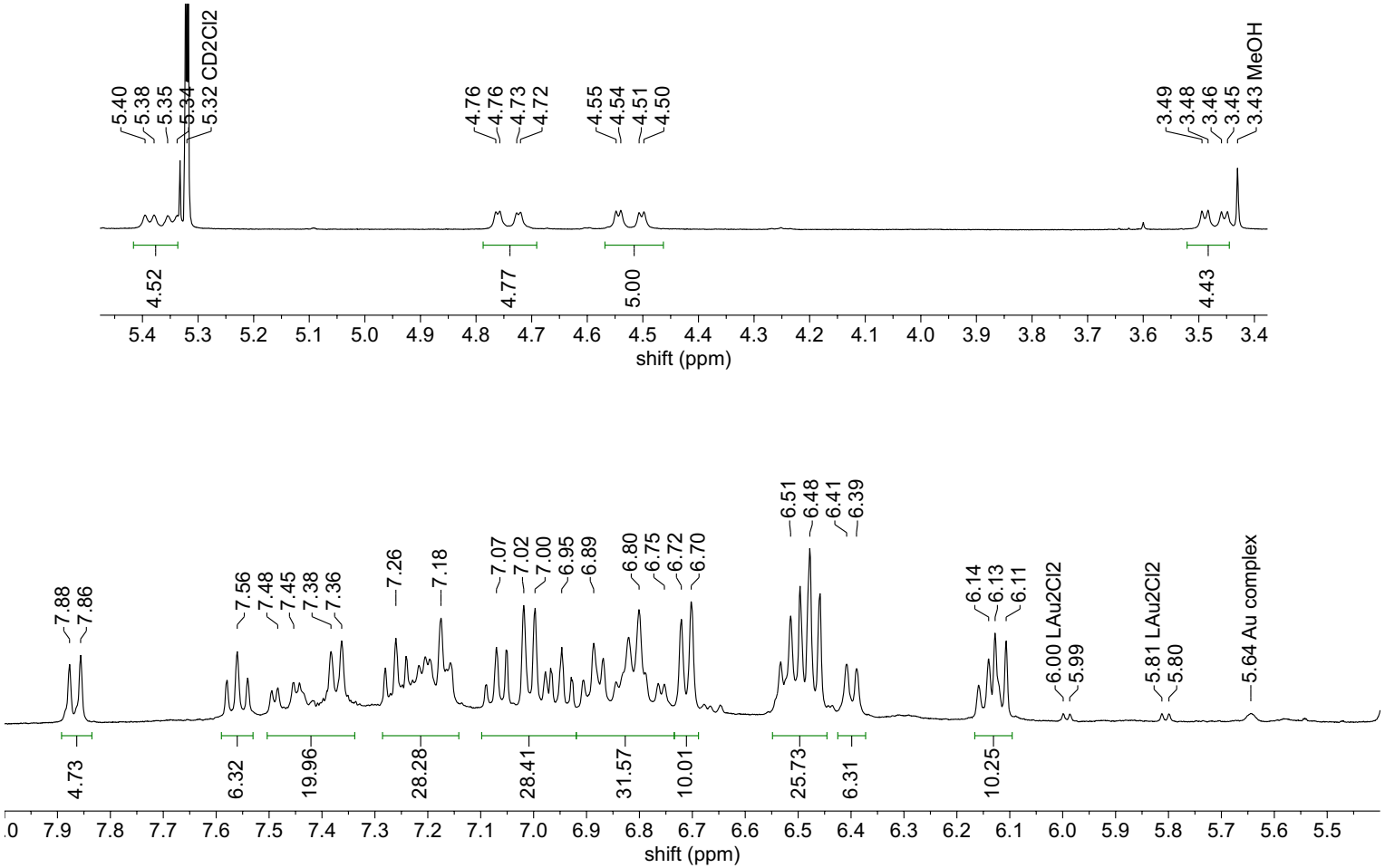

Figure S66. ^{1}H NMR spectrum (CD_2Cl_2, 600 MHz) of **^{13}C-[3a]**Cl_3 showing expanded aryl and alkyl regions. ESI-MS suggests the Au complex is $[L_2Au_2]Cl_2$.

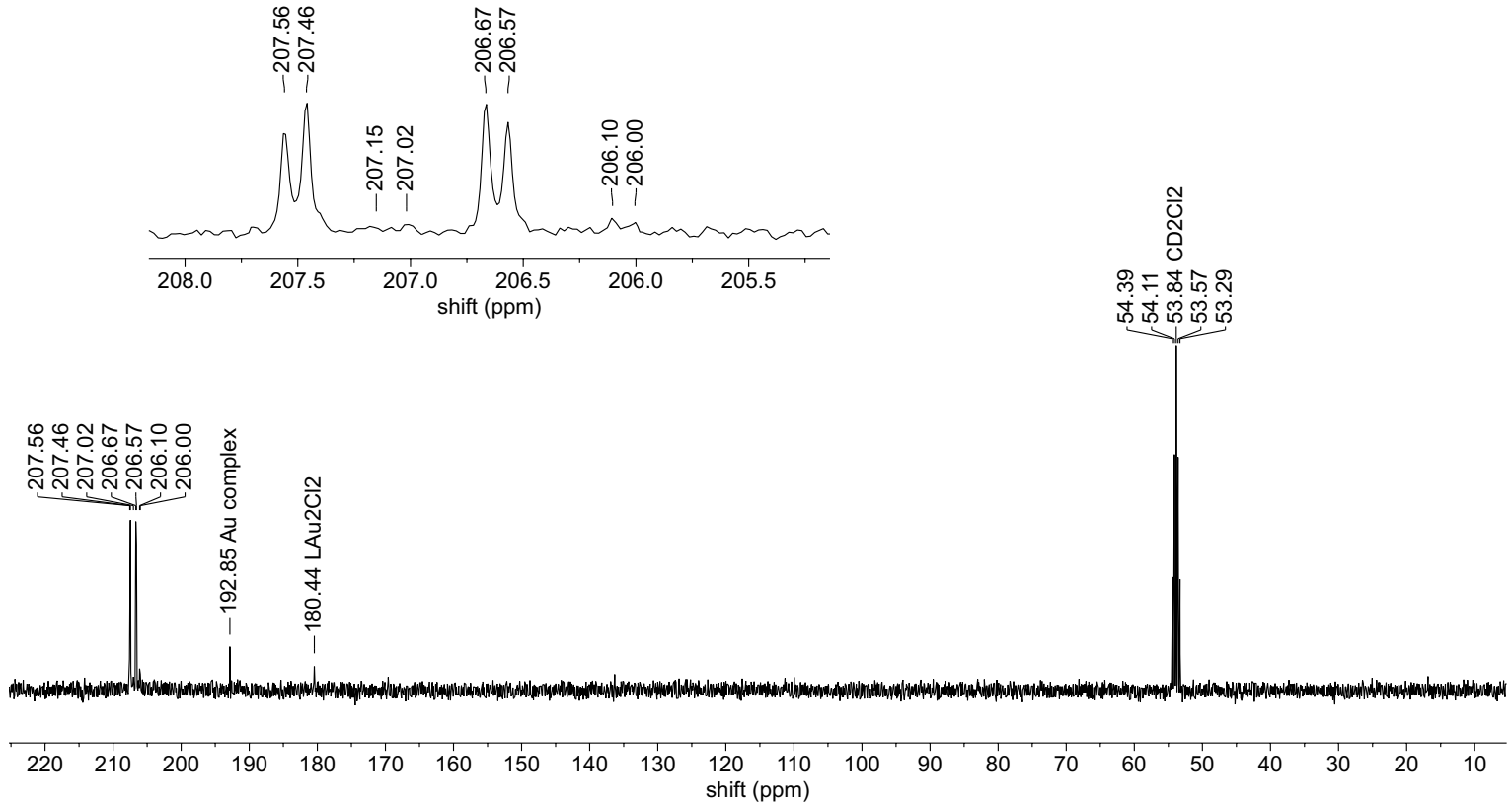

Figure S67. $^{13}C\{^{1}H\}$ NMR spectrum (CD_2Cl_2, 151 MHz) of **^{13}C-[3a]**Cl_3. ESI-MS suggests the Au complex is $[L_2Au_2]Cl_2$.

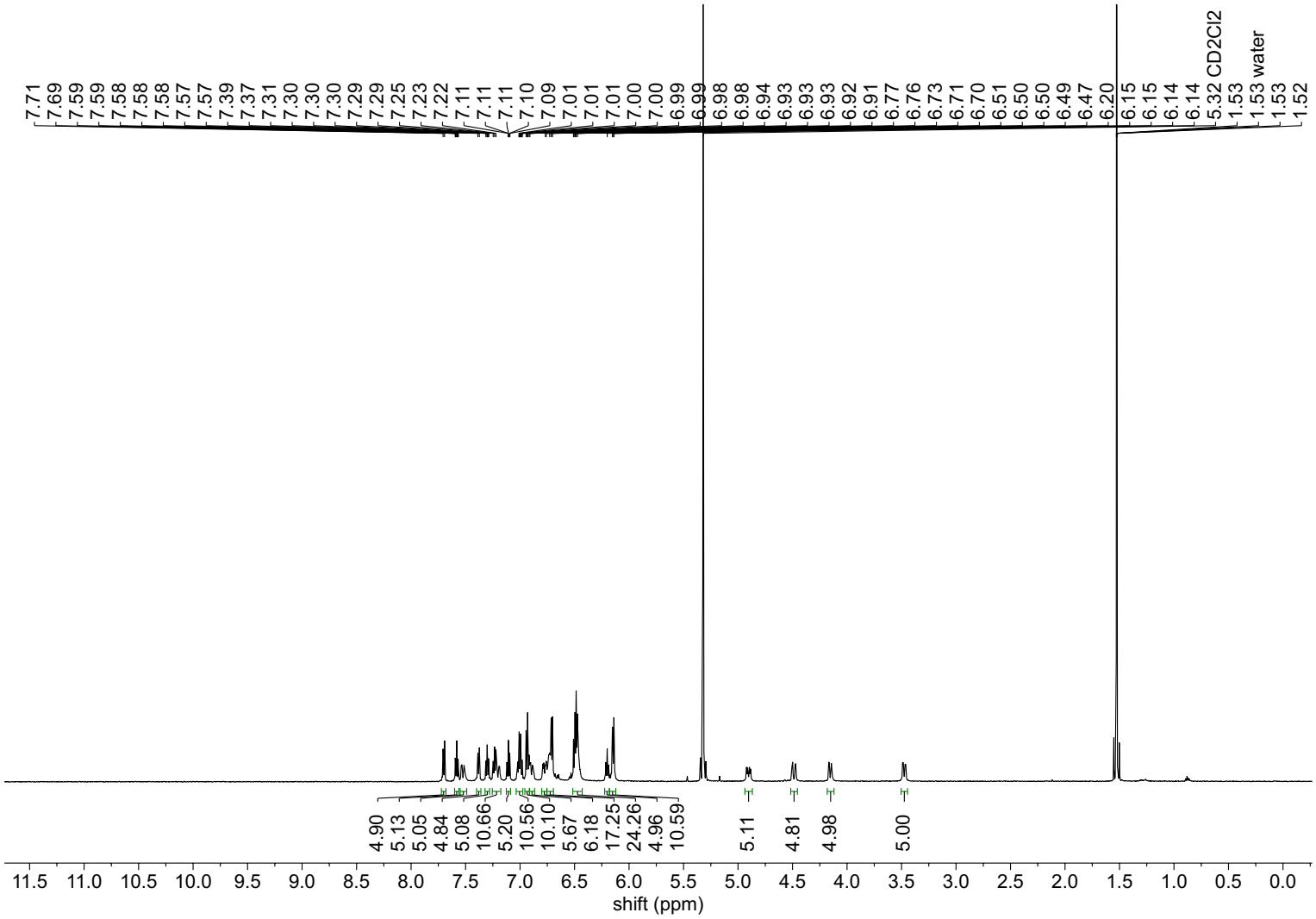

Figure S68. ^{1}H NMR spectrum (CD_2Cl_2, 600 MHz) of **^{13}C-[3a]**$[PF_6]_3$.

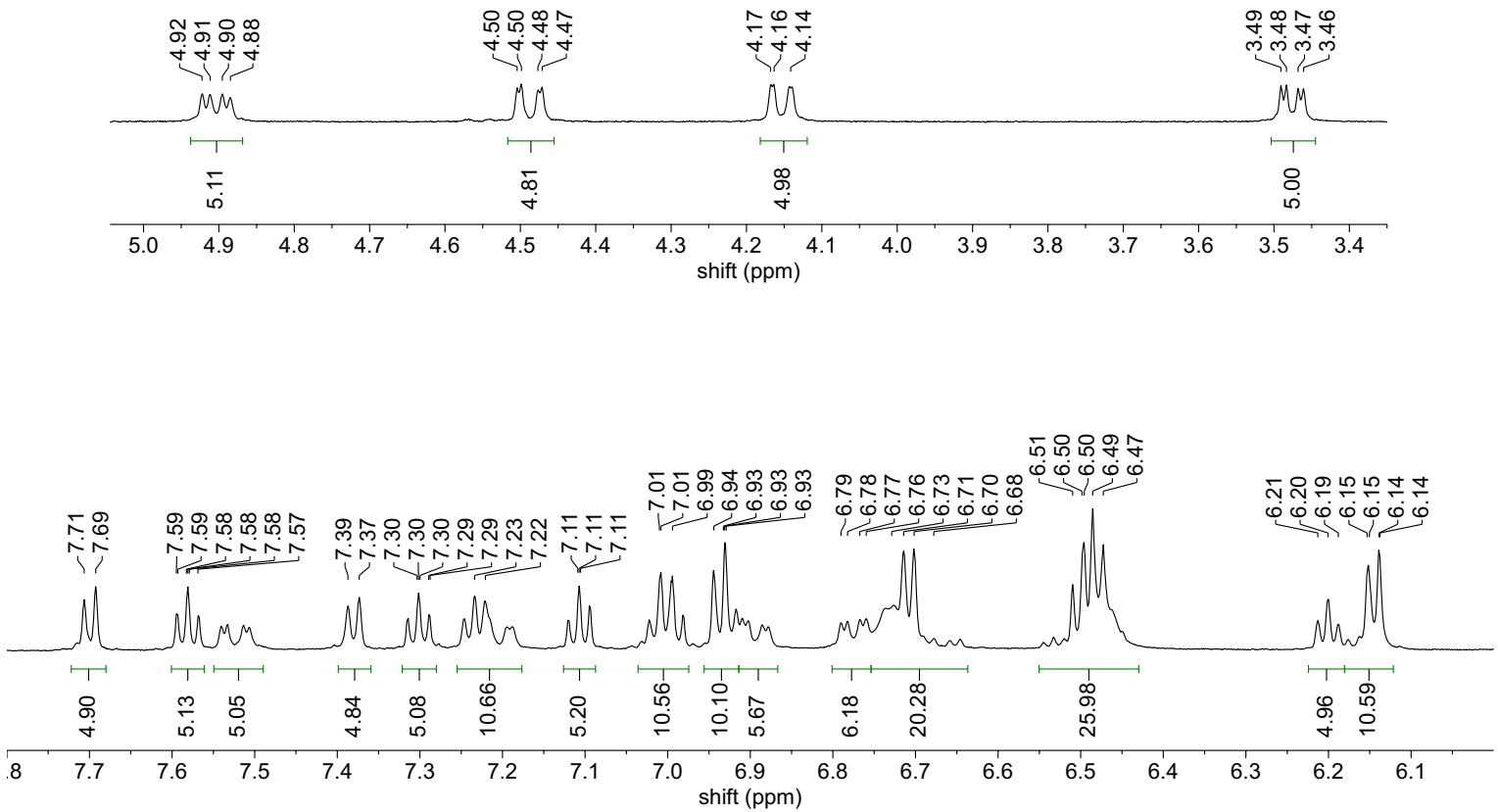

Figure S69. ^{1}H NMR spectrum (CD_2Cl_2, 600 MHz) of **^{13}C-[3a]**$[PF_6]_3$ showing expanded aryl and alkyl regions.

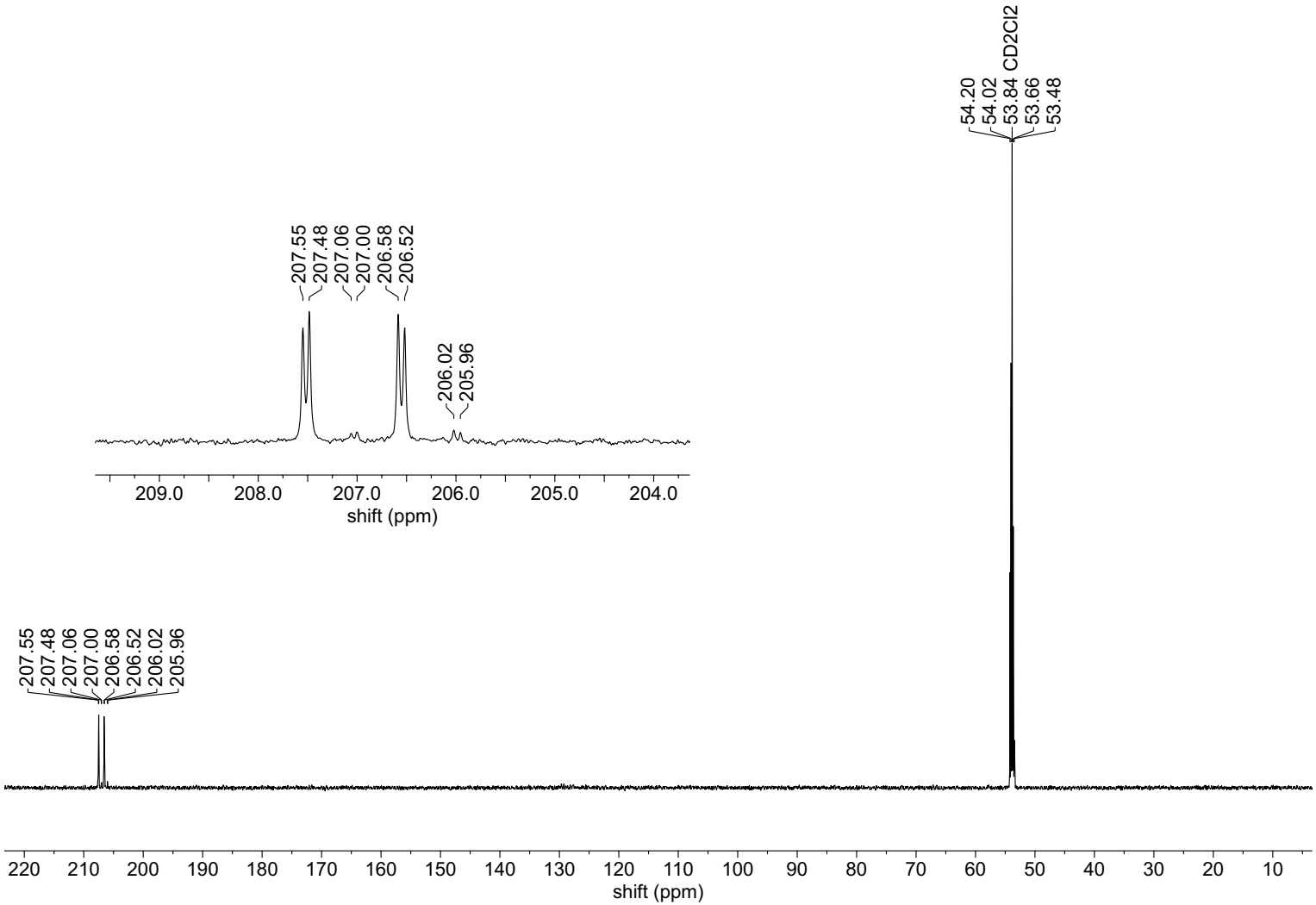

Figure S70. $^{13}C\{^{1}H\}$ NMR spectrum (CD_2Cl_2, 151 MHz) of **^{13}C-[3a]**$[PF_6]_3$.

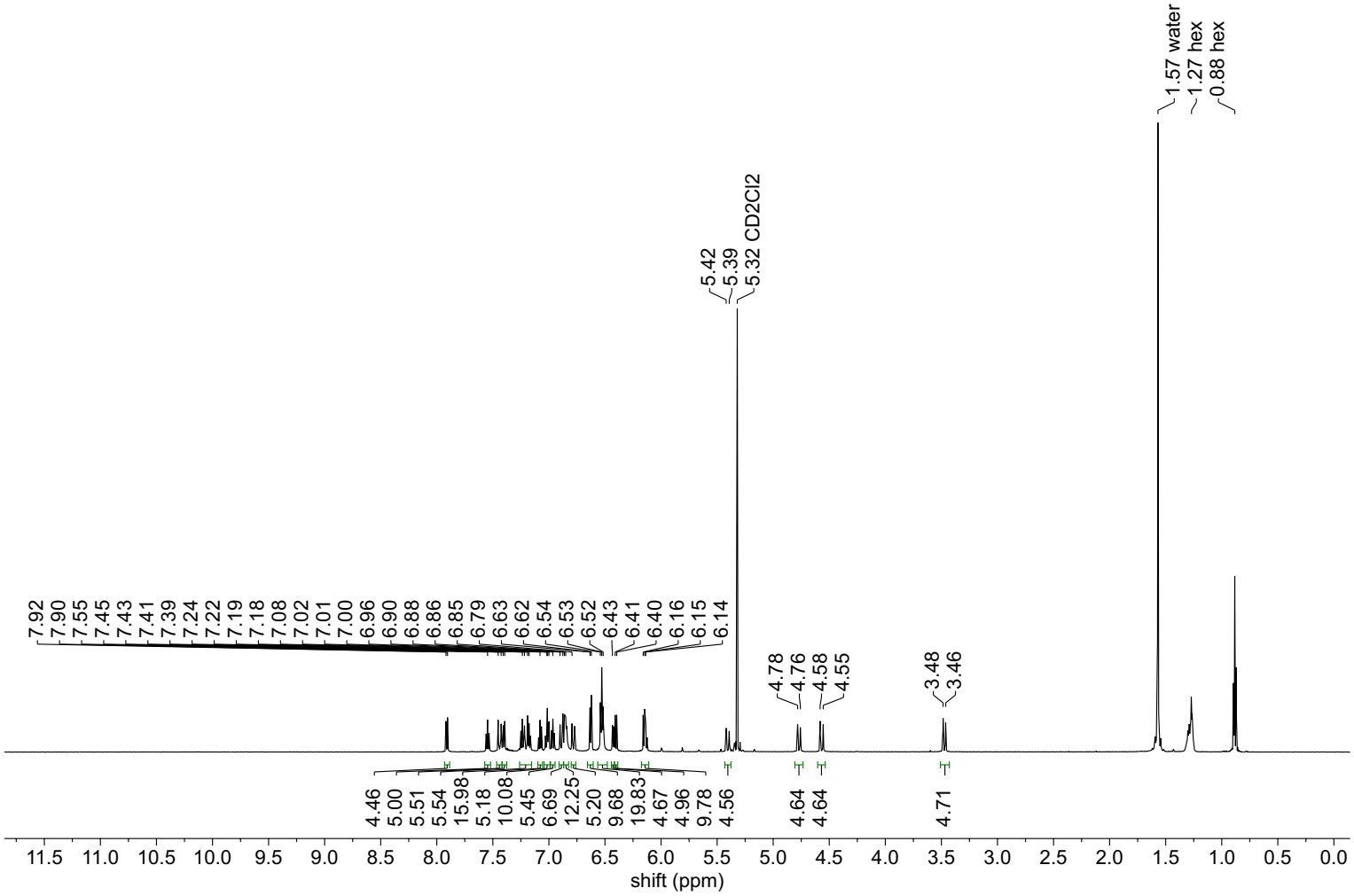

Figure S71. ^{1}H NMR spectrum (CD_2Cl_2, 600 MHz) of [**3b**]Br_3.

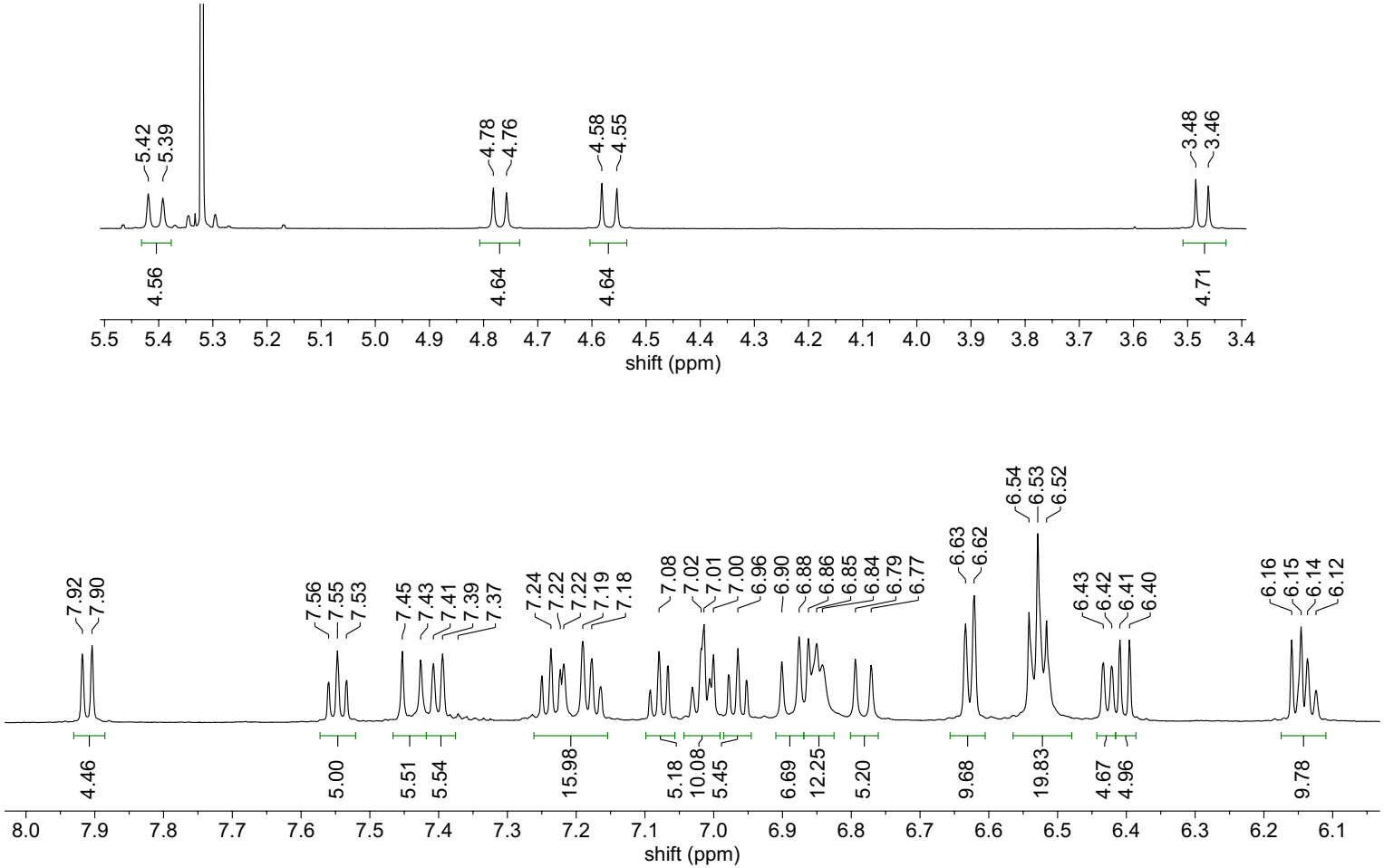

Figure S72. ^{1}H NMR spectrum (CD_2Cl_2, 600 MHz) of [**3b**]Br_3 showing expanded aryl and alkyl regions.

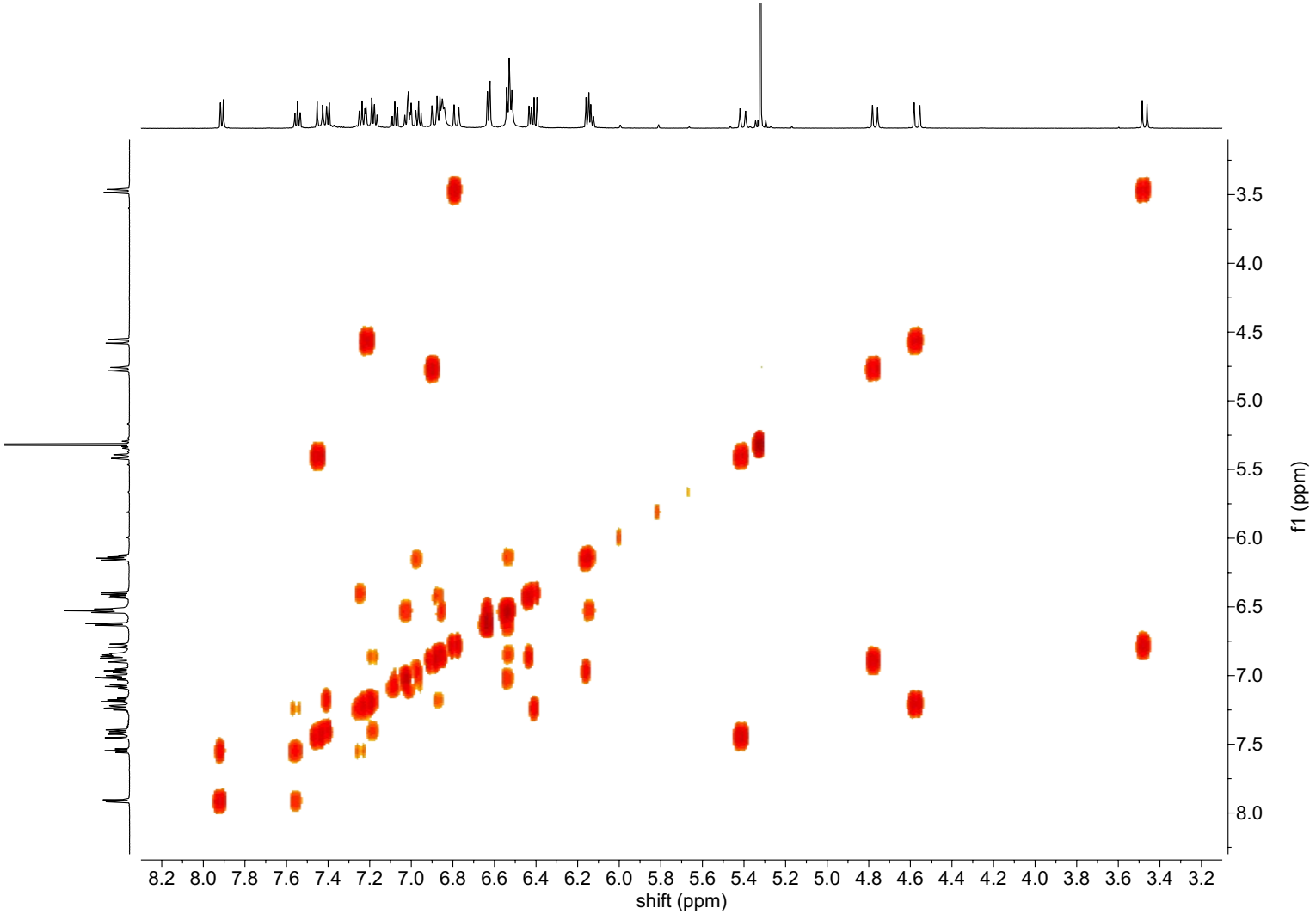

Figure S73. ^{1}H-^{1}H COSY NMR spectrum (CD_2Cl_2, 600 MHz) of [**3b**]Br_3.

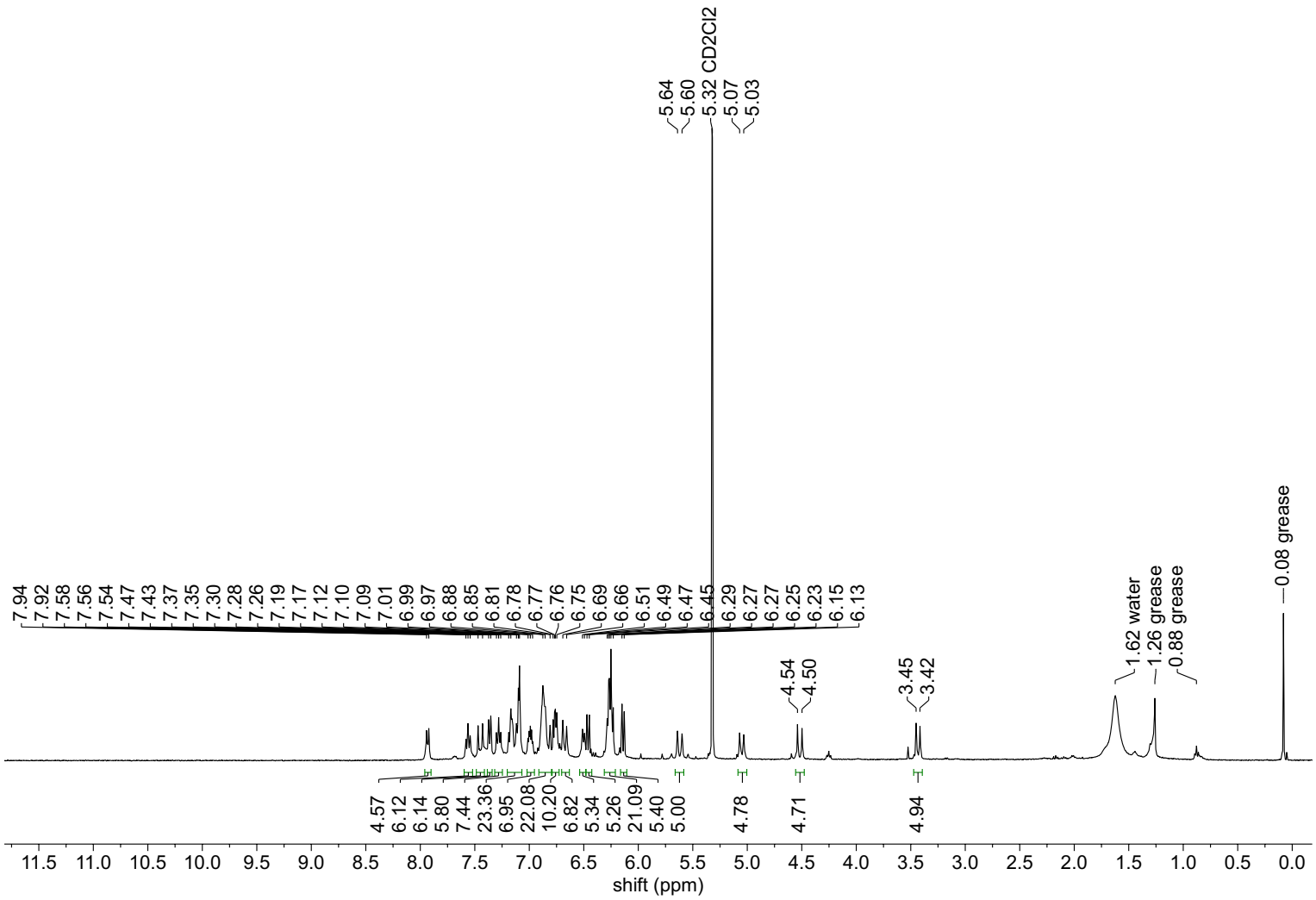

Figure S74. ^{1}H NMR spectrum (CD_2Cl_2, 600 MHz) of [**3c**]Cl_3.

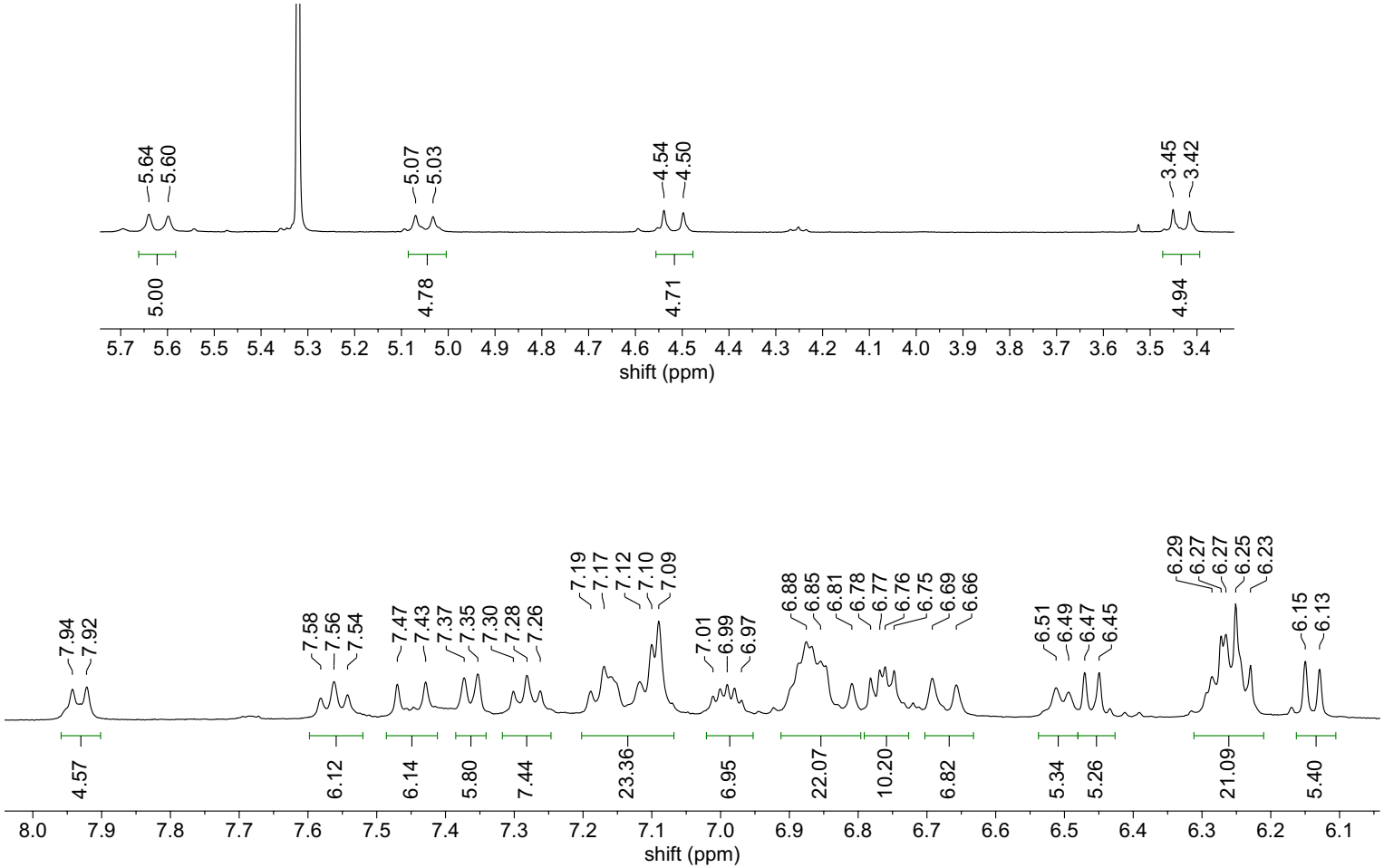

Figure S75. ^{1}H NMR spectrum (CD_2Cl_2, 600 MHz) of [**3c**]Cl_3 showing expansion aryl and alkyl regions.

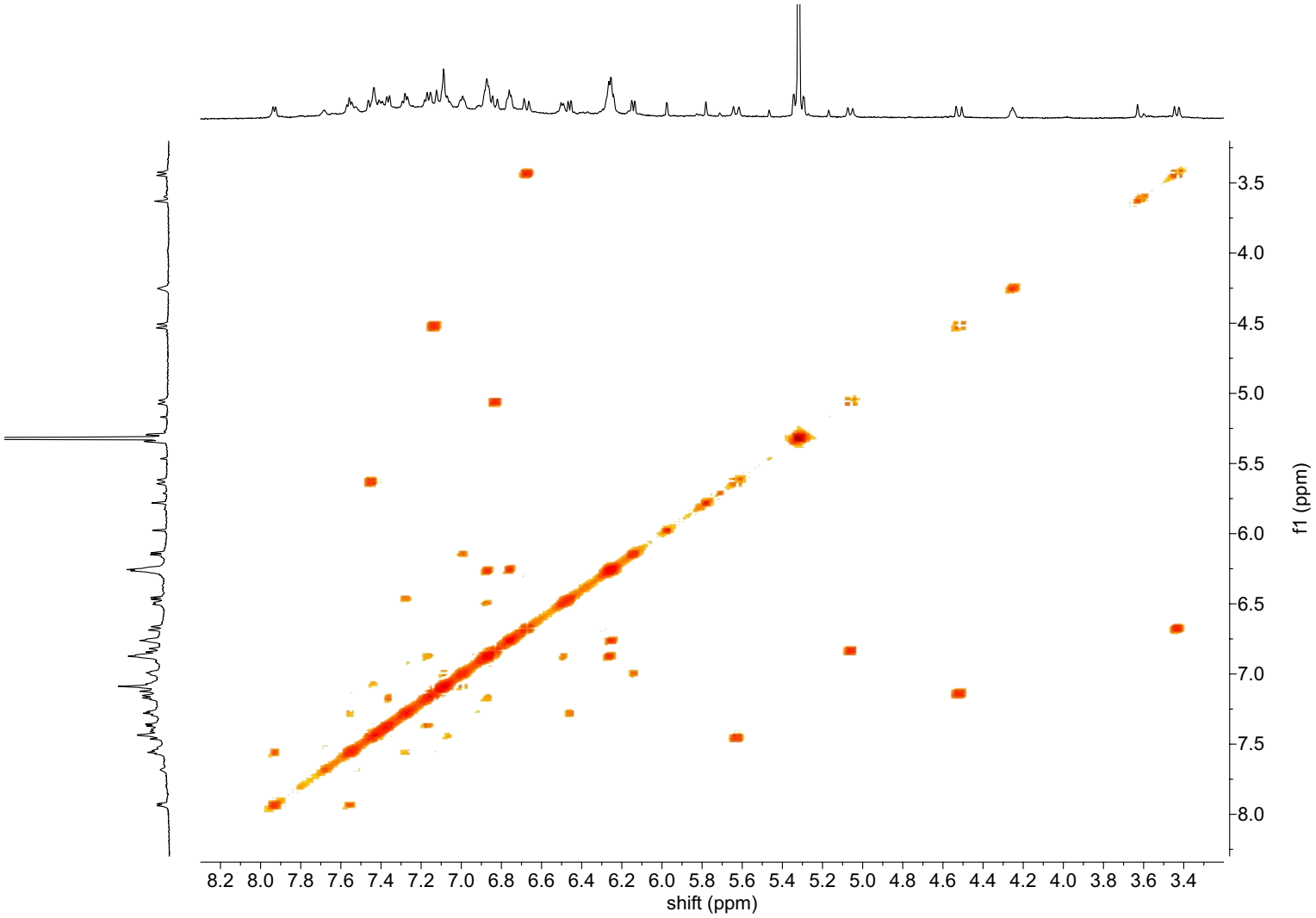

Figure S76. ^{1}H-^{1}H COSY NMR spectrum (CD_2Cl_2, 600 MHz) of [**3c**]Cl_3.

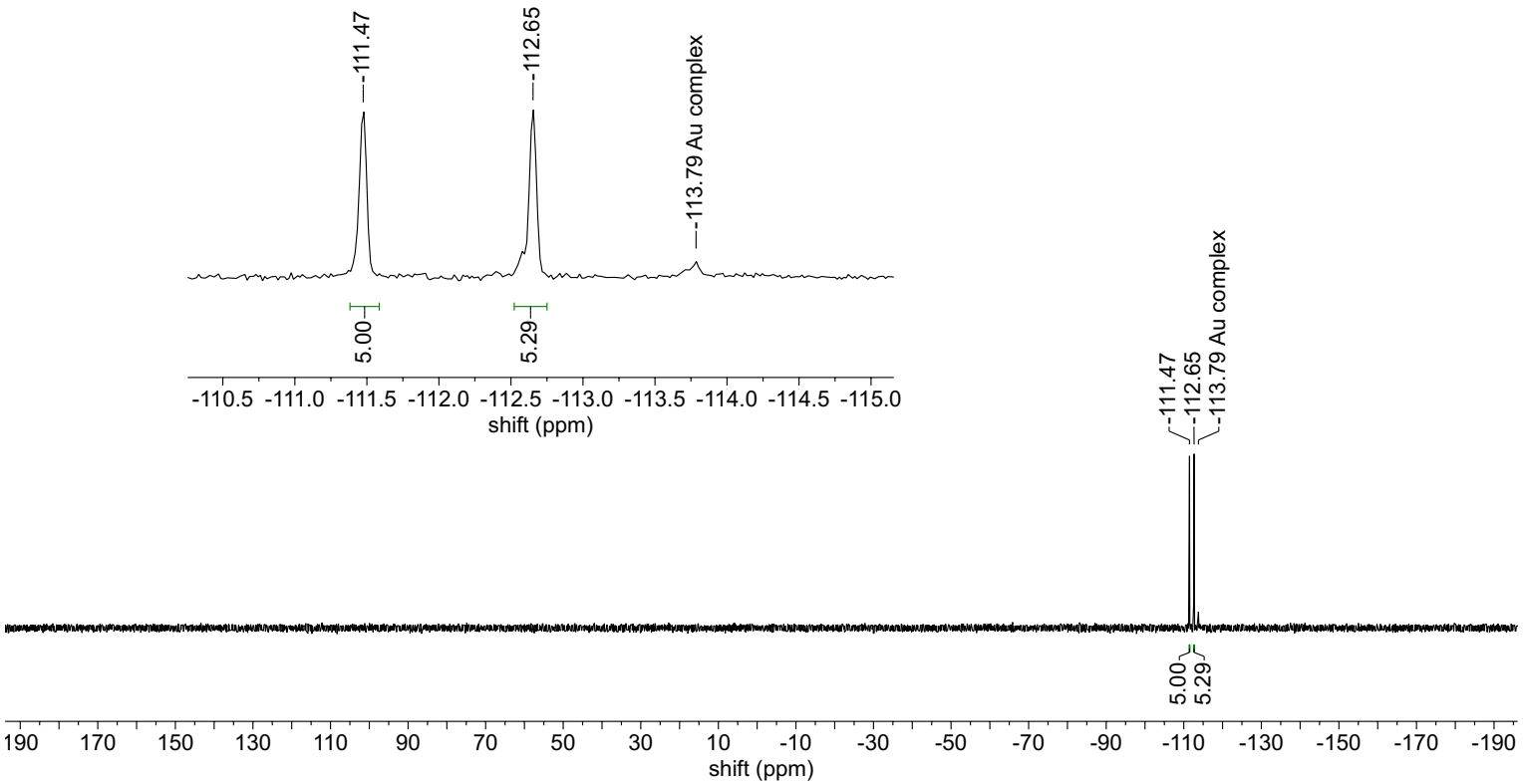

Figure S77. ^{19}F NMR spectrum (CD_2Cl_2, 376 MHz) of **[3c]**Cl_3. ESI-MS suggests the Au complex is $[L_2Au_2]Cl_2$.

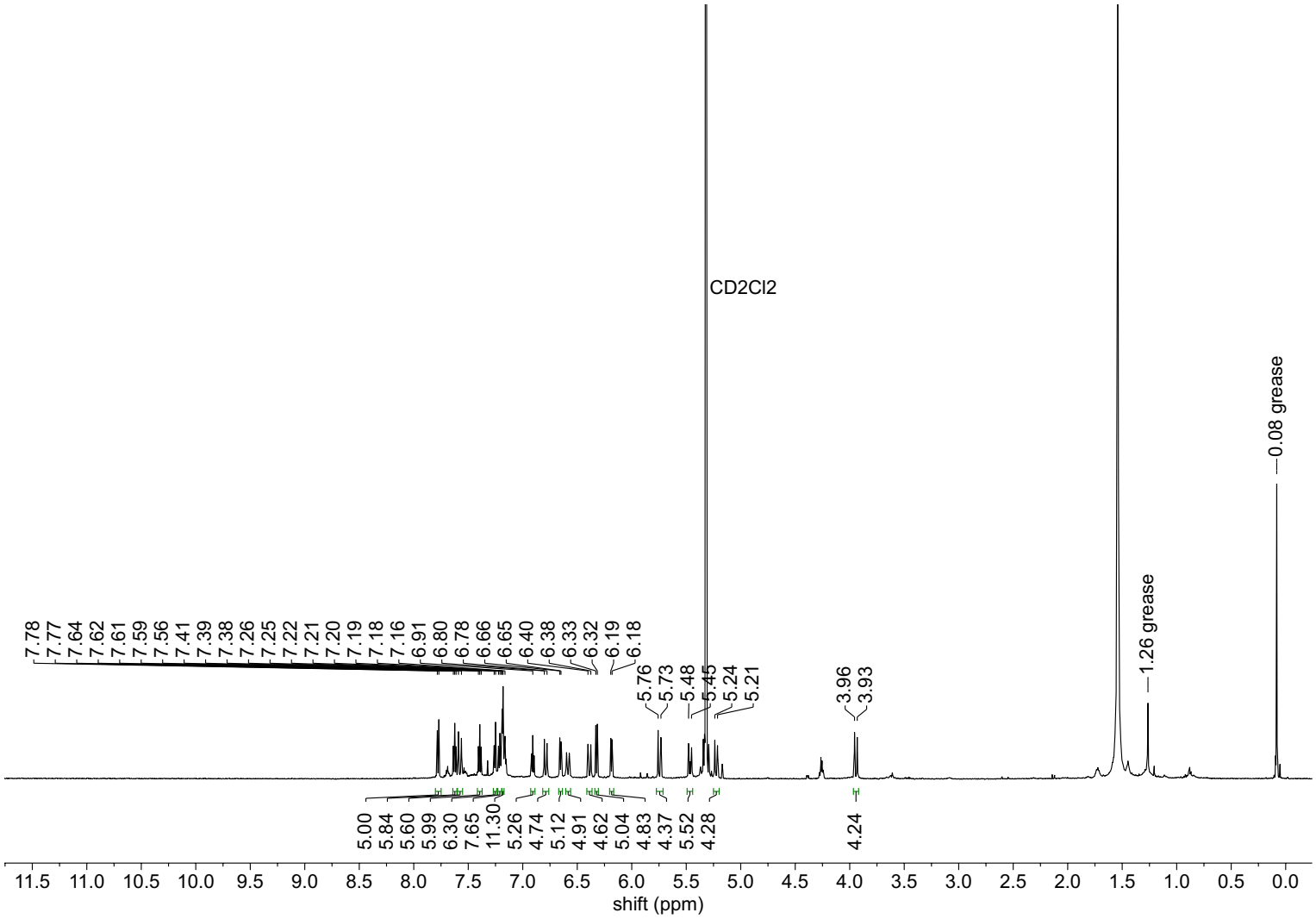

Figure S78. ^{1}H NMR spectrum (CD_2Cl_2, 600 MHz) of [**3d**]Br_3.

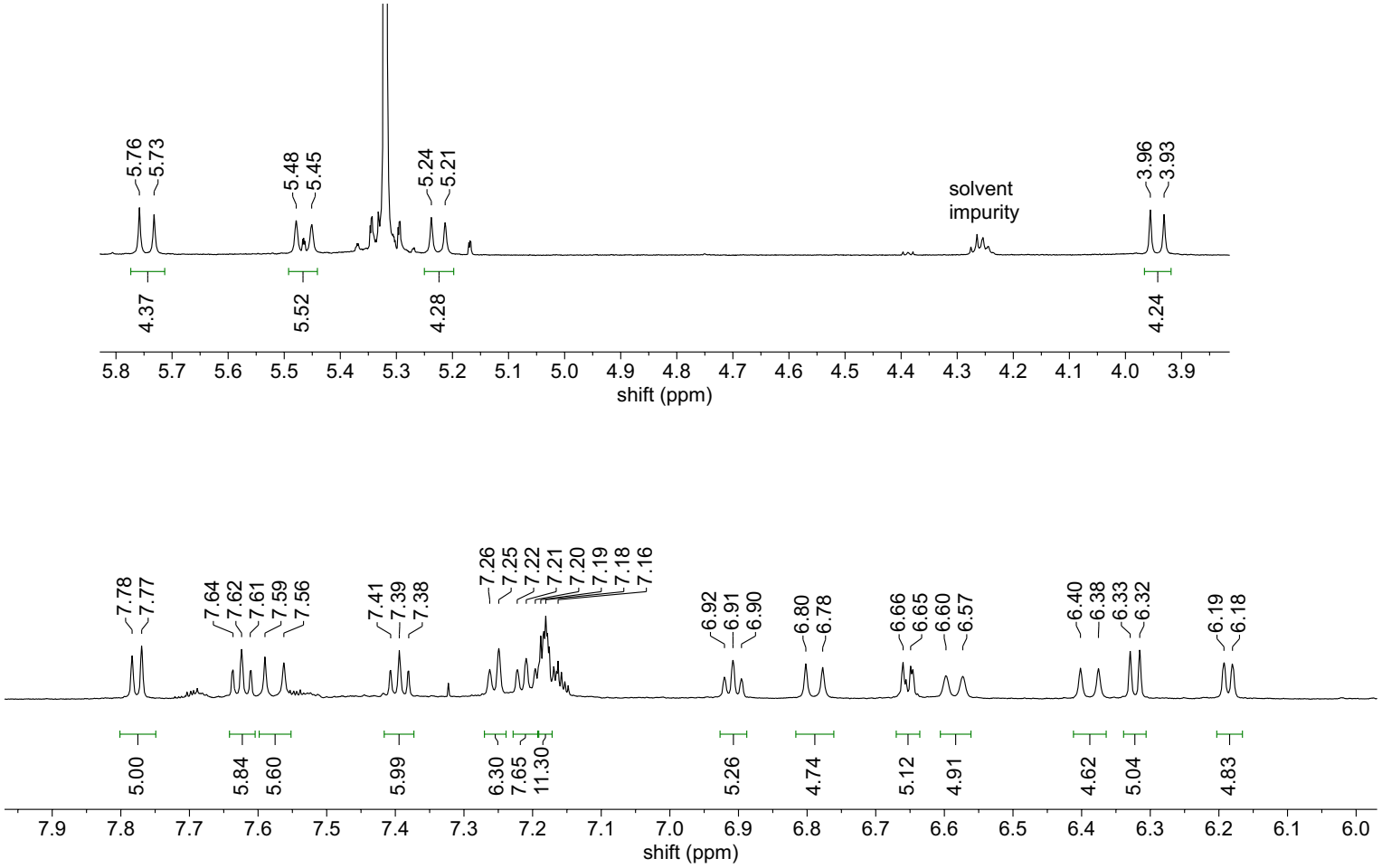

Figure S79. ^{1}H NMR spectrum (CD_2Cl_2, 600 MHz) of [**3d**]Br_3 showing the expanded aryl and alkyl regions.

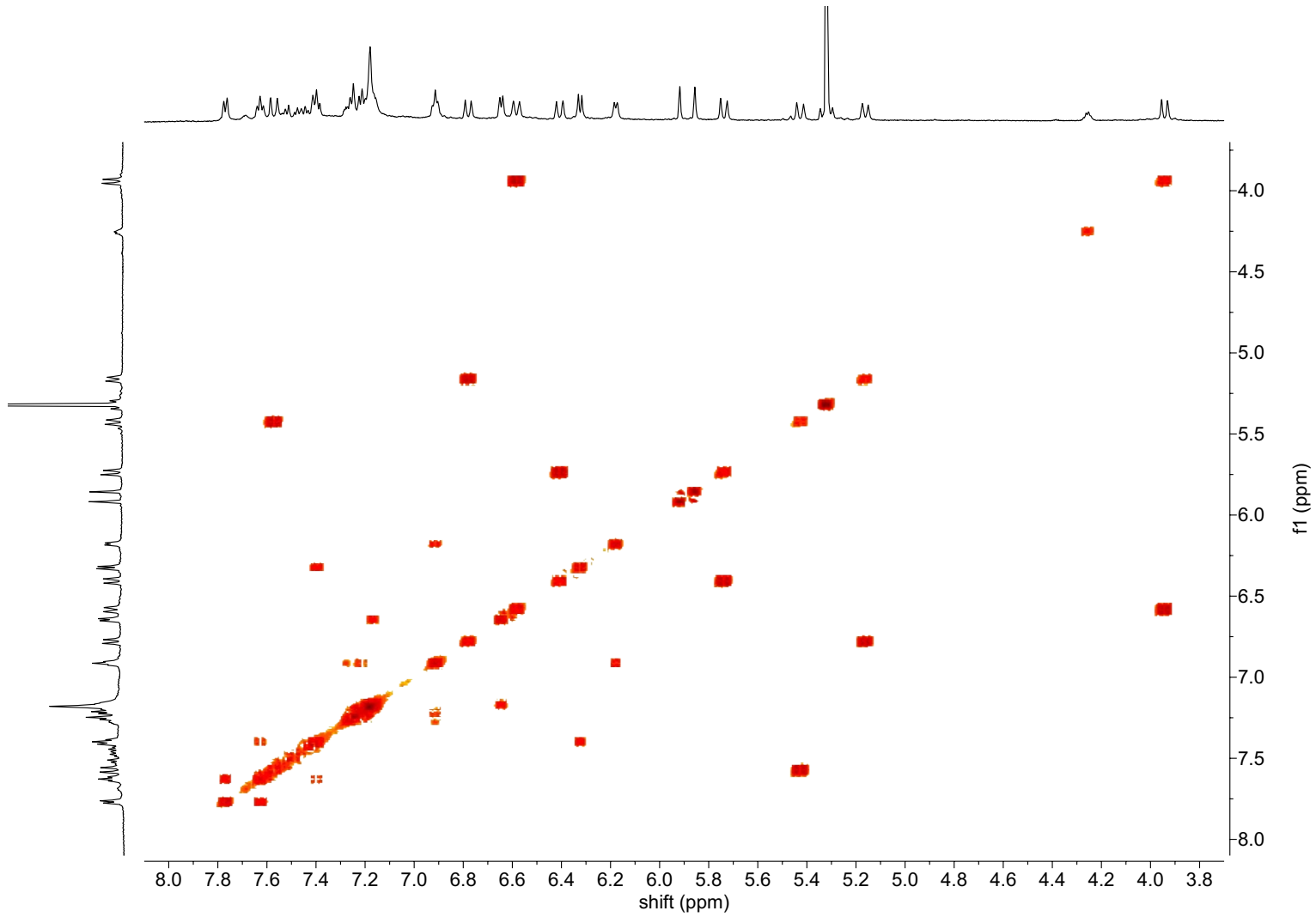

Figure S80. ^{1}H-^{1}H COSY NMR spectrum (CD_2Cl_2, 600 MHz) of [**3d**]Br_3.

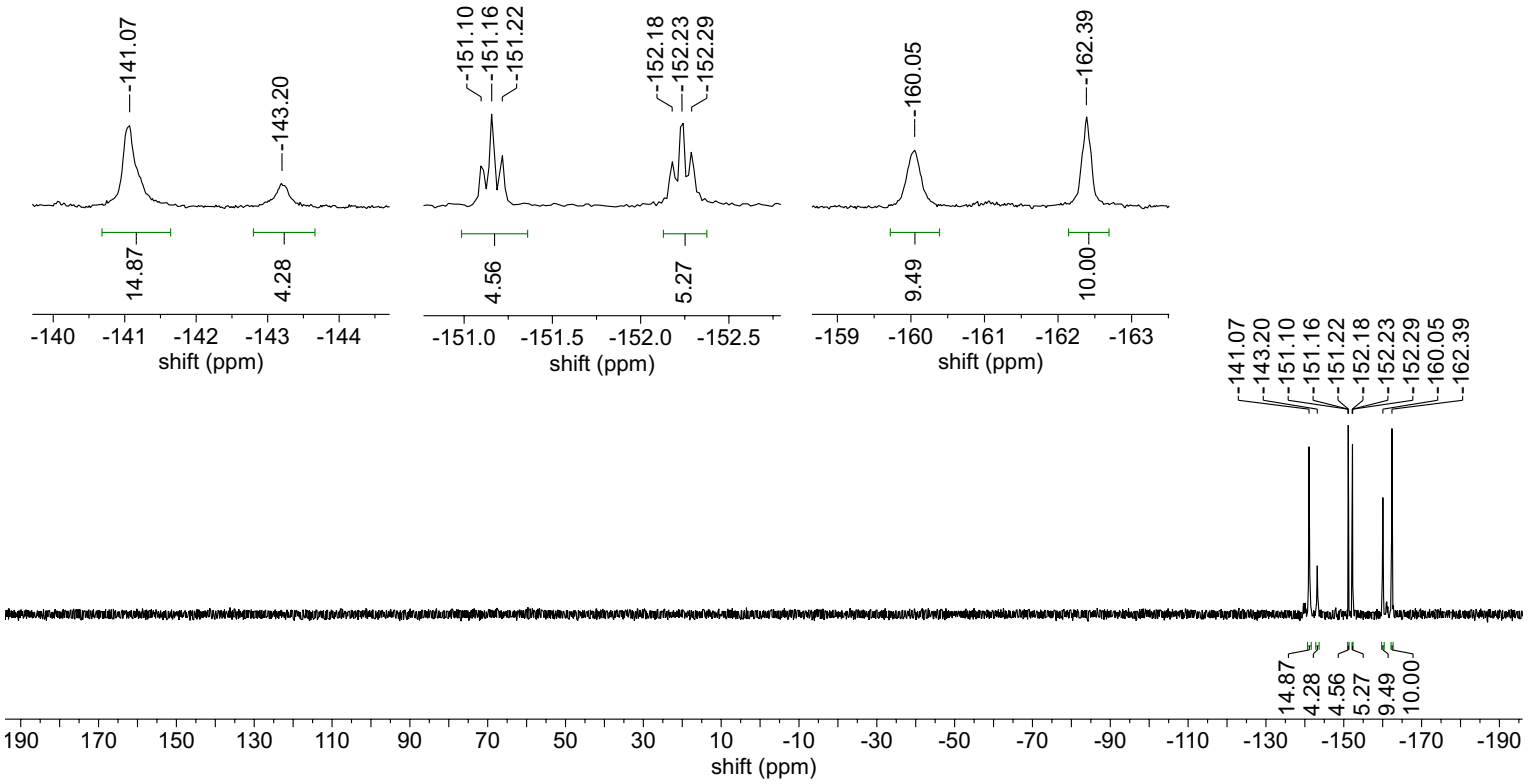

Figure S81. ^{19}F NMR spectrum (CD_2Cl_2, 376 MHz) of **[3d]**Cl_3.

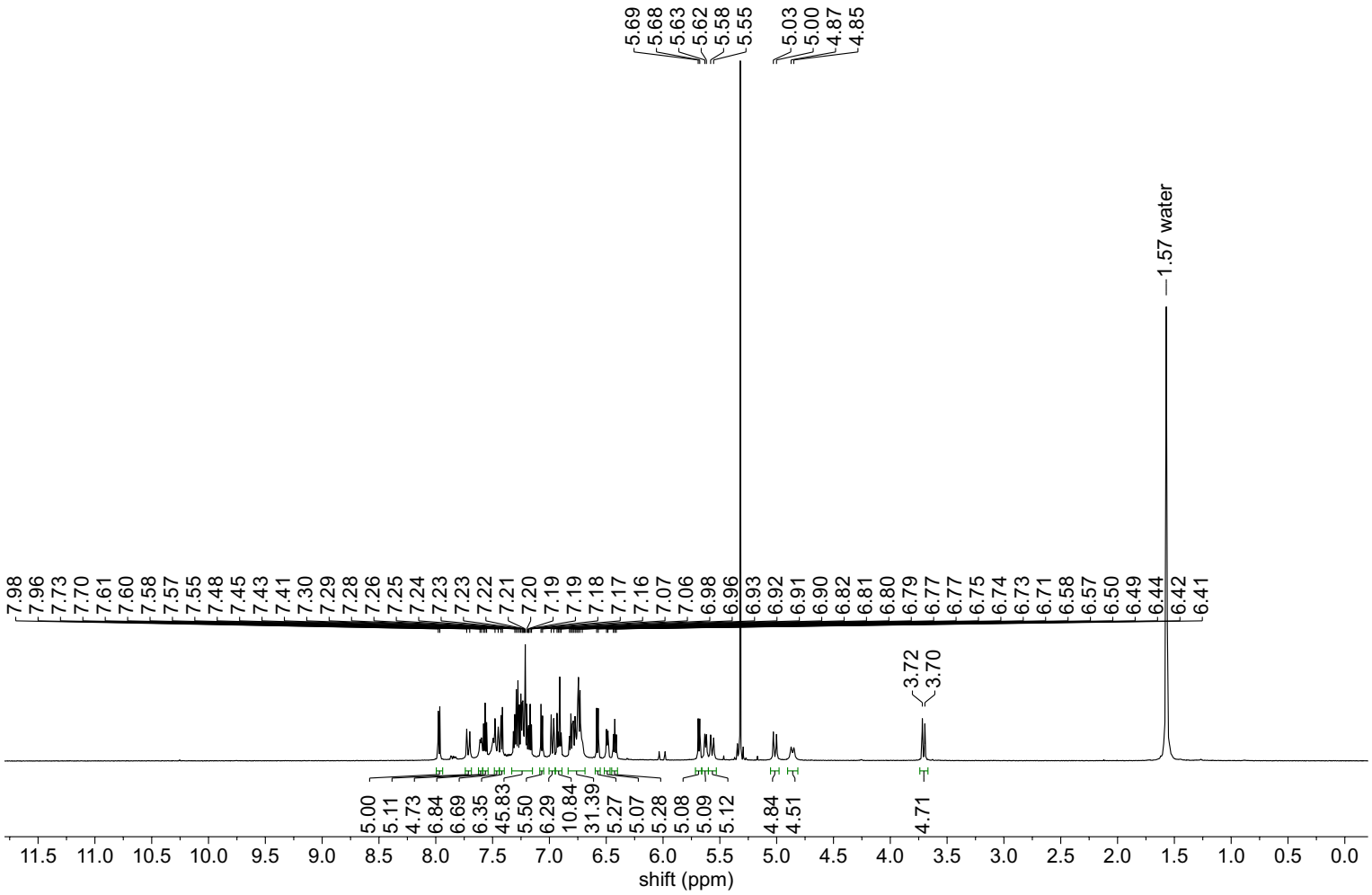

Figure S82. ^{1}H NMR spectrum (CD_2Cl_2, 600 MHz) of [**3e**]Br_3.

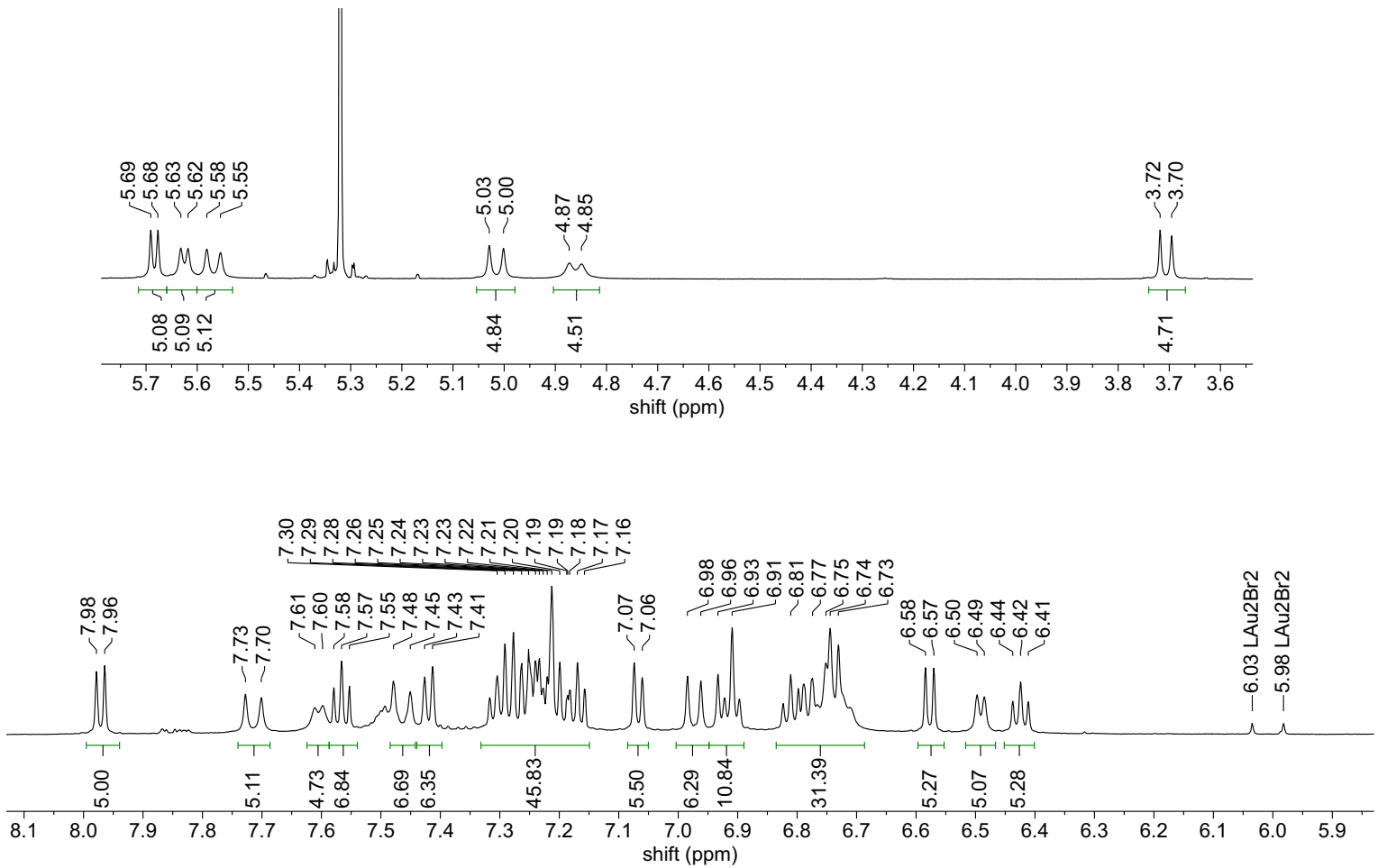

Figure S83. ^{1}H NMR spectrum (CD_2Cl_2, 600 MHz) of [**3e**]Br_3 showing the expanding aryl and alkyl regions.

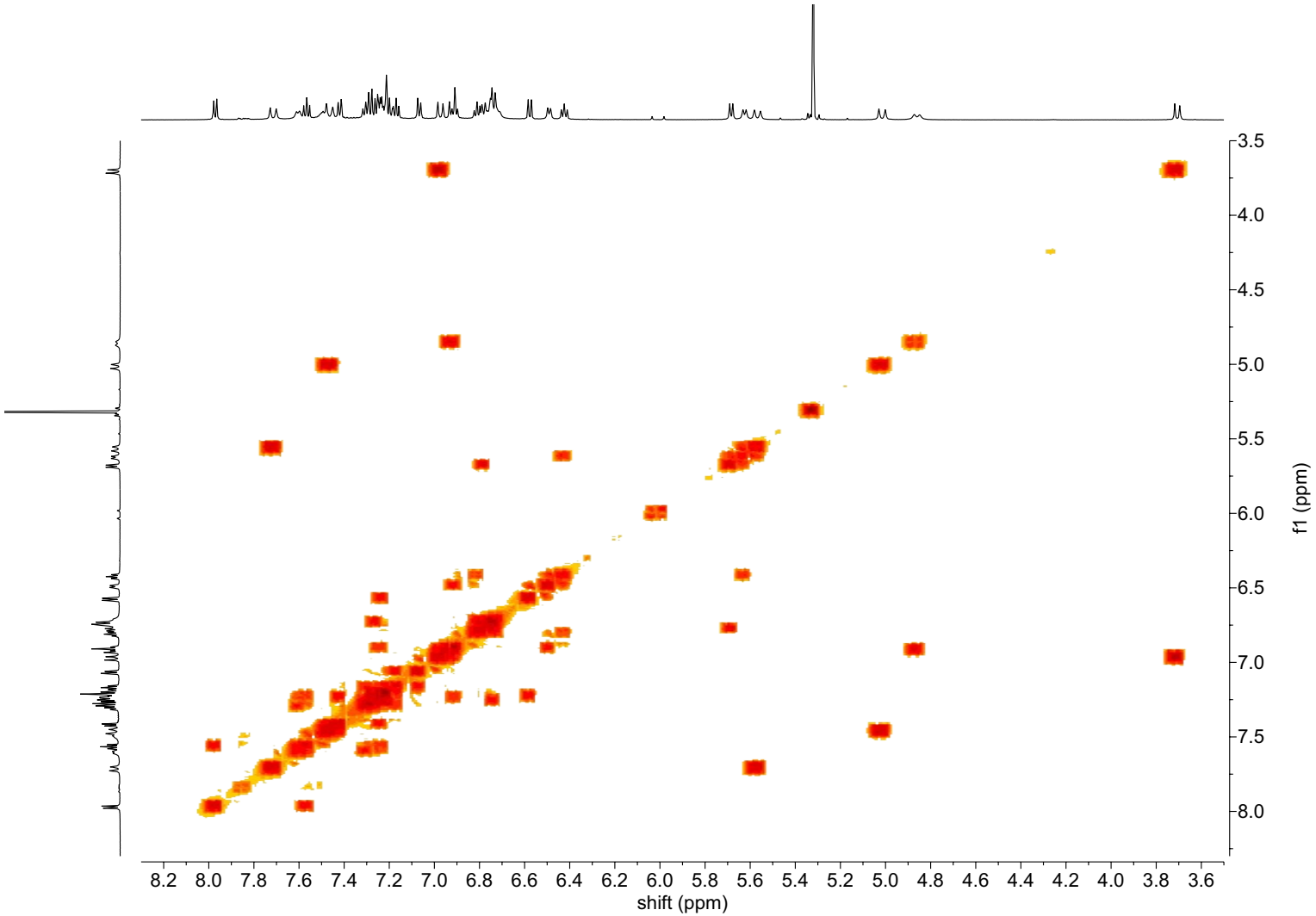

Figure S84. ^{1}H-^{1}H COSY NMR spectrum (CD_2Cl_2, 600 MHz) of [**3e**]Br_3.

4 References

1. Holz, J.; Ayerbe Garcia, M.; Frey, W.; Krupp, F.; Peters, R., Diastereoselective synthesis, structure and reactivity studies of ferrocenyloxazoline gold(I) and gold(II) complexes. *Dalton. Trans.* **2018,** *47*, 3880-3905.
2. Kose, O.; Saito, S., Cross-coupling reaction of alcohols for carbon-carbon bond formation using pincer-type NHC/palladium catalysts. *Org. Biomol. Chem.* **2010,** *8*, 896-900.
3. Mathias, L. J.; Overberger, C. G., Carbon-13 nuclear magnetic resonance chemical shifts of substituted benzimidazoles and 1,3-diazaazulene. *J. Org. Chem.* **1978,** *43*, 3526-3530.
4. Tessier, J.; Schmitzer, A. R., Benzimidazolium salts prevent and disrupt methicillin-resistant Staphylococcus aureus biofilms. *RSC Advances* **2020,** *10*, 9420-9430.
5. Wright, B. D.; Deblock, M. C.; Wagers, P. O.; Duah, E.; Robishaw, N. K.; Shelton, K. L.; Southerland, M. R.; DeBord, M. A.; Kersten, K. M.; McDonald, L. J.; Stiel, J. A.; Panzner, M. J.; Tessier, C. A.; Paruchuri, S.; Youngs, W. J., Anti-tumor activity of lipophilic imidazolium salts on select NSCLC cell lines. *Med. Chem. Res.* **2015,** *24*, 2838-2861.
6. Dinda, J.; Adhikary, S. D.; Seth, S. K.; Mahapatra, A., Carbazole functionalized luminescent silver(i), gold(I) and gold(III)–N-heterocyclic carbene complexes: a new synthetic disproportionation approach towards Au(I)–NHC to provide Au(III)–NHC. *New J. Chem.* **2013,** *37*, 431-438.
7. Fatima, T.; Haque, R. A.; Iqbal, M. A.; Razali, M. R., A new approach for the synthesis of tetrabenzimidazolium salt as a precursor for the tetra-N-heterocyclic carbene dinuclear silver(I) complex. *J. Organomet. Chem.* **2017,** *831*, 50-54.
8 (a) Parker, C. A.; Rees, W. T. Correction of fluorescent spectra and measurement of fluorescent quantum yield. *Analyst* **1960**, *85*, 587-597; (b) Demas, J. N.; Crosby, G. A., Measurement of photoluminescence quantum yields. *J. Phys. Chem.* **1971**, *75*, 991-1024; (c) Rhys-Williams, A. T.; Winfield, S. A.; Miller, J. N. Relative fluorescence quantum yields using a computer controlled luminescence spectrometer. *Analyst* **1983**, *108*, 1067-1071; (d) Eaton, D. F. Reference materials for fluorescence measurements. *Pure & Appl. Chem.* **1988**, *60* (7), 1107-1114; (e) Forgues, F. S.; Lavabre, D. Are fluorescence quantum yields so tricky to measure? A demonstration using familiar stationery products. *J. Chem. Educ.* **1999**, *76*, 1260-1264.
9 Seybold P. G.; Gouterman M. Porphyrins XIII: Fluorescence spectra and Quantum Yields. *J. Mol. Spectrosc.* **1969**, *31*, 1-13.
10 CRC Handbook of Chemistry and Physics, Internet Version **2005**, David R. Lide, ed., *CRC Press*, Boca Raton, FL, 2005.
11. Sheldrick, G. M., SHELXT - integrated space-group and crystal-structure determination. *Acta Crystallogr A Found Adv* **2015,** *71*, 3-8.
12. (a) Baker, M. V.; Brown, D. H.; Simpson, P. V.; Skelton, B. W.; White, A. H.; Williams, C. C., Palladium, rhodium and platinum complexes of ortho-xylyl-linked bis-N-heterocyclic carbenes: Synthesis, structure and catalytic activity. *J. Organomet. Chem.* **2006,** *691*, 5845-5855; (b) Yılmaz, Ü.; Şireci, N.; Deniz, S.; Küçükbay, H., Synthesis and microwave-assisted catalytic activity of novel bis-benzimidazole salts bearing furfuryl and thenyl moieties in Heck and Suzuki cross-coupling reactions. *Appl. Organomet. Chem.* **2010,** *24*, 414–420.
13. (a) Narouz, M. R.; Takano, S.; Lummis, P. A.; Levchenko, T. I.; Nazemi, A.; Kaappa, S.; Malola, S.; Yousefalizadeh, G.; Calhoun, L. A.; Stamplecoskie, K. G.; Häkkinen, H.; Tsukuda, T.; Crudden, C. M., Robust, Highly Luminescent Au_{13} Superatoms Protected by N-Heterocyclic Carbenes. *J. Am. Chem. Soc.* **2019,** *141*, 14997-15002; (b) Shichibu, Y.; Konishi, K., HCl-induced nuclearity convergence in diphosphine-protected ultrasmall gold clusters: a novel synthetic route to "magic-number" Au_{13} clusters. *Small* **2010,** *6*, 1216-1220.